ROLE OF SNARE-DEPENDENT GLIOTRANSMITTERS RELEASE IN ALZHEIMER'S DISEASE: FROM ASTROCYTES TO BEHAVIOUR

DANIELA SOFIA DA COSTA ABREU

A dissertation submitted in partial fulfillment of the requirements for the Degree of Masters in Biomedical Research (Specialization Area: Neuroscience) at Faculdade de Ciências Médicas | NOVA Medical School of NOVA University Lisbon

December 2021

nms.unl.pt

ROLE OF SNARE-DEPENDENT GLIOTRANSMITTERS RELEASE IN ALZHEIMER'S DISEASE: FROM ASTROCYTES TO BEHAVIOUR

Daniela Sofia da Costa Abreu

Supervisors: Sandra Henriques Vaz, PhD, Senior Postdoctoral Researcher at iMM/FMUL

Co-Supervison: Maria José Diógenes, PhD, Associate Professor at FMUL

FCM|NMS Supervisor: Hugo Vicente Miranda, PhD, Principal Investigator/Assistant Professor at CEDOC/NMS

A dissertation submitted in partial fulfillment of the requirements for the Degree of Masters in Biomedical Research (Specialization Area: Neuroscience)

December 2021

The experimental work contained in this master thesis was performed at the Instituto de Medicina Molecular João Lobo Antunes, Faculdade de Medicina, Universidade de Lisboa and the Instituto de Farmacologia e Neurociências, Faculdade de Medicina, Universidade de Lisboa, under the supervision of Sandra Henriques Vaz, PhD and co-supervision of Maria José Diógenes, PhD. Financial support was provided by Fundação para a Ciência e para a Tecnologia (FCT, PTDC/BTM-SAL/32147/2017) and H2020-WIDESPREAD-05-2017-Twinning (EpiEpinet) under grant agreement No. 952455.

Acknowledgments

Em primeiro lugar, gostaria de agradecer à professora Ana Sebastião, pela oportunidade de me tornar membro da sua (gigante) equipa. Obrigada por trabalhar diariamente no sentido de nos proporcionar as melhores condições de trabalho, e pela preocupação que demonstra por todos nós.

Um obrigado muito especial à pessoa a quem realmente devo a concretização desta tese de mestrado: a minha orientadora, Sandra. Obrigada pelas palavras de aconchego e de força, sempre pronunciadas no momento certo. Obrigada por me receberes de braços abertos, pela paciência, e por criares um ambiente seguro, onde não só tenho permissão para ter sucesso, mas também para falhar. Obrigada, por todas as vezes em que ficaste acordada até tarde e trabalhaste aos fins de semana, só para me conseguires dar feedback e me ajudares a tornar uma melhor investigadora. Espero não te ter desiludido, e ter estado à altura das tuas expectativas.

Ao Hugo e à Mizé, por terem aceitado serem meus orientadores e trabalharem em conjunto com a Sandra no sentido de levar este projeto a bom porto.

Ao grupo que me acolheu (e me fez sentir acolhida), *astropeople*. Um gigante obrigada Sara, Mariana S, Joana R, Oksana, Filipa, Mariana V e Joana G! Por todos os dias de *setup* que vos pedinchei, por todas as culturas falhadas que fiz ao longo do ano, por todas as exaustivas experiências de comportamento que se tornaram mais fáceis graças a vocês… Obrigada pela amizade dentro e fora do laboratório. Foi um privilégio crescer no mundo da ciência ao vosso lado.

E é importante lembrar que a vida profissional é um aspeto da vida, e não a vida concreta. Como tal, agradeço aos meus amigos. Aos que fiz no mestrado e que me fizeram sentir acolhida nesta cidade tão grande que é Lisboa. Mas também aos meus amigos de Aveiro, em especial à Mariana, Soares, Laura e às minhas pedaças (Filo, Mariana e Inês). Sem vocês teria sido muito mais difícil.

Um agradecimento muito especial à minha família. Obrigada mãe, por todas as vezes em que te sacrificaste e te deixaste para segundo plano, para que eu conseguisse correr atrás dos meus sonhos. Obrigada Sónia, por todas as vezes em que me tentaste arrancar da frente do computador com o objetivo de me fazeres parar escrever esta (interminável) tese, mesmo que para isso tivessemos de fazer 3 bolos no espaço de dois dias. Vocês são a luz que me orienta na escuridão. E quantas vezes me tiraram de lá. Obrigada por tornaram tudo isto possível.

Por fim, obrigada Pedro. Obrigada pela tua compreensão, carinho, amor, dedicação, e por carregares todas as minhas cruzes como se fossem tuas. Este trabalho também é teu.

Um sincero obrigada a todos.

Invictus

Do fundo desta noite que persiste
A me envolver em breu - eterno e espesso,
A qualquer deus - se algum acaso existe,
Por mi'alma insubjugável agradeço.

Nas garras do destino e seus estragos,
Sob os golpes que o acaso atira e acerta,
Nunca me lamentei - e ainda trago
Minha cabeça - embora em sangue - ereta.

Além deste oceano de lamúria,
Somente o Horror das trevas se divisa;
Porém o tempo, a consumir-se em fúria,
Não me amedronta, nem me martiriza.

Por ser estreita a senda - eu não declino,
Nem por pesada a mão que o mundo espalma;
Eu sou dono e senhor de meu destino;
Eu sou o comandante de minha alma.

William Ernest Henley

Scientific production

The scientific content of the present dissertation has been discussed in several national conferences both in poster and oral sessions:

- **Abreu DS**, Gomes JI, Sottomayor MN, Ribeiro FF, Vicente Miranda H, Marques MC, Summavielle T, Socodato R, Relvas JB, Sebastião AM, Déglon N, Vaz SH (2021) "Astrocyte's dysregulation: a central hub in Alzheimer's disease pathophysiology?" XVII Meeting of the Portuguese Society for Neuroscience, December 1st-3rd, Portugal [Poster communication]
- **Abreu DS**, Gomes JI, Sottomayor MN, Ribeiro FF, Vicente Miranda H, Marques MC, Summavielle T, Socodato R, Relvas JB, Sebastião AM, Déglon N, Vaz SH (2021) "Astrocyte-driven changes in synaptic plasticity and memory function in Alzheimer' disease" V Symposium Portuguese Glial Network, November 30th, Portugal [Oral communication]
- **Abreu DS**, Gomes JI, Vicente Miranda H, Sebastião AM, Diógenes MJ, Vaz SH (2021) "Astrocytes in Alzheimer's disease: friends, foes and potential therapeutic targets" iMed Conference, October 7th, Portugal [Oral communication, **Finalist**]
- **Abreu DS**, Gomes JI, Sottomayor M, Solano F, Ribeiro F, Sebastião AM, Vaz SH (2021) "Astrocytes: a model to study synaptic plasticity, learning and memory, and disease research" EpiEpiNet Summer School - Epileptogenesis & Epilepsy Network, September 27th- October 1st, Portugal [Poster communication]
- **Abreu DS**, Gomes JI, Vicente Miranda H, Sebastião AM, Diógenes MJ, Vaz SH (2021) "Astrocytes as potential targets to reduce neurotoxicity in Alzheimer's disease" 16th YES (Young European Scientist) Meeting, September 16-19th, Portugal [Oral communication, **2nd place**]
- **Abreu DS**, Gomes JI, Fonseca-Gomes J, Vicente Miranda H, Sebastião AM, Diógenes MJ, Vaz SH (2021) "Impact of astrocytes in neurotoxicity mediated by amyloid-β: potential role of D-serine" AIMS Meeting – Annual International (bio)Medical Students Meeting, March 18th-21st, Portugal [Poster communication]
- **Abreu DS**, Pinto S, Gomes JI, Fonseca-Gomes J, Vicente Miranda H, Sebastião AM, Diógenes MJ, Vaz SH (2021) "Gliotransmission role upon amyloid-β mediated excitotoxicity" SPF Meeting 2021- Annual Meeting of Pharmacology Portuguese Society, February 17-19th, Portugal [Oral communication]

Table of Content

List of Figures and Tables ..... **XI**

List of Abbreviations ..... **XIII**

Resumo **1**

Abstract **3**

1. Introduction **5**

1.1. Astrocytes 5

1.1.1. Development of the astroglia concept 5

1.1.2. Electrophysiological properties 6

1.1.3. Functions 7

1.2. The Tripartite Synapse 9

1.2.1. Ca^{2+}-dependent gliotransmission 9

1.2.2. Gliotransmitters 12

1.2.2.1. Glutamate 12

1.2.2.2. D-serine 14

1.3. Synaptic plasticity, memory, and the hippocampus 18

1.3.1. Patient H.M and the history of memory 18

1.3.2. Hippocampal anatomy 18

1.3.3. Synaptic plasticity 19

1.3.4. NMDAR-dependent LTP 20

1.3.5. Cognitive and behavioral evaluation of rodent models 22

1.4. Alzheimer's disease 24

1.4.1. Discovery and clinical manifestation of Alzheimer's disease 24

1.4.2. Pathological hallmarks of Alzheimer's disease 24

1.4.3. Astrocytic gliotransmitters in Alzheimer's disease 27

2. Rationale and Aims **31**

2. Materials and Methods **33**

2.1. Genetic model: Transgenic dominant-negative SNARE (dn-SNARE) mice 33

2.1.1. Animal's genotyping 34

2.2. *In vivo* AAV-AD model 36

2.3. *Ex-vivo* electrophysiological recordings 37

2.3.1. Preparation of acute hippocampal slices 38

2.3.2. Drug treatment 38
2.3.3. Extracellular recordings of field excitatory postsynaptic potentials (fEPSPs) and Long-Term Potentiation (LTP) induction 39
2.4. Western blot 41
2.5. Immunofluorescence assays 42
2.6. FRET-base live-cell imaging in astrocytes 43
2.6.1. Primary cultures of astrocytes 43
2.6.2. FRET biosensor for glutamate assay 44
2.6.2.1. Growing of bacterial cultures 44
2.6.2.2. Plasmid DNA purification from E. coli 45
2.6.2.3. Fluorescence principles and FRET 46
2.7. Behavioral tests 48
2.7.1. Open-field test 50
2.7.2. Y-maze spontaneous alternation 51
2.7.3. Object Location Task 52
2.7.4. Barnes Maze 53
2.7.5. Morris Water Maze 55
3. Results 58
3.1. Role of astrocytic signaling in the modulation of synaptic plasticity, and cognitive functions 58
3.1.1. Validation of the dn-SNARE mouse model 58
3.1.1.1. Transgene detection and quantification 58
3.1.1.2. Immunofluorescence analysis 59
3.1.2. Electrophysiological testing of dn-SNARE mice: Synaptic plasticity 61
3.2. The role of SNARE-dependent gliotransmitters release Aβ-mediated toxicity on hippocampal synaptic plasticity 62
3.3. Astrocytes as the main source of D-serine 64
3.3.1. Synaptic plasticity: Wt and dn-SNARE hippocampal slices perfused with D-serine 64
3.3.2. Synaptic plasticity: Wt and dn-SNARE hippocampal slices perfused with L-serine . 66
3.4. LTP-impairment triggered by Aβ-oligomers was rescued by supplying exogenous D-serine 68
3.5. The role of SNARE-dependent gliotransmitters release in Alzheimer's disease: memory and learning impairment 70
3.5.1. Validation of the AD model: Western blot quantification 70
3.5.2. Validation of the AD model: Immunofluorescence analysis 71

3.5.2.1. Human APP immunostaining 72
3.5.2.2. Total APP immunostaining 74
3.5.3. Behavioral analysis 76
3.5.3.1. Open-Field Test 76
3.5.3.2. Y-maze spontaneous alternation 77
3.5.3.3. Object location test 78
3.5.3.4. Barnes Maze 79
3.5.3.5. Morris Water Maze 83
3.5.4. Long-term potentiation of AAV-PS1 or AAV-APP/PS1 injected dn-SNARE and Wt mice 86
3.6. $A\beta_{1-42}$-oligomers increase glutamate release by astrocytes 88
4. Discussion 91
4.1. The dn-SNARE mice model 91
4.2. Role of gliotransmission in $A\beta_{1-42}$ effects in synaptic plasticity 93
4.3. Role of gliotransmission in AD-like APP processing 97
5. Conclusion 103
6. References 105

List of Figures and Tables

Figures

Figure 1: Scheme of the tripartite synapse and Ca2+-dependent gliotransmission 11

Figure 2: Mechanisms of glutamate release from astrocytes 13

Figure 3: Serine shuttle pathway between neurons and astrocytes 17

Figure 4: Schematics of the hippocampal neuronal circuitry 19

Figure 5: NMDAR-dependent LTP mechanism 22

Figure 6: Amyloid precursor protein (APP) processing pathways 25

Figure 7: Schematic functioning of the transgenic dn-SNARE mice 34

Figure 8: Schematic illustration of electrode positions in CA1 region of hippocampal slice and diagram of field excitatory postsynaptic potential (fEPSP) 39

Figure 9: Vector Map of pDisplay FLIPE-600n 46

Figure 10: Characterization of a FRET-based biosensor for the quantification of glutamate released from cultured astrocytes 47

Figure 11: Experimental design 50

Figure 12: Schematic representation of the OFT 51

Figure 13: Schematic representation of the Y-maze continuous spontaneous alternation task 52

Figure 14: Diagram of OLT tasks 53

Figure 15: Schematic representation of Barnes Maze test 55

Figure 16: Schematic representation of the MWM test 57

Figure 17: Quantification of the transgene reporter GFP in the hippocampus of Wt and dn-SNARE mice 59

Figure 18: dn-SNARE transgene expression is astrocyte-specific 60

Figure 19: SNARE-dependent gliotransmission modulates LTP 61

Figure 20: Blocking SNARE-dependent gliotransmission reverts LTP impairment mediated by $A\beta_{1-42}$ oligomers 63

Figure 21: D-serine tends to increase LTP only in animals with compromised gliotransmission 65

Figure 22: L-serine does not alter LTP in animals with compromised gliotransmission 67

Figure 23: D-serine rescues the deficit of Aβ-induced LTP 69

Figure 24: Quantification of human APP and total APP expression in the hippocampus of Wt and dn-SNARE mice 3 months after AAV-PS1 and AAV-APP/PS1 injections 71

Figure 25: Human APP expression in hippocampal slices of Wt and dn-SNARE animals three months after AAV-PS1 and APP/PS1 injection 73

Figure 26: Total APP expression in hippocampal slices of Wt and dn-SNARE animals three months after AAV-PS1 and APP/PS1 injection 75

Figure 27: Assessment of motor function, exploration, and anxious-like behaviors by OFT of Wt and dn-SNARE mice 3 months after AAV-APP/PS1 and AAV-PS1 injections 77

Figure 28: Y-maze spontaneous alternation to evaluate spatial working memory performance of Wt and dn-SNARE mice 3 months after AAV-APP/PS1 and AAV-PS1 injections 78

Figure 29: Spatial memory performance, in OLT, of Wt and dn-SNARE mice 3 months after AAV-PS1 and AAV-APP/PS1 injection 79

Figure 30: Learning performance in the Barnes Maze test of Wt and dn-SNARE mice 3 months after AAV-PS1 and AAV-APP/PS1 injection 81-82

Figure 31: Spatial learning evaluation on probe trial from Barnes Maze test of Wt and dn-SNARE mice 3 months after AAV-PS1 and AAV-APP/PS1 injection 83

Figure 32: Learning performance in the MWM test of Wt and dn-SNARE mice 3 months after AAV-PS1 and AAV-APP/PS1 injection 85

Figure 33: Synaptic plasticity changes in LTP in Wt and dn-SNARE mice three months after AAV-PS1 or AAV-APP/PS1 injection 87

Figure 34: $A\beta_{1-42}$ oligomers induce an increase in glutamate release by astrocytes 88

Tables

Table 1: PCR mix used for the genotyping of Wt and dn-SNARE animals 35

Table 2: PCR conditions used for the genotyping of Wt and dn-SNARE animals 36

List of Abbreviations

Aβ	Amyloid β-peptide
AAV	Adeno Associated Virus
aCSF	Artificial cerebrospinal fluid
AD	Alzheimer's disease
AICD	Amyloid precursor protein intracellular fragment
AMPA	α-amino-3-hydroxy-5-methyl-4-isoxazolepropionic acid
AMPAR	α-amino-3-hydroxy-5-methyl-4-isoxazolepropionic acid
APP	Amyloid precursor protein
APS	Ammonium persulfate
Asc-1	Alanine/serine/cysteine transporter 1
ASCT	Alanine/serine/cysteine/threonine transporter
ATP	Adenosine triphosphate
BBB	Brain blood barrier
BSA	Bovine serum albumin
CA1	Cornu Ammonis 1
CA3	Cornu Ammonis 3
Ca^{2+}	Calcium
CFP	Cyan fluorescent protein
Cl^-	Chloride
CNS	Central nervous system
CSF	Cerebrospinal fluid
CTF	C-terminal fragment of APP
CZ	Central zone
DAAO	D-amino acid oxidase
DAPI	4',6'-diamidino-2-phenylindole
DG	Dentate Gyrus
dn-SNARE	Dominant-negative SNARE
Dox	Doxycycline
EAAT1	Excitatory amino acid transporter 1
EAAT2	Excitatory amino acid transporter 2

EGFP	Enhanced green fluorescence protein
eNMDAR	Extrasynaptic NMDA receptor
EPSP	Excitatory postsynaptic potentials
ER	Endoplasmic reticulum
FBS	Fetal bovine serum
fEPSP	Field excitatory postsynaptic potential
FRET	Fluorescence resonance energy transfer
GABA	Gamma-aminobutityric acid
GFAP	Glial fibrillary acidic protein
GLAST	Glutamate aspartate transporter
GLT-1	Glutamate transporter-1
GPCR	G-protein-coupled receptors
H_2O	Water
hGFAP	Human glial fibrillary acidic protein
IP3	Inositol (1,4,5)-triphosphate
IP_3R	Inositol (1,4,5)-triphosphate receptor
IP_3R2	Inositol (1,4,5)-triphosphate receptor type 2
ITI	Inter-trial interval
IZ	Intermediate zone
K^+	Potassium
KO	Knockout
LTP	Long term potentiation
Mg^{2+}	Magnesium
MWM	Morris water maze
mGluR	Metabotropic glutamate receptor
Na^+	Sodium
NFT	Neurofibrillary tangles
NMDA	N-methyl-D-aspartate
NMDAR	N-methyl-D-aspartate receptor
NOR	Novel Object Recognition test
OFT	Open Field Test
OLT	Object location task
PBS	Phosphate-buffered saline

PCR	Polymerase chain reaction
PHGDH	D-3-phosphoglycerate dehydrogenase
Phospho-tau	Phosphorylated tau
PIP2	Phosphatidylinositol 4,5-bisphosphate
PLC	Phospholipase C
PS1	Presenilin 1
PS2	Presenilin 2
PSFV	Presynaptic fiber volley
PZ	Peripheral zone
RT	Room temperature
sAPP	Soluble amyloid precursor protein
SDS-PAGE	Sodium dodecyl sulphate polyacrylamide gel electrophoresis
SNAP-23	Synaptosome-associated protein of 23 kDa
SNARE	Soluble N-ethyl maleimide-sensitive fusion protein attachment protein receptor
sNMDAR	Synaptic NMDA recetor
SR	Serine racemase
TAE	Tris-Acetate-EDTA
TBS-T	Tris-buffered saline with Tween® 20
tetO	Tetracycline operator
tTA	Tetracycline transactivator
VAMP2	vesicle-associated membrane protein 2
VAMP3	vesicle-associated membrane protein 3
YFP	Yellow fluorescent protein
Wt	Wild-type

Resumo

Apesar dos avanços no conhecimento dos mecanismos neurotóxicos e dos aspetos clínicos da doença de Alzheimer (AD), a sua etiologia permanece pouco clara. As espécies tóxicas do péptido β-amiloide (Aβ) desregulam a sinalização de Ca^{2+} nos astrócitos, levando a gliotransmissão anómala. Sabe-se que os gliotransmissores glutamato e D-serina ativam recetores NMDA (NMDARs), que são fundamentais na plasticidade sináptica (ex.: potenciação de longo prazo (LTP)) e na memória, podendo ser neuroprotetores (sinápticos, sNMDAR) ou iniciar vias de morte celular (extra-sinápticos, eNMDAR). Assim, levantámos a hipótese de que o Aβ: (1) exacerba a liberação de glutamato dos astrócitos, ativando excessivamente os eNMDAR e aumentando a excitabilidade neuronal e, concomitantemente, (2) diminui a liberação de D-serina, reduzindo a ativação dos sNMDAR, comprometendo a plasticidade sináptica com subsequente disfunção da memória. Assim, o nosso objetivo foi investigar como é que alterações na sinalização astrócitos-neurónios suprimem os mecanismos de plasticidade sináptica e contribuem para os déficits de memória observados na AD. Utilizamos murganhos transgénicos dn-SNARE, onde a gliotransmissão dependente de SNARE é seletivamente comprometida nos astrócitos. Para estudar a plasticidade sináptica, induzimos um protocolo de LTP nas fatias de hipocampo dos animais dn-SNARE e Wt incubadas com oligomeros $Aβ_{1-42}$ (200 nM) e/ou D-serina (10 µM). Em paralelo, injetamos no hipocampo de animais dn-SNARE e Wt vetores AAV que transportam a forma mutada da proteína precursora de amiloide humana (APP) e presenilina 1 (PS1), de modo a mimetizar o padrão de expressão da APP observado no hipocampo de pacientes com AD. Os animais foram submetidos a três testes de comportamento: *open field* (OFT) (locomoção, ansiedade e exploração), Y-maze de alternância espontânea (memória de trabalho espacial) e *Morris water maze* (MWM) (memória espacial e de longa duração). Adicionalmente, culturas primárias de astrócitos foram transfetadas com um biossensor de FRET para avaliar o impacto da presença de oligomeros de $Aβ_{1-42}$ (200 nM) na liberação de glutamato pelos astrócitos. O nosso trabalho mostra que: (1) o comprometimento da gliotransmissão recupera a inibição da LTP mediada pelos oligomeros de $Aβ_{1-42}$; (2) os astrócitos libertam mais glutamato na presença de oligomeros de $Aβ_{1-42}$; e (3) a D-serina promove a ativação dos sNMDAR e potencializa a indução de LTP, mesmo na presença de oligomeros de $Aβ_{1-42}$. Os resultados preliminares dos testes de comportamento sugerem que apenas no MWM o comprometimento da gliotransmissão parece melhorar os déficits de memória causados pelo processamento de APP. Os nossos resultados atribuem um papel central aos astrócitos na plasticidade sináptica e à disfunção de memória na AD, abrindo portas para abordagens e novos alvos terapêuticos para o tratamento da AD.

Abstract

Although new insight has been gained about the neurotoxic mechanisms and the clinical aspects of Alzheimer's disease (AD), the actual neuropathogenic processes remain unclear. Amyloid-β (Aβ) toxic species, an AD hallmark, induce an astrocytic Ca^{2+}-signaling dysregulation with consequent abnormal gliotransmission. Glutamate and D-serine gliotransmitters activate NMDA receptors (NMDARs), which play an important role in synaptic plasticity (eg: long-term potentiation (LTP)) and memory function, and can be neuroprotective (synaptic, sNMDAR) or initiate cell death pathways (extrasynaptic, eNMDAR). Thus, we hypothesize that Aβ: (1) exacerbates astrocytic glutamate release, excessively activating eNMDARs and increasing neuronal excitability; (2) and reduces D-serine release, poorly activating sNMDAR, which overall leads to the disruption of synaptic plasticity with subsequent memory impairment. Therefore, we aim to investigate how, in AD, changes in astrocyte-neuron signaling suppress synaptic plasticity mechanisms and contribute to memory deficits. To clarify this, we used dn-SNARE transgenic mice, where SNARE-dependent gliotransmission is selectively disrupted in astrocytes. To study synaptic plasticity, we induced an LTP protocol in hippocampal slices, from dn-SNARE and Wt animals, incubated with $A\beta_{1-42}$ oligomers (200 nM) and/or D-serine (10 µM). In parallel, we injected in the hippocampus of dn-SNARE and Wt mice AAV vectors carrying the mutated form of human amyloid precursor protein (APP) and presenilin 1 (PS1), to mimic the pattern of APP expression observed in the hippocampus of human AD patients. Then, the animals were submitted to the open field test (OFT) (locomotion, anxiety, and exploration), Y-maze spontaneous alternation (spatial working memory), and Morris water maze (MWM) (spatial and long-term memory). Additionally, primary astrocyte cultures were transfected with a FRET-glutamate biosensor, to evaluate the impact of $A\beta_{1-42}$ oligomers (200 nM) on glutamate release by astrocytes. Our work shows that the etiology and treatment of AD can be mechanistically linked via astrocytes since: (1) impairing gliotransmission restores LTP inhibition mediated by $A\beta_{1-42}$ oligomers; (2) astrocytes release more glutamate in the presence of $A\beta_{1-42}$ oligomers; (3) D-serine enhances sNMDAR activation and potentiates LTP induction, even in the presence of $A\beta_{1-42}$ oligomers. Besides, behavioral preliminary results suggest that AAV-APP/PS1 injection does not induce an alteration in OFT nor Y-maze test. However, in MWM, gliotransmission impairment seems to ameliorate memory deficits caused by AD-like APP processing, suggesting a role of astrocytes in memory decline in the early stage of AD. Together, our results place astrocyte at the central hub for synaptic plasticity and memory dysfunction in AD, opening the search for innovative approaches and targets for AD treatment.

1. Introduction

Astrocytes, the most abundant glial cell type in the central nervous system (CNS), for a long time were considered a non-excitable cell type that operated as a “glue”, providing only passive metabolic and mechanical support to adjacent neurons (Hu et al., 2016). However, much progress has been made in understanding the role of astrocytes in the maintenance of CNS homeostasis. Nowadays, it is known that astrocytes interact with neurons, by regulating the concentration and exchange of ions, H_2O, neurotransmitters, energy, and metabolic substrates, by controlling neurogenesis and synaptogenesis, and by being involved in the formation and maintenance of the brain-blood barrier (BBB) (Lanciotti et al., 2013). This led to the concept of the “tripartite synapse” that incorporated astrocytes as a third functional component of the synapse (Araque et al., 1999; Perea and Araque, 2009). The tripartite synapse concept considers that neurotransmitters released from neurons also bind receptors on the adjacent astrocytes, activating signaling pathways that induce an increase of the intracellular calcium (Ca^{2+}) levels in astrocytes, which in turn release gliotransmitters that modulate neuronal excitability and synaptic transmission. Moreover, there is an emerging conception of astrocytes contributing to neuropathological processes, either by loss or pathological modification of their function (Adamsky and Goshen, 2017). In Alzheimer's disease (AD), the formation of amyloid β-peptide (Aβ) induces a Ca^{2+}-signaling dysregulation in astrocytes, and consequent dysregulation of astrocytic gliotransmission (Chow et al., 2010; Kuchibhotla et al., 2009; Pillai and Nadkarni, 2019; Takano et al., 2007; Talantova et al., 2013). Knowing that Ca^{2+}-dependent release of gliotransmitters can occur in a SNARE-dependent manner, the main aim of this master thesis was to investigate how changes in SNARE-dependent gliotransmitter release from astrocytes contribute to AD-related molecular pathology and lead to aberrant synaptic signaling and deficits in learning and memory. Therefore, the following introduction addresses the main concepts: astrocytes, tripartite synapse, gliotransmission, synaptic plasticity, and AD pathology.

1.1. Astrocytes

1.1.1. Development of the astroglia concept

The concept “neuroglia” was introduced by Rudolf Virchow, in 1856, to refer to the “connective substance” in the brain, most likely without cellular content, that held neurons together (Virchow, 1856). Just over a decade later, the histological revolution occurred in 1873 when Camillo Golgi

developed the silver-chromate staining technique, which, for the first time, allowed neurophysiologists to appreciate the true structure of neurons (Golgi, 1873). Further, in 1893 the term “astrocyte”, which referred to the stellate morphology of these cells, was introduced by Michael von Lenhossek (Lenhossek, 1891).

The application of Golgi staining led to a characterization of astrocytes into two major morphological groups based on their morphology and anatomical location (Garwood et al., 2017): the protoplasmic astrocytes (Andriezen, 1893) of the grey matter and the fibrous astrocytes (Kölliker, 1889) of the white matter. Both types of astrocytes express the glial fibrillary acidic protein (GFAP), an intermediate filament protein classically used as a marker for astrocytes (Tabata, 2015). These studies were followed by Santiago Ramón y Cajal, who characterized astrocytes in brain tissue, and anticipated the idea of active neuronal-glial interactions as a substrate for brain function (Ramón y Cajal, 1913). Besides, over the years, several different types of astrocytes have been described: Bergmann glia, in the cerebellum, that extend long processes to enwrap and control Purkinje cells (Haim and Rowitch, 2016); Müller cells, involved in the development of the retina's architecture and circuitry (Willbold and Layer, 1998); protoplasmic velate astrocytes, that support granule cells in the cerebellum (Haim and Rowitch, 2016); and type B cells, that provide a neurogenic microenvironment for subventricular zone cells (Haim and Rowitch, 2016; Lim and Alvarez-Buylla, 1999). These different types of astrocytes display regional differences and/or specificities in terms of morphological and physiological properties, and protein expression patterns (Haim and Rowitch, 2016), highlighting the importance of astrocytic function in complex brain processing.

1.1.2. Electrophysiological properties

Unlike neurons, astrocytes are not electrically excitable, being unable to conduct action potentials. Thus, astrocytes were traditionally considered contributors to the structural organization of the brain (Oberheim et al., 2011). However, astrocytes are not electrically silent cells. They exhibit a chemically excitable system capable to maintain and modulate neuronal activity by sensing and responding to environmental signals (Guerra-Gomes et al., 2018). In addition, they also express voltage- and ligand-activated channels, allowing potassium (K^+), sodium (Na^+), Ca^{2+}, and chloride (Cl^-) ions to pass through the membrane, which was previously thought to be exclusive from neurons (Hu et al., 2016).

In 1990, Cornell-Bell and co-workers observed that cultured astrocytes could respond to glutamate by increasing cytoplasmic Ca^{2+} levels and initiate the propagation of a Ca^{2+} wave between adjacent cultured astrocytes (Cornell-Bell et al., 1990). These were the first indications that astrocyte networks could constitute a long-range signaling system within the brain. Nevertheless, it is now known that Ca^{2+} waves are implicated in gliotransmitter release and potentially play an important role in other astrocyte functions (Araque et al., 1999; Perea and Araque, 2009). The Ca^{2+} wave is a result of the inositol (1,4,5)-triphosphate (IP_3) receptors (IP_3R) activation, which leads to the release of internal stores of Ca^{2+}, that ultimately propagate to neighboring astrocytes through gap junctions mainly constituted by connexin 43 (Bender et al., 2016).

Astrocytes are also a critical determinant of other extracellular ions homeostasis, such as K^+. In fact, the ionic channel expression pattern of astrocytes is dominated by K^+ channels (Dallérac et al., 2013). One of the important roles of astrocytes is to uptake K^+ released by active neurons, by a process called "K^+ clearance". Extracellular K^+ is a major player in maintaining the resting membrane potential of neurons, meaning that even minor increases in the extracellular K^+ concentration can alter the probability of a neuron firing an action potential (Bellot-Saez et al., 2017). Defective extracellular K^+ clearance mechanisms have been associated with several neurological diseases, including AD. This was validated by Vitvitsky and colleagues, that demonstrated, by the analysis of postmortem brain samples of individuals with and without AD, that Aβ-induced astrocytic Na^+ and K^+ imbalances (Vitvitsky et al., 2012), highlighting the role of astrocytes in preventing extracellular K^+ levels from reaching a toxic concentration. Thereby, astrocytes exhibit functional electrical properties sensitive to neuronal activity and are capable of modulating neurotransmission.

1.1.3. Functions

The traditional view of astrocytes as simple supportive cells for neurons is being replaced by a new vision in which astrocytes play a wide range of functions for the regulation of the brain network. Due to their distribution in the CNS, and to the structural and biochemical features, astrocytes sense and dynamically respond to changes in the microenvironment (Lanciotti et al., 2013).

Astrocytes' participate in the arrangement of some functional structures, as is the case of the BBB (Gordon et al., 2007) and gap junctions, by which astrocytes are interconnected, forming an astrocyte-astrocyte syncytium, for the exchange of small molecules and ions (Lanciotti et al., 2013),

or to modulate the activity of adjacent oligodendrocytes and neurons (Verkhratsky et al., 2014). Moreover, astrocytes also form the tripartite synapse with neurons, which provides the proper structural and functional conditions for neuron-astrocyte communication (Araque et al., 1998b, 1999), contributing to cognitive functions and behavior (Halassa et al., 2009; Sardinha et al., 2017).

Astrocytes contribute to the regulation of the neuronal microenvironment through tight control of local ion and transmitters concentrations. They are responsible for the clearance and recycling of neurotransmitters and metabolism-derived products from the synapse (Verkhratsky et al., 2014). For instance, glutamate, the major excitatory neurotransmitter in the CNS involved in synaptic transmission and plasticity, is removed from the synaptic cleft primarily via glutamate transporters GLT-1 (glutamate transporter-1 also called excitatory amino acid transporter 2 or EAAT2), and GLAST (glutamate aspartate transporter also known as excitatory amino acid transporter 1 or EAAT1), which are mainly expressed in the astrocytic membrane (Bender et al., 2016). Thus, astrocytes protect neurons from glutamate-mediated excitotoxicity, by maintaining low extracellular glutamate concentrations (Lanciotti et al., 2013). Although both neurons and astrocytes express glutamate transporters, glutamate uptake is predominantly performed by astrocytes (Rothstein et al., 1996). After being uptaked by astrocytes, glutamate is converted into glutamine by the astrocyte-specific enzyme glutamine synthetase (Lanciotti et al., 2013). Glutamine is then released back in the extracellular space to be uptaken by adjacent neurons, where it is converted to glutamate and gamma-aminobutyric acid (GABA), the principal inhibitory neurotransmitter in the CNS (Verkhratsky et al., 2014). In addition, astrocytes provide metabolic support to brain activity by taking up glucose, the only glutamate precursor that crosses the BBB in sufficient quantities, from the blood circulation, via glucose transporters, where it can either be stored as glycogen or metabolized in the glycolytic pathway to be delivered to neurons (Lanciotti et al., 2013).

Astrocytes also influence myelination by releasing cytokines and growth factors that affect oligodendrocyte progenitor proliferation and differentiation, or by secreting regulatory proteins that promote the myelinating activity of oligodendrocytes. For example, Alexander's disease, a leukodystrophy characterized by myelin degeneration, is a consequence of a mutation in the GFAP gene, which leads to astrocyte dysfunction, demonstrating that astrocyte development and normal white matter function are correlated (Molofsky et al., 2012).

Lastly, by their intimate relationship with neurons, astrocytes modulate neuronal function and information processing, playing a vital role in the coordination of synaptic networks. As a response

to the neurotransmitters released by neurons, astrocytes may release transmitters termed gliotransmitters, including glutamate, D-serine, adenosine triphosphate (ATP), adenosine, and GABA, mainly through Ca^{2+}-dependent vesicular release. In turn, the gliotransmitters can affect neuronal activity, by binding to their respective receptors on neurons, modulating their firing frequency and synaptic transmission (Bender et al., 2016; Halassa et al., 2009).

1.2. The Tripartite Synapse

The revaluation of the "astroglia" term started with the "tripartite synapse" concept, proposed by Araque and colleges in 1999, which incorporated the astrocytes as the third functional component of the synapse, demonstrating the existence of bidirectional communication between astrocytes and neurons (Araque et al., 1999). This concept is based on the ability of astrocytes to sense neurotransmitters released during neuronal activity and respond to them, by releasing gliotransmitters that modulate synaptic function (Perea and Araque, 2009).

1.2.1. Ca^{2+}-dependent gliotransmission

Astrocytic gliotransmitters are released mainly by Ca^{2+}-dependent exocytosis via vesicular mechanisms (Santello et al., 2012), but also through non-exocytotic mechanisms, such as anion channels, functional unpaired connexons hemichannels/connexins, purinergic receptors, reversal of uptake by amino acid transporters, and by exchange via the cystine-glutamate antiporter (Malarkey and Parpura, 2008; Santello et al., 2012). However, the Ca^{2+}-dependent exocytotic vesicular is the most extensively studied and the best characterized up to date (Santello et al., 2012).

Astrocytes express receptors, that are mainly G-protein-coupled receptors (GPCRs) from Gq subtype, that sense the neurotransmitters and neuromodulators released from the presynaptic neuron (Agulhon et al., 2008; Perea and Araque, 2009; Santello et al., 2012). This process results in both postsynaptic neuronal membrane and perisynaptic astrocytic membrane activation, ultimately leading to the generation of a postsynaptic potential in the neuron, and an increase in intracellular Ca^{2+} levels in the astrocyte (Figure 1) (Agulhon et al., 2008; Santello et al., 2012). The astrocytic Ca^{2+} is released from intracellular stores via stimulation of GPCR-Gq that activates phospholipase C (PLC), which then hydrolyzes the membrane lipid phosphatidylinositol 4,5-bisphosphate (PIP2) to generate diacylglycerol and IP_3 (Figure 1) (Agulhon et al., 2008). In turn, IP_3 activates IP_3R, which leads to Ca^{2+}

release from the endoplasmic reticulum (ER) with the subsequent release of gliotransmitters, including excitatory and inhibitory amino acids (D-serine, glutamate, aspartate, GABA and glycine), ATP, and related nucleotides and nucleosides, eicosanoids and other lipid mediators, neuropeptides, neurotrophins (nerve growth factor and brain-derived neurotrophic factor, cytokines (interleukins, interferons, and tumor necrosis factors alpha, and growth factors (Figure 1) (Agulhon et al., 2008; Santello et al., 2012). Interestingly, astrocytes lacking the astrocyte-specific IP_3R, the IP_3R type 2 (IP_3R2) are unable of releasing Ca^{2+} from internal stores either spontaneously or in response to agonists of Gq-coupled GPCRs (Petravicz et al., 2008), evidencing that IP_3R2 is the primary functional IP_3R in astrocytes. A recent study suggested that mice lacking IP_3R2 exhibited remote and spatial memory deficits, and abnormalities in the process of selectively weakening specific sets of synapses (Pinto-Duarte et al., 2019). In the same paper, the authors demonstrated that these deficits could be prevented by supplementation with D-serine (Pinto-Duarte et al., 2019), confirming the key roles of astrocytic Ca^{2+} signals on neural circuits function and cognitive behavior.

Ca^{2+}-mediated gliotransmission comprises the release of vesicles containing gliotransmitters via exocytosis. Astrocytes express the protein machinery involved in vesicle fusion essential for soluble N-ethyl maleimide-sensitive fusion protein attachment protein receptor (SNARE) complex formation, including vesicle-associated membrane protein 2 (VAMP2), also referred to as synaptobrevin II or its homolog cellubrevin (VAMP3), syntaxin 1, synaptosome-associated protein of 23 kDa (SNAP-23), as well as several auxiliary proteins to this complex, such as synaptotagmin (Figure 1) (González-arias and Perea, 2019; Parpura and Zorec, 2010).

In the dn-SNARE mouse model, used to study the implication of astrocytic signaling (Pascual et al., 2005), the expression of the cytoplasmic domain of synaptobrevin II selectively in astrocytes, which acted as a dominant-negative SNARE (dn-SNARE) (Pascual et al., 2005), resulted in a reduction of glutamate (Zhang et al., 2004), ATP (Pankratov and Lalo, 2015), and D-serine (Pankratov and Lalo, 2015) release from astrocytes. Besides, through the generation of the dn-SNARE mouse model, Philip Haydon and his team showed that the magnitude of theta-burst long-term potentiation (LTP) was smaller in dn-SNARE animals in comparison to wild-type (Wt) (Pascual et al., 2005). Even though the model validity was questioned (Fujita et al., 2014), further studies have shown that it is a reliable model to dissect the role of gliotransmitter release (Lalo et al., 2021b; Pascual et al., 2005; Sardinha et al., 2017; Sultan et al., 2015)(Sardinha et al., 2017).

Once released, gliotransmitters feedback on neurons (Figure 1) to inhibit or enhance neuronal activity and, thereby, modify synaptic plasticity and subsequent behavior (Allen and Barres, 2009; Araque et al., 1999; Perea et al., 2009; Santello et al., 2019). Altogether these studies demonstrate that astrocytes express proteins necessary for gliotransmitters release through a vesicle-related mechanism that modulates synaptic plasticity.

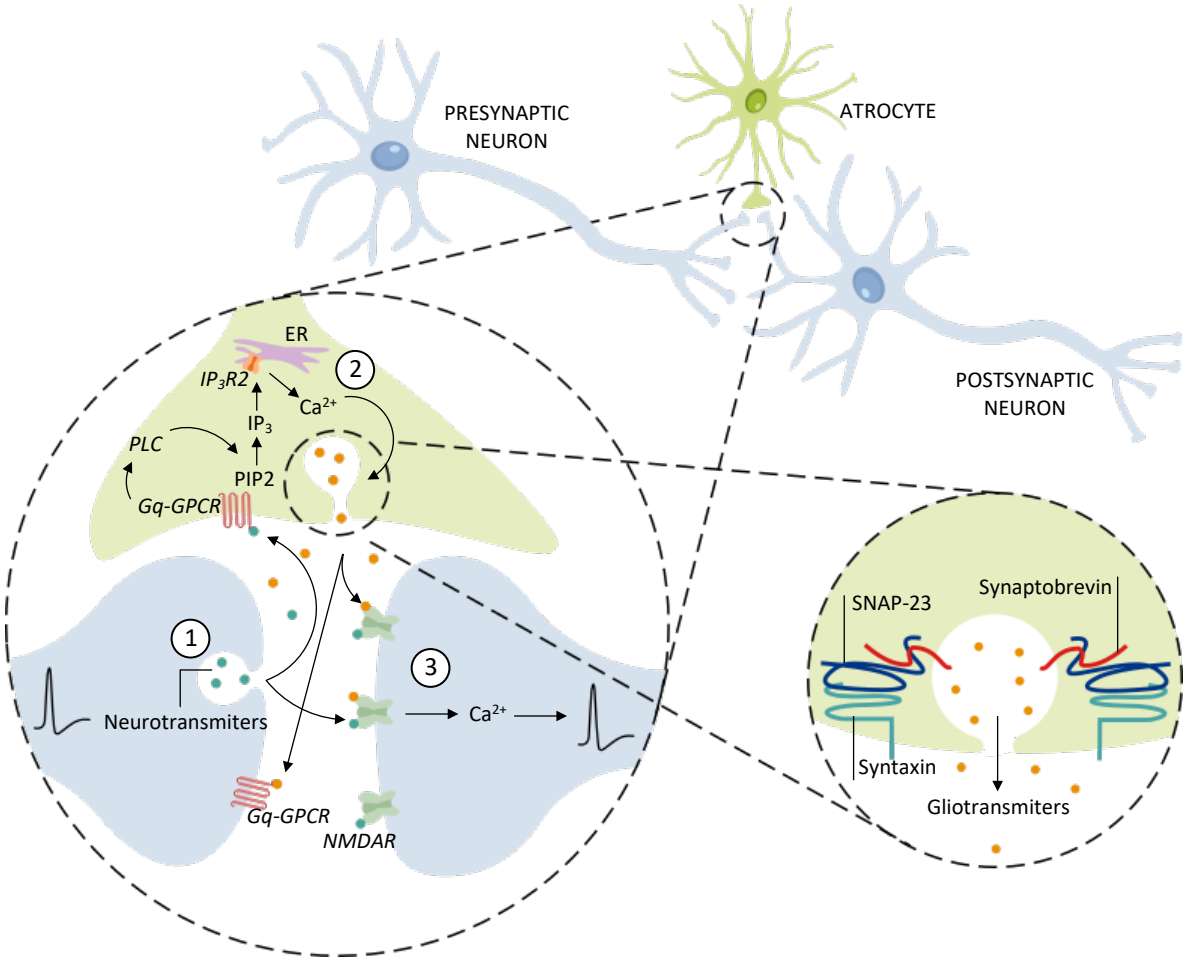

Figure 1: Scheme of the tripartite synapse and Ca^{2+}-dependent gliotransmission. 1. The release of neurotransmitters upon neuronal stimulation will activate astrocytic Gq-GPCR coupled to PLC. **2.** With Gq stimulation, PLC is activated to cleave the PIP2 into IP_3. The IP_3 originated binds to IP_3R2 in the ER, triggering the release of Ca^{2+} from intracellular stores. In turn, this transient increase in intracellular Ca^{2+} mediates the release of gliotransmitters contained in synaptic-like vesicles, through the formation of a SNARE complex between vesicle SNARE (synaptobrevin) and astrocyte membrane SNAREs (syntaxin and SNAP-23). **3.** The released gliotransmitters act on presynaptic and postsynaptic receptors, modulating neuronal excitability and synaptic transmission. ER: Endoplasmic reticulum. IP_3: Inositol (1,4,5)-triphosphate Gq-GPCR: Gq-protein coupled receptors. IP_3R2: Inositol (1,4,5)-triphosphate receptor type 2. PLC: Phospholipase C.

1.2.2. Gliotransmitters

Astrocytes arise as key modulators and mediators of synaptic neurotransmission and plasticity, by releasing gliotransmitters as a response to the neurotransmitters released during synaptic activity (Perea and Araque, 2009). For the purpose of this thesis, only glutamate and D-serine gliotransmitters will be explained in detail.

1.2.2.1. Glutamate

Glutamate, the principal excitatory neurotransmitter in the brain, is functionally involved in the regulation of synaptic plasticity, particularly the LTP (Hu et al., 2016). By controlling the balance between glutamate uptake and release (Figure 2), astrocytes can maintain glutamate homeostasis, support normal neuronal function, and protect against glutamate excitotoxicity (Mahmoud et al., 2019). Like in neurons, glutamate receptors present on astrocytes include metabotropic glutamate receptors (mGluR) and the three classes of ionotropic receptors: α-amino-3-hydroxy-5-methyl-4-isoxazolepropionic acid (AMPA) receptors (AMPAR), kainic acid receptors, and N-methyl-D-aspartate (NMDA) receptors (NMDAR) (Skowrońska et al., 2019). When glutamate is released from excitatory neurons (Figure 2), it activates type 1 and 5 mGluRs in astrocytes, causing an elevation of the astrocytic intracellular Ca^{2+}, which in turn triggers glutamate release from astrocytes (Mahmoud et al., 2019). Astrocytes can release glutamate via various routes to modulate synaptic transmission (Figure 2), including: (A) Ca^{2+}-mediated exocytosis (Chapter 1.2.1.); (B) Ca^{2+}-activated anion channels that are permeable to glutamate and open upon activation of a Gq-coupled GPCR; (C) diffusion through purinergic receptors where glutamate is released in exchange with the uptake of ATP; (D) cystine/glutamate antiporters that allow glutamate release in exchange of cystine uptake; (E) reversal of glutamate uptake transporters, whereby glutamate uptake transporters in astrocytes can reverse and start to release glutamate in a Ca^{2+}-independent mechanism (most likely in pathological conditions); and by (F) gap junctions hemichannels, in which connexin and pannexin proteins that form the gap junctions between astrocytes and hemichannels that allow the passage of glutamate from the cytoplasm of astrocytes to the extracellular space (Araque et al., 1999; Mahmoud et al., 2019; Malarkey and Parpura, 2008; Park et al., 2009; Parpura and Zorec, 2010). Then, astrocytic glutamate can modulate synaptic transmission by activating NMDARs (Angulo et al., 2004) and/or non-NMDAR (Araque et al., 1998a), such as presynaptic mGluRs (Araque et al., 1998a; Perea and Araque, 2007). Coriously, GABA release from interneurons activates GABA-

receptors in astrocytes and induces a rise in their intracellular Ca^{2+} levels, which in turn triggers glutamate release that contributes to the potentiation of inhibitory synaptic transmission (Kang et al., 1998). Therefore, glutamate released by astrocytes is directly involved in synaptic transmission and plasticity.

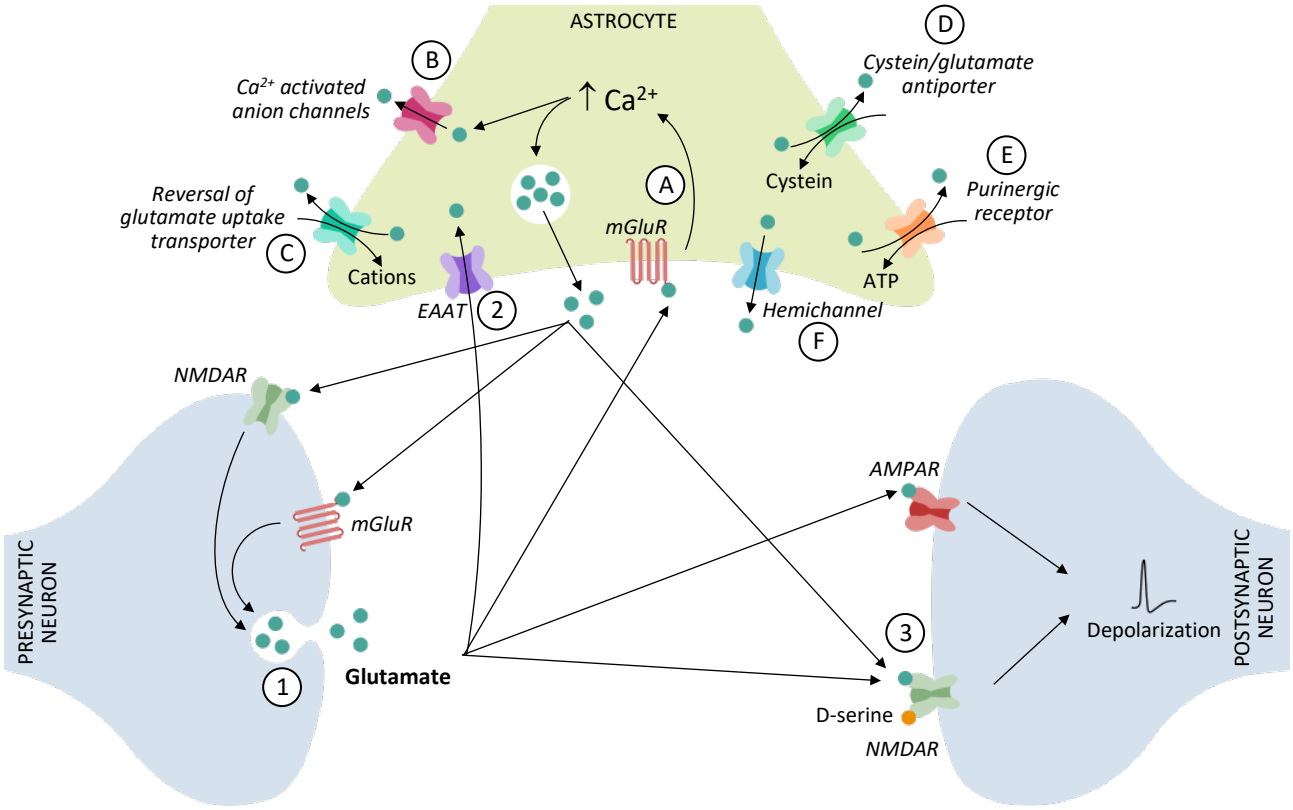

Figure 2: Mechanisms of glutamate release from astrocytes. 1. After the release of glutamate (green circle) from the presynaptic neurons, some glutamate activates NMDARs and AMPARs of the adjacent postsynaptic neuron to transmit excitatory impulses, while the majority of glutamate is captured by astrocytes via their glutamate uptake transporters EAAT (**2**), which are expressed on the surface of the astrocytic peri-synaptic processes. Astrocytes have a wide variety of glutamate release mechanisms: **A.** Ca^{2+}-mediated exocytosis (elevations of astrocyte intracellular Ca^{2+} evoked by Gq-coupled GPCRs like mGluR activation); **B.** Ca^{2+} activated anion channels (stimulation of GPCRs in astrocytes increases intracellular Ca^{2+}); **C.** Reversal of uptake transporters (in cases of severe ischemia or stroke); **D.** Cystine/glutamate antiporters (exchange with cystine uptake); **E.** Purinergic receptor (exchange with the uptake of ATP); **F.** Hemichannels (gap junction channels that allow the passage from the cytoplasm to the extracellular space). **3.** Then, glutamate released from astrocytes stimulates neuronal presynaptic group mGluRs or NMDAR, inducing more glutamate release from presynaptic neurons. Astrocytic glutamate also acts on postsynaptic neurons to activate, in conjugation with D-serine (orange circle), NMDAR-dependent synaptic plasticity mechanisms. ATP: Adenosine triphosphate. EAAT: Excitatory amino acid transporter 2. mGluR: Metabotropic glutamate receptor

Under physiological conditions, the concentration of glutamate in the extracellular space must be maintained very low to prevent excessive stimulation of glutamate receptors and subsequent neuronal excitotoxicity (Armada-Moreira et al., 2020; Gonçalves-Ribeiro et al., 2019; Mahmoud et al., 2019). In fact, many CNS disorders are characterized by the loss of glutamate uptake by astrocytes, as is the case of traumatic brain injury (Landeghem et al., 2006), Huntington's disease (Hassel et al., 2008), amyotrophic lateral sclerosis (Vaz et al., 2021), and AD (González-Reyes et al., 2017), where patients exhibit a reduction in EAAT2, associated with accumulation of extracellular glutamate. This impairment in the synaptic clearance of glutamate, together with the excessive release, can further contribute to the increase in extracellular glutamate concentration. This glutamate will then overstimulate NMDA, AMPA, and kainic acid receptors, inducing an excessive intracellular Ca^{2+} influx in neurons and initiating intracellular cascades, leading to apoptotic neuronal loss (Armada-Moreira et al., 2020). These excitotoxic mechanisms have been implicated in neurodegenerative disease, including Parkinson's disease (Trudler et al., 2021) and AD (Talantova et al., 2013), in which Ca^{2+}-dependent release of glutamate from astrocytes activates glutamate receptors, including extrasynaptic NMDARs (eNMDARs) on neurons, that will enhance cell death pathways and consequently reduce neuronal survival (Armada-Moreira et al., 2020). Overall these studies suggest that dysregulated glutamate uptake and release by astrocytes contributes to the development of psychiatric disorders, neuronal dysfunction, and neurodegeneration.

1.2.2.2. D-serine

In the 1990s, Hashimoto group detected for the first time the presence of D-serine in rodents and humans' brains, especially enriched in regions close to the NMDARs, which suggested an influence on neurotransmission and related processes (Hashimoto et al., 1993b, 1993a, 1992). The first evidence for the role of D-serine as an NMDAR co-agonist was made by Mothet and collaborators, by using D-amino acid oxidase (DAAO) to deplete D-serine from cultured neurons and brain slices, and the results pointed that the removal of D-serine reduces NMDAR-mediated transmission, while exogenous applications allow complete recovery (Mothet et al., 2000). Accordingly, D-serine is now accepted as a co-agonist of NMDAR, acting on GluN1/GluN2A subunits-containing NMDARs for its full activation (Coyle et al., 2020; Martineau et al., 2014). However, the primary site of D-serine synthesis and release remains controversial.

D-serine is synthesized from L-serine by the enzyme serine racemase (SR), which is expressed in both neurons and astrocytes (Williams et al., 2006). An initial study generated mice with a conditional deletion of D-3-phosphoglycerate dehydrogenase (PHGDH), the enzyme necessary for L-serine synthesis that is expressed exclusively in astrocytes, and demonstrated that both L- and D-serine levels were decreased in the cerebral cortex and hippocampus in the absence of L-serine (Yang et al., 2010), highlighting that L-serine is a key factor for maintaining D-serine levels in the brain and that astrocytes are the primary source of L-serine for D-serine synthesis. Additionally, by using conditional cell-specific SR-knockout (KO) mice, the deletion of neuronal SR reduced by ~70% LTP formation at *Cornu Ammonis* 3 (CA3)-*Cornu Ammonis* 1 (CA1) synapses, while deletion of SR in astrocytes had no impact on LTP induction (Benneyworth et al., 2012), suggesting that SR is predominant in neuronal populations, and not in astrocytes. Remarkably, Henneberger and colleagues, by using hippocampal slices, provided evidence that astrocytic D-serine release relies on Ca^{2+}-dependent exocytosis (Henneberger et al., 2010). By clamping intracellular Ca^{2+} in the astrocytes at *Schaffer collateral*-CA1 synapses, LTP was abolished, an effect that was rescued by the administration of D-serine (Henneberger et al., 2010), emphasizing the important contribution of D-serine for LTP establishment.

Nonetheless, although neurons are the major producers of D-serine in the brain, astrocytic D-serine is more abundant than neuronal D-serine in most brain regions (Martineau et al., 2014, 2013; Williams et al., 2006). To explain the opposing localizations of SR and D-serine, Wolosker proposed the “Serine shuttle” hypothesis (Figure 3) that illustrates the main mechanisms regulating SR activity and D-serine dynamics in the brain (Wolosker, 2011). Briefly, astrocytes are the primary and only source of *de novo* L-serine needed for D-serine production, since astrocytes express PHGDH, the key enzyme that catalyzes the formation of L-serine from glucose (Ivanov and Mothet, 2019; Martineau et al., 2014; Wolosker, 2011) (Figure 3). Then, L-serine initially produced in astrocytes shuttles to neurons via the astrocytic alanine/serine/cysteine/threonine transporter (ASCT), where is captured by the neuronal alanine/serine/cysteine transporter 1 (Asc-1) (Wolosker, 2011) (Figure 3). Once L-serine gets into neurons, SR uses L-serine to produce D-serine, pyruvate, and ammonia by an α,β-elimination reaction (Wolosker, 2011) (Figure 3). However, SR α,β-elimination activity can also act on D-serine, in which part of D-serine synthesized by SR is converted to pyruvate and ammonia, limiting the D-serine concentration in neurons (Foltyn et al., 2005). Afterward, D-serine produced in neurons is released and can be subsequently taken up by astrocytes, where it is stored (Wolosker,

2011) (Figure 3). Neuronal D-serine is mainly released in response to depolarization, while astrocytes release D-serine mainly through Ca^{2+}- and SNARE-dependent exocytosis (Martineau et al., 2014). Therefore, Wolosker hypothesis proposes that the higher content of D-serine in astrocytes is related to their low SR expression, which prevents D-serine metabolism via α,β-elimination (Martineau et al., 2014; Wolosker, 2011). This is supported by a study that showed a decrease in NMDAR activation by using fluoroacetate, a glial toxin that prevents the release of gliotransmitters (Le Bail et al., 2015). This effect could be reverted by the perfusion of L-serine (Le Bail et al., 2015), providing evidence that the removal of glial coverage decreases the metabolic support of L-serine to neurons for the service of synthesizing D-serine, leading to reduced D-serine synthesis and consequently affecting synaptic transmission. Moreover, Neame and collaborators reported that inhibition of astrocytic PHGDH suppresses the *de novo* synthesis of L-and D-serine and reduces the NMDAR synaptic potentials and LTP at the *Schaffer collateral*-CA1 synapse (Neame et al., 2019), supporting the serine shuttle mechanism between astrocytes and neurons in generating the NMDAR co-agonist D-serine. Additionally, deletion of SR in glutamatergic neurons abolished D-serine synthesis similarly to PHGDH inhibition, suggesting that neurons are the predominant manufacturers of the newly synthesized D-serine (Neame et al., 2019). Lastly, PHGDH-derived glycine regulates D-serine by tonic inhibition of SR, and by promoting D-serine release through the Asc-1 transporter, playing a role in the activation of synaptic NMDARs (Neame et al., 2019). These results suggest that most of the D-serine is of neuronal origin and its production depends on both the astrocytic L-serine export and the intracellular levels of glycine.

Moreover, abnormal levels of D-serine have been reported in different brain disorders and neurodegeneration. For instance, in the blood, CSF, and postmortem brain tissue of patients with schizophrenia, a psychiatric disorder linked to NMDAR hypofunction, was found diminished D-serine levels accompanied by higher DAAO activity (the enzyme that degrades D-serine) (Guercio and Panizzutti, 2018; Wolosker, 2018). Mutation in DAAO is associated with familial amyotrophic lateral sclerosis, which deregulates D-serine metabolism, increasing D-serine levels and potentiating excitotoxic effects mediated through the NMDAR activation, ultimately leading to neurodegeneration of motor neurons (Kondori et al., 2018). Nevertheless, there is no consensus on the involvement of D-serine in AD. Madeira *et al*. have reported that AD patients have increased levels of D-serine in the CSF and some brain regions, due to the action of soluble Aβ oligomers, and that D-serine levels are correlated with memory impairments (Madeira et al., 2015). Moreover, a

meta-analysis concluded that D-serine levels in the serum and CSF in patients with AD were significantly higher than those in the control groups (Chang et al., 2020). Contrary, a recent study revealed no significant alterations in serum and CSF concentrations of D-serine in AD patients throughout AD progression, compared to non-demented controls (Nuzzo et al., 2020). Overall, these findings indicate that dysregulation of the serine shuttle can be implicated in neuronal disorders, opening doors for new strategies to restore D-serine homeostasis in these conditions.

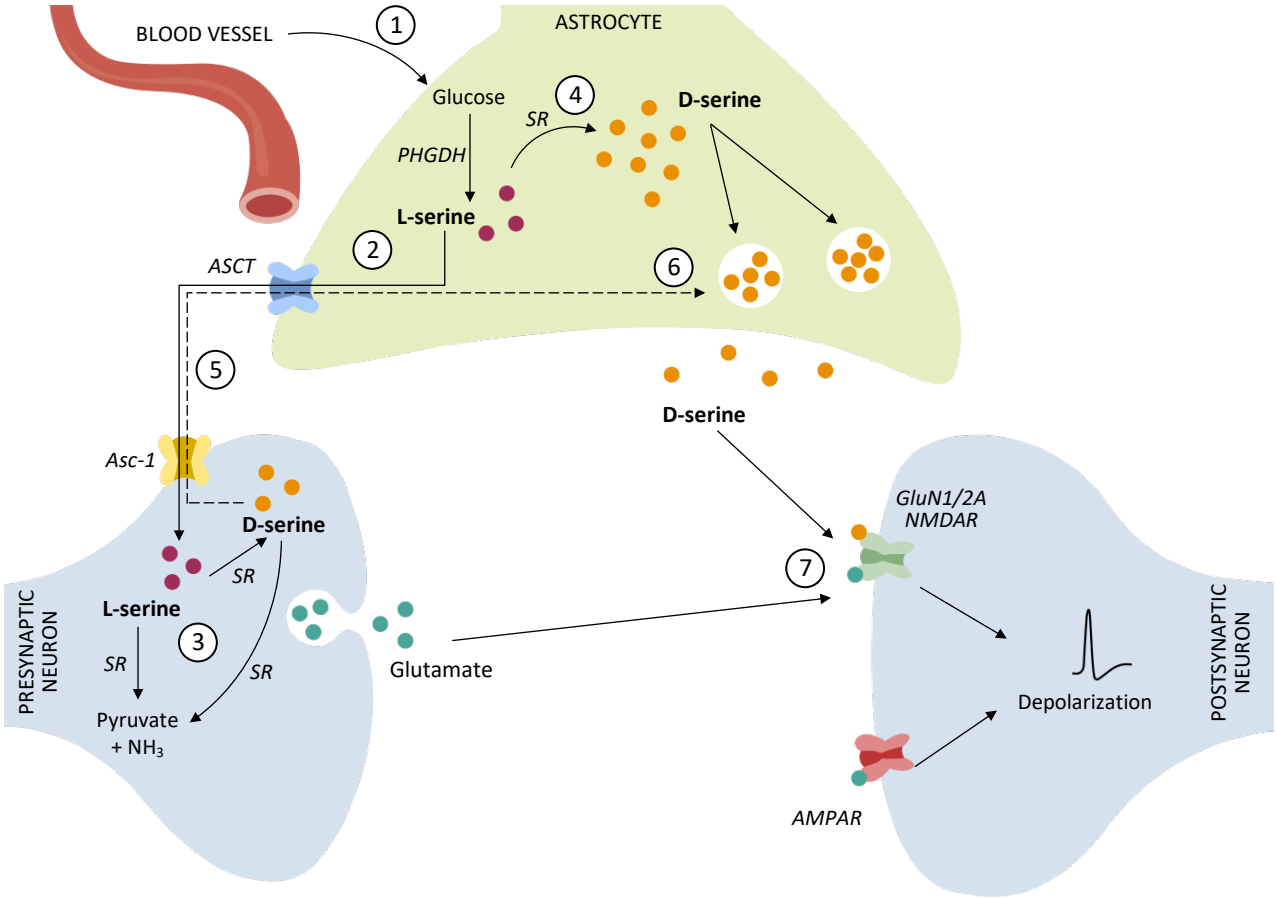

Figure 3: Serine shuttle pathway between neurons and astrocytes. 1. L-Serine is mostly synthesized from glucose in astrocytes by the PHGDH enzyme. **2.** Subsequently, L-serine is released from astrocytes (continuous line) by the ASCT and is then taken up into neurons via Asc-1 transporter. **3.** Neuronal SR produces D-serine, pyruvate, and ammonia by α,β-elimination. SR also degrade D-serine itself, limiting the accumulation of D-serine in neurons. A similar process also happens inside astrocytes (**4**). **5.** Then, D-serine is delivered back to the extracellular space (dashed line) through Asc-1, where it acts directly on NMDAR, or can shuttle again into astrocytes, where it accumulates in glial vesicles (**6**). Neuronal D-serine release occurs following depolarization, while astrocytic D-serine release mainly occurs through exocytosis (dependent on an increase in cytosolic Ca^{2+} and on SNARE proteins). **7.** Once in the synaptic cleft, D-serine binds to synaptic NMDAR-containing GluN1/GluN2A subunits, where it promotes functional plasticity at synapses or neurotoxicity in pathological conditions. Asc-1: ASCT: alanine/serine/cysteine transporter 1 Alanine/serine/cysteine/threonine transporter. PHGDH: D-3-phosphoglycerate dehydrogenase. SR: Serine racemase

1.3. Synaptic plasticity, memory, and the hippocampus

1.3.1. Patient H.M and the history of memory

The hippocampus, located in the inferior temporal lobe, is responsible for the formation and storage of memory, and it's one of the most studied areas in the mammalian CNS (Vago et al., 2014). Its role in memory was partially determined by studying patient H.M., who had both sides of his hippocampus removed in an attempt to cure his epilepsy (Scoville and Milner, 1957). Following surgery, H.M seizures disappeared and he presented normal intelligence quotient and short-term memory, but could no longer encode new information into long-term memory (Vago et al., 2014). However, he could acquire a new skill (procedural tasks), showing improvement across trials, without any memory of having encountered the task before (Vago et al., 2014), suggesting for the first time the existence of implicit and explicit learning abilities. Nonetheless, he could remember events that occurred before the surgery, which advocated that the hippocampal region is an important player in memory encoding and to form stable and long-term memories, but might not be the final repository for these memories (Vago et al., 2014).

1.3.2. Hippocampal anatomy

The hippocampus (Figure 4) is a structure that includes the dentate gyrus (DG), comprised of granule cells, and CA3 and CA1 areas, containing pyramidal neurons (Temido-Ferreira et al., 2019). In the principal feed-forward circuit involved in the process of information, the hippocampus receives unidirectional input from layer II perforant neurons of the entorhinal cortex, that enter the DG, and make excitatory synaptic contact with the dendrites of granule cells (Neves et al., 2008) (Figure 4). Then, the granule cells of the DG project their axons (mossy fibers) to the dendrites of CA3 pyramidal cells . After, the axons from the CA3 pyramidal neurons (*Schaffer collaterals*) and CA2 axons project to the *stratum radiatum* to synapse with CA1 pyramidal cells (Temido-Ferreira et al., 2019). The *stratum pyramidale* layer contains the cell bodies of the excitatory pyramidal neurons, while the *stratum radiatum* layer contains the axons from the *Schaffer collaterals* projections (Temido-Ferreira et al., 2019). The most well-characterized and well-studied glutamatergic synapse of the hippocampus is the *Schaffer collaterals*-CA1 synapse (Temido-Ferreira et al., 2019).

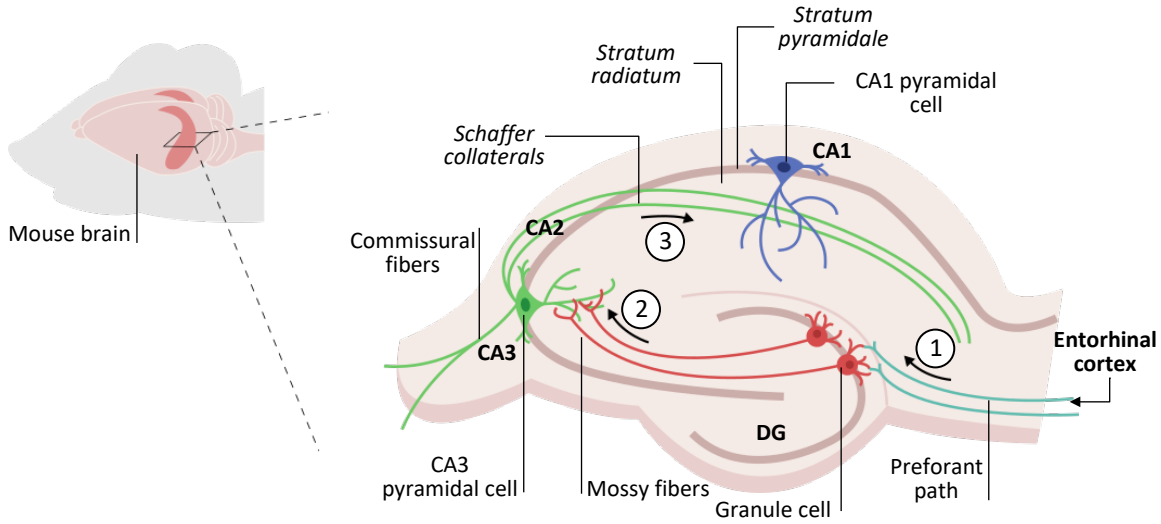

Figure 4: Schematics of the hippocampal neuronal circuitry. 1. Neuronal afferents inputs originating from the entorhinal cortex project through the perforant pathway to the granule cells of the DG which, in turn, (**2**) project via mossy fibers to CA3 pyramidal cells. **3.** Then, CA3 pyramidal cells project via the *Schaffer collaterals* to CA1 pyramidal cells. Axons from CA1 then project back to the entorhinal cortex, completing the circuit. CA1: Cornu Ammonis 1. CA3: Cornu Ammonis 1. DG: Dentate gyrus

1.3.3. Synaptic plasticity

In the late 1940s, Donald Hebb postulated that synaptic connections are the basis of mental associations (Hebb, 1949). Hebb proposed that "cells that fire together wire together", which means that associative memories are formed in the brain by coincident presynaptic and postsynaptic activity, which results in strengthening of the synaptic connection between the pre- and postsynaptic neuron (Bliss et al., 2018; Hebb, 1949). However, it was not until the early 1970s that experimental evidence for the existence of this activity-dependent change in synaptic strength was published. Bliss and Lømo observed in electrophysiological studies that repetitive trains of stimuli in the perforant path induced long-lasting excitatory postsynaptic potentials (EPSP) that increased the efficiency of transmission at synapses on DG granule cells (Bliss and Lømo, 1973), a plastic process that is now recognized as LTP. Briefly, LTP is the mechanism in which connections between co-active neurons are strengthened by specific patterns of stimulation, such as high-frequency stimulation or theta (θ)-bust stimulation, so that subsequent activation by incoming stimulation of only a part of the assembly can lead to activation of the whole assembly, thereby recapitulating the activity elicited by the original event (Neves et al., 2008). Besides, the θ-burst patterned neural activity is characteristic of the spike trains of CA1 pyramidal neurons during spatial learning tasks

and, in contrast, θ-bursting occurs relatively infrequently during behavioral events less directly related to learning (Otto et al., 1991). LTP is characterized by three properties: 1. Cooperativity: LTP can only be induced by the coincident activation of a critical number of synapses; 2. Input specificity: specific synapses are activated; and 3. Associativity: the simultaneous activation of two separate inputs, one of which is weak and fails to undergo LTP on its own, when tetanized together with a strong input exhibit LTP (Citri and Malenka, 2008). The diversity of synaptic plasticity mechanisms is expanded by the existence of long-term depression (LTD), the opposing process to LTP (Bliss et al., 2018). LTD reflects a long-lasting decrease in the efficiency of synaptic transmission following a continuous low-frequency stimulation, that might serve as a learning mechanism, or a process of ensuring homeostatic stability, by preventing an increase in overall activity in potentiated networks, thus controlling synaptic plasticity (Neves et al., 2008; Temido-Ferreira et al., 2019). To summarize, synaptic plasticity is the experience-mediated structural and functional changes in the connections between neurons, which results in changes to neural circuits (Ota et al., 2013).

This experience-dependent synaptic change has been widely studied due to its role in mechanisms of learning and memory storage. The initial evidence suggestive of a link between LTP and memory emerged from the work of Barnes, which demonstrated that rats with the most durable LTP in a given age group tended to show the best spatial learning (Barnes, 2003, 1979). Also, a faster decay of LTP is associated with behavioral forgetting in young and old animals, highlighting the importance of LTP for sustaining a memory (Barnes, 2003, 1979). In addition, Nabavi and co-workers provided compelling evidence for a role in learning and memory, by demonstrating that a certain memory can be inactivated and reactivated with LTD and LTP, respectively (Nabavi et al., 2014).

1.3.4. NMDAR-dependent LTP

LTP in the hippocampal CA1 region, broadly representative of LTP at excitatory synapses, is dependent on NMDAR activation and primarily involves a postsynaptic modification (Citri and Malenka, 2008). The NMDAR is a type of glutamate receptor permeable to Ca^{2+} ions, in which the channel is blocked by magnesium (Mg^{2+}) at resting membrane potential (Bliss et al., 2018) (Figure 5). During synaptic transmission, the presynaptic neuron releases glutamate that binds to both the NMDAR and AMPARs. Then, Na^{+} flows through the AMPAR channel but not through the NMDAR channel because of the presence of Mg^{2+} (Citri and Malenka, 2008). Periods of high-frequency stimulation will activate AMPAR and initiate the influx of Na^{+} that depolarizes the postsynaptic

neuron (Citri and Malenka, 2008) (Figure 5). Simultaneously, the presynaptically released glutamate bind and activate the astrocytic mGluRs on astrocyte processes enveloping synapses, leading to an intercellular Ca^{2+} wave propagation that triggers exocytosis of the D-serine containing synaptic-like vesicles (Agulhon et al., 2012). After, due to strong membrane depolarization, the Mg^{2+} withdraws from the NMDAR and the subsequent activation of the NMDAR, by the binding of both glutamate and a co-agonist (glycine or D-serine), and allows both Na^{+} and Ca^{2+} to flow into the postsynaptic neuron (Agulhon et al., 2012; Citri and Malenka, 2008) (Figure 5). The increase in cytosolic Ca^{2+} in the postsynaptic neuron activates Ca^{2+}-dependent proteins, such as calcium/calmodulin-dependent kinase II that leads to the phosphorylation of a variety of proteins including AMPARs, causing an increase in the conductance of the AMPAR channel, and promoting the incorporation of AMPARs into the postsynaptic membrane, which results in the upregulation of their activity, leading to a larger postsynaptic response to glutamate (Citri and Malenka, 2008). Remarkably, the size of the postsynaptic density and dendritic spine is increased, culminating in an enlargement of the potentiated synapses that requires transcription and local dendritic protein synthesis to supply the essential proteins necessary for maintaining synaptic strength (Citri and Malenka, 2008) (Figure 5). Further understanding of the processes behind LTP will certainly contribute to our understanding of learning and memory mechanisms, as well as provide insight into the pathophysiology of a wide variety of brain disorders.

NMDAR can be found in the synapse (synaptic NMDAR, sNMDAR) or outside the synapse (extrasynaptic NMDAR, eNMDAR), playing different roles in synaptic plasticity (Shipton et al., 2014). These receptors require the binding of a co-agonist (glycine or D-serine) and the agonist (glutamate) to GluN1 and GluN2A-D subunits, respectively (Hardingham and Bading, 2010; Shipton et al., 2014). Briefly, sNMDAR activation leads to the stimulation of signaling cascades associated with neuroprotection and survival. These receptors are mainly enriched with GluN2A subunits, that have more affinity for D-serine than for glycine (Papouin et al., 2012). Contrastingly, eNMDAR preferentially initiates cell death pathways, by disturbing the communication between the synapse and the nucleus at various levels (Hardingham and Bading, 2010). These are mostly composed of GluN2B subunits that are more sensitive to glycine than to D-serine (Papouin et al., 2012). It is already described that LTP is mediated by sNMDARs, while eNMDARs do not contribute to this form of plasticity (Papouin et al., 2012). In addition, synaptic loss associated with neurodegenerative diseases (including AD and Huntington's disease) may be caused by an imbalance of sNMDAR and

eNMDAR signaling (Hardingham and Bading, 2010). Interestingly, eNMDARs were found to accumulate at points in close contact with adjacent glia cell processes (Petralia et al., 2010), highlighting the role of astrocytic glutamate in the modulation of NMDAR.

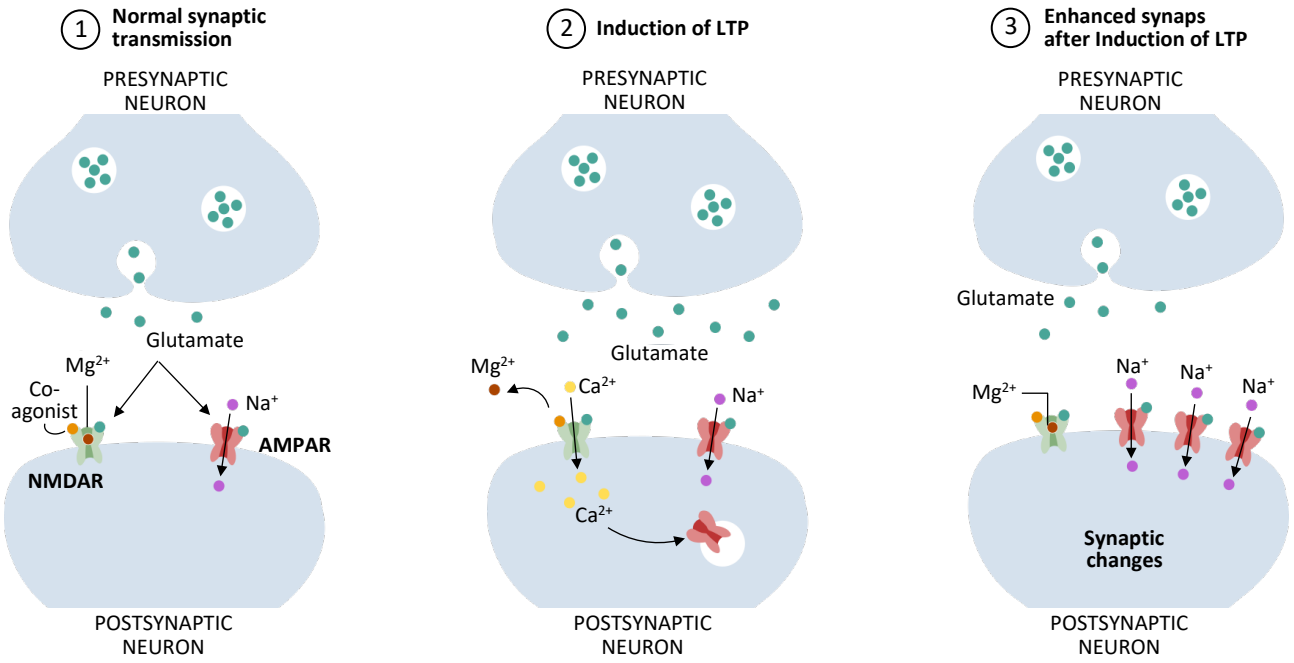

Figure 5: NMDAR-dependent LTP mechanism. 1. Normally, the NMDAR is inactive because it is blocked with an Mg^{2+} molecule. Therefore, glutamate release only activates AMPAR. **2.** Repeated activation of AMPAR allows entry of Na^{+} ions. Eventually, the voltage-dependent Mg^{2+} blockade of the NMDAR is removed, and the NMDAR is now fully activated by glutamate (NMDAR agonist, green) and D-serine/glycin (NMDAR co-agonist, orange) binding, allowing Ca^{2+} ions to enter. The Ca^{2+} influx affects the metabolic machinery of the neuron, which results in the addition of more AMPAR to the postsynaptic membrane. **3.** The synapse has thus been strengthened and it will respond more rapidly and strongly to future releases of glutamate. This process makes the synapse stronger and more likely to be activated in the future.

1.3.5. Cognitive and behavioral evaluation of rodent models

The study of learning and memory requires the development and use of experimental model systems that can be utilized both to characterize the fundamental behaviors associated with memory and to explore the underlying mechanisms. Therefore, the selection of appropriate cognitive tasks for mice is crucial.

Tests of exploratory activity that rely on spontaneous exploration of the apparatus, such as the Open Field Test (OFT) are useful to assess the baseline activity of the animals (Seibenhener and Wooten, 2015). Animals in an open arena or box exhibit thigmotaxis ("wall-hugging" behavior), which can be

used to measure anxiety levels (Sweatt, 2009). These results are important to consider when interpreting other behavioral tests.

The Y-maze is widely used to test working memory, a process for short-term active maintenance of information that depends on the prefrontal cortex (Sweatt, 2009). The three identical arms evoke active exploration, and the pattern of arm entries, as well as the total number of entries, can be informative. The working memory interpretation of alternation asserts that preference for the least recently visited arm indicates memory for the history of arm entries (Gold et al., 2013).

The object location task (OLT) and the novel object recognition task (NOR) test the inherent preference of mice for novelty. The OLT primarily evaluates spatial learning, which relies heavily on hippocampal activity. In contrast, the NOR evaluates non-spatial learning of object identity, which relies on both hippocampus and perirhinal regions (Denninger et al., 2018).

Maze learning has been widely used to probe for the role of the hippocampus in rodent learning and memory. Both Barnes Maze (dry) and Morris Water Maze (MWM) (wet) allow an assessment of the animals' capacity to use spatial cues to locate a hidden escape location (Sweatt, 2009). Distal cues should not be very close to the apparatus or indicative of the escape location or reward, to avoid simple visual discrimination learning without a spatial component. The Barnes Maze is a plastic disk elevated above the floor with a series of escape ports along its perimeter, and animals' performance can be quantitated, for instance, by counting the number of errors (an attempt to enter a non-escape hole) an animal makes before finding the escape hole (Pitts, 2018). Similarly, in the MWM, rodents rely on distal cues to navigate in an open swimming arena to locate a submerged escape platform. For instance, by virtually dividing the pool into four equal quadrants, then measuring the amount of time that the animal spends searching in each quadrant and the number of times that it crosses the exact place where the platform had been located during training is indicative that the animal has learned the location of the platform (Vorhees and Williams, 2006). Generally, in these paradigms, experimental groups are compared with controls to estimate the impact of such manipulation by extracting a cognitive readout.

1.4. Alzheimer's disease

Of the various dementing illnesses, our understanding of AD has progressed the farthest at the molecular level. That does not mean that our understanding of AD is good, but rather that we have at least a few clues as to what is happening.

1.4.1. Discovery and clinical manifestation of Alzheimer's disease

Alzheimer's disease (AD) pathology was first characterized in 1906 by Alois Alzheimer. He described how one of his patients, Auguste Deter, was suffering from progressive changes in her personality, rapidly worsening memory weakness and pronounced psychosocial impairments. Following her death, Alois Alzheimer examined the brain in detail that showed the histological features that are today associated with AD: dramatic brain shrinkage, the presence of dense plaque-like deposits scattered around nerve cells, and the presence of dense like tangle structures localized within cellular structures (Cipriani et al., 2011; Graeber et al., 1997).

Currently, AD is the most common form of dementia, and it represents close to 75% of all dementia cases, affecting 5% of the population older than 65 years, and 30% of the population older than 85 years (Carrillo-Mora et al., 2014). Besides, due to population aging, the number of people with AD is estimated to increase every 20 years (Carrillo-Mora et al., 2014). The early-onset familial form of AD is very rare and is linked to the inheritance of autosomal dominant mutations on the genes encoding for amyloid precursor protein (APP) and presenilins 1 and 2 (PS1 and 2) (Sweatt, 2009). The most common form is the late-onset sporadic form, in which the highest risk factor is aging and the inheritance of the epsilon-4 allele type of apolipoprotein E (Sweatt, 2009). The clinical features of AD include gradual impairment of short-term memory, and in more advanced stages the deterioration of long-term memory, accompanied by personality and behavioral changes, ultimately leading to the patients' inability to perform daily activities (Canada, 2014; Dézsi et al., 2015).

1.4.2. Pathological hallmarks of Alzheimer's disease

AD clinical signs and symptoms are correlated with selective dysfunction (and ultimately death) of neurons in neural circuits and brain regions critical for memory and cognition, including the hippocampus, amygdala, neocortex, anterior thamalus, the basal forebrain cholinergic system, and the mono-aminergic brainstem system (Sweatt, 2009). The key breakthrough in understanding the

molecular pathology of AD came with the identification that amyloid plaques are comprised of aggregates of amyloid-beta (Aβ) peptides. The Aβ is a peptide of 38-42 amino acids produced in virtually all neurons through sequential proteolytic processing of a membrane-attached type-1 protein, called APP, by means of two enzymatic complexes: the β- and γ-secretases (Carrillo-Mora et al., 2014). APP extracellular domain functions include cell surface receptor, cell adhesion, neurite outgrowth and synaptogenesis, while APP intracellular domain has been implicated in cell migration, synapse remodeling, cell signaling and axonal transport (Zheng and Koo, 2006). This integral membrane glycoprotein possesses a cytoplasmic (C-terminal) and an extracellular domain (N-terminal), and can be processed either by a non-amyloidogenic or an amyloidogenic pathway (Figure 6) (Gralle and Ferreira, 2007). In physiological conditions, within the non-amyloidogenic pathway (Figure 6, left), APP is cleaved by α-secretase, releasing soluble APPα (sAPPα). Then, the C-terminal fragment of APP that remains anchored to the membrane (CTFα) is once again proteolyzed by the γ -secretase, producing the fragment p3 ($Aβ_{17–40/42}$) and releasing the APP intracellular domain (AICD) fragment, that does not appear to contribute to AD pathology (Carrillo-Mora et al., 2014). On the other hand, in the amyloidogenic pathway (Figure 6, right), the APP is first proteolyzed by the β-secretase, which generates soluble APPβ (sAPPβ) and the CTFβ fragment that remains attached to the membrane (Carrillo-Mora et al., 2014). The latter is cleaved by the γ -secretase complex, forming the $Aβ_{1-38/42}$ peptide and releasing the AICD fragment inside the cell (Carrillo-Mora et al., 2014). Nonetheless, both sAPPα and sAPPβ have similar neurotrophic properties that protect against Aβ neurotoxicity and thus are not deleterious *per se* (Chasseigneaux and Allinquant, 2012).

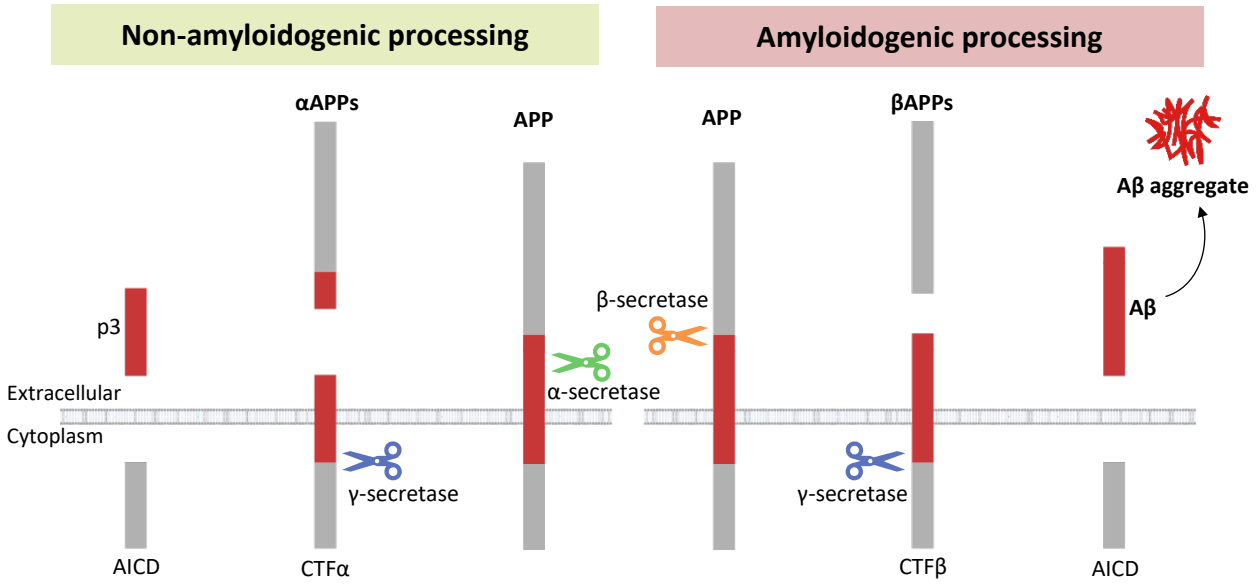

Figure 6: Amyloid precursor protein (APP) processing pathways. The transmembrane protein APP can be processed by two pathways: the amyloidogenic pathway and the non-amyloidogenic pathway. In the non-amyloidogenic pathway

(left), α-secretase cleaves APP, releasing the APP C-terminal fragment (CTFα) and soluble amyloid precursor protein α (sAPPα). The CFTα is then cleaved by γ-secretase to release the APP intracellular domain (AICD) and P3 fragment. Conversely, in the amyloidogenic pathway (right), β-secretase cleaves APP to release the soluble fragment βAAPs and produce the CFTβ fragment. Further, CFTβ is cleaved by γ-secretase, resulting in the release of Aβ peptide and AICD. Aβ: amyloid-beta. AICD: amyloid precursor protein intracellular domain. APP: Amyloid precursor protein. APPs: soluble amyloid precursor protein derivated. CTF: carboxyl-terminal fragments.

Aβ monomers undergo structural changes leading to the assembly to form oligomeric species that aggregate to further generate protofibrils that then mature and elongate into insoluble fibrils (Reiss et al., 2018). A study comparing the effects of fibrillar versus oligomeric Aβ infused both into the left lateral ventricle of rats found that both Aβ forms caused a decline in spatial learning and memory, but the impairment induced by Aβ oligomers was more severe than that by Aβ fibrils, and these effects were accompanied by increased neurodegeneration and greater inflammatory response (He et al., 2012), which supports the primacy of oligomeric Aβ as the main source of neurotoxicity.

Both APP processing pathways are present in healthy individuals and AD patients, however, studies suggest that pathological changes associated with AD may arise from an imbalance between production and clearance of Aβ peptides, which favors the amyloidogenic pathway, as well as an increase in $A\beta_{1-40}/A\beta_{1-42}$ ratio (amyloid cascade hypothesis) (Sweatt, 2009). The presence of the additional two hydrophobic amino acids in $A\beta_{1-42}$ makes it much more susceptible to aggregation into soluble oligomers compared to $A\beta_{1-40}$, further emphasizing how increased levels of $A\beta_{1-42}$ might be a major underlying cause of AD (Bitan et al., 2003). Nonetheless, the exact mechanism by which Aβ oligomers disturb synaptic transmission and memory is unknown. Studies using animal models have revealed that Aβ peptides suppress LTP in rat hippocampal slices (Chen et al., 2000), by inducing aberrant glutamate release from neurons (Brito-Moreira et al., 2011) and astrocytes with subsequent eNMDAR-mediated excitotoxicity (Talantova et al., 2013), which underscores NMDARs as possible pharmacologic therapeutic targets for the future.

Another neuropathological feature of AD is neurofibrillary tangles (NFTs), which comprise aggregates of poorly soluble filaments, being the principal component hyperphosphorylated isoforms of the microtubule-associated protein tau (Sweatt, 2009). Tau hyperphosphorylation has been demonstrated to occur downstream of Aβ oligomerization, consequently causing microtubule destabilization and disrupted cytoskeleton structure, which culminates in the formation of

intracellular NFTs, with loss of neuronal and synaptic function (Tu et al., 2014). Curiously, phosphorylated tau (phospho-tau) colocalizes with Aβ in synaptic terminals from both postmortem AD human brain (Fein et al., 2008) and transgenic AD mouse brain (Takahashi et al., 2010). Additionally, Talantova et al. also reported that Aβ increases glutamate release by astrocytes, which in turn activated eNMDARs, increasing phospho-tau levels (Talantova et al., 2013). In the tau hypothesis, modifications of tau protein phosphorylation are the primary cause of AD pathology. However, Lewis and colleagues suggested that alterations in tau phosphorylation occur after altered APP processing since transgenic mice overexpressing tau and APP exhibited increased formation of tau positive tangles when compared to mice only overexpressing tau (Lewis et al., 2013). Thus, these results support the premise that Aβ is the primary mechanism of AD pathogenesis and that other disease hallmarks, including NFTs, are a consequence of the imbalance between Aβ production and clearance, and that pathological interactions between Aβ and phospho-tau may have a causative role in Aβ-induced synaptic dysfunction and disintegration of the neuronal network.

Current FDA-approved therapeutics are acetylcholinesterase inhibitors, that enhance cholinergic neurotransmission through inhibition of enzyme acetylcholinesterase, and NMDAR antagonists, that block NMDAR-mediated activity (Kumar and Singh, 2015). However, these drugs target the disease symptoms, providing temporary relief to a specific subset of AD patients (Kumar and Singh, 2015). More recently, Biogen's aducanumab was also approved by the FDA, not for ameliorating cognitive symptoms in AD patients, but for removing Aβ (Tanzi, 2021). Taken together, these findings emphasize the importance of investigating Aβ toxicity and the need for better therapeutics.

1.4.3. Astrocytic gliotransmitters in Alzheimer's disease

The neurodegenerative phenomenon in AD was, for decades, thought to be associated with neuronal dysfunction. However, as discussed earlier, glia cells are important for homeostasis in brain function and any disruption in this homeostasis can be critical for the nervous system. During the last few years, astrocytes' role and interactions with neurons have been the focus of research, and the evidence suggests a role for astrocyte-neuron signaling dysfunction as a critical contributor to pathology for most neurodegenerative diseases, including AD (Nanclares et al., 2021).

A critical process sustained by astrocytes at various stages of AD is their reactivity, which is characterized by morphological, molecular, and functional changes of astrocytes in response to

pathological situations in the surrounding tissue, that may include toxic gains-of-function, or loss of their physiological functions (Escartin et al., 2021). Several experiments have documented that exposure to Aβ disturbs Ca^{2+}-signaling and homeostasis in astrocytes, triggering astrocytic Ca^{2+} increases both in cell cultures and transgenic mice models of AD (Chow et al., 2010; Kuchibhotla et al., 2009; Takano et al., 2007). Accordingly, inhibiting the Ca^{2+}-dependent protein phosphatase calcineurin (that was shown to orchestrate biochemical cascades leading to astrocyte activation) in astrocytes improved cognitive and synaptic function, reduced glial activation, and lower amyloid levels in the transgenic APP/PS1 AD mouse model (Furman et al., 2012).

As explained in Chapter 1.2.2.1. astrocytes are the key protectors against excitotoxicity and are predominant elements in glutamate homeostasis. Perturbations at the astrocytes level can lead to excessive extracellular glutamate, which can cause hyperexcitability to the point of excitotoxicity and neuronal death (Talantova et al., 2013). Glutamate clearance is maintained mainly by astroglia-specific glutamate transporters EAAT1 and EAAT2, that when dysregulated cause neurological disorders (Lanciotti et al., 2013). In APP/PS1 AD mouse model, Aβ plaques are correlated to a regional reduction and dysfunction of GLT-1 that causes impaired glutamate clearance rates (Hefendehl et al., 2016). Similarly, the reduction of EAAT2 activity in the early stages of AD has been reported to be correlated with cognitive decline (Masliah et al., 1996). Moreover, regarding astrocytes involvement in toxic glutamate release, Talantova and collaborators described that, in hippocampal slices from 3xTg-AD mice model of AD, the extracellular presence of Aβ near to astrocytes is associated with extrasynaptic glutamate release and consequent eNMDAR activation, that precipitate loss of dendrites and spines (Talantova et al., 2013). Besides, eNMDAR activation is followed by a decrease in miniature excitatory postsynaptic currents, which corresponds to the initial synaptic dysfunction, and is then accompanied by an increase in synaptic loss and additional cognitive impairments (Talantova et al., 2013). These results are suggestive that an increase in glutamate release by astrocytes may underlie the dysregulation of cognition and synaptic function and plasticity stereotypical of AD.

Considering that eNMDAR activity inhibits neuroprotective pathways and signals neuronal injury, whereas sNMDAR activity stimulates neuroprotective transcriptional and antioxidant pathways (Hardingham and Bading, 2010), the preservation of sNMDARs activity is essential to maintain neuronal survival when targeting AD. As explained in detail in Chapter 1.2.2.2. D-serine is a gliotransmitter that has been linked to learning and memory by its actions on sNMDARs (Van-Horn

et al., 2013). However, the D-serine role in AD has been controversial. Increased levels of D-serine were observed in postmortem hippocampal and cortical samples (Madeira et al., 2015) and serum (Piubelli et al., 2021) of AD patients. Moreover, APP/PS1 mice AD, levels of both D-serine and SR (the enzyme responsible for D-serine production) are also elevated (Madeira et al., 2015). Besides, Balu and co-workers showed that SR is up-regulated in reactive astrocytes in the entorhinal cortex and hippocampus of subjects with AD, and increases with disease progression (Balu et al., 2019). Additionally, an increase in signaling pathways associated with eNMDAR activation in the hippocampus of an aged AD mouse model was also verified (Balu et al., 2019), suggesting that the D-serine effect may depend on the disease stage. Nonetheless, Nuzzo et al. analyzed D-serine concentrations in the blood serum and CSF of patients representing the whole clinical spectrum of AD and found no alterations in comparison to the control group (Nuzzo et al., 2020). Curiously, D-serine administration was demonstrated to ameliorate cognitive, learning and memory and motor functions in $A\beta_{1-42}$ injected mice, by regulating NMDAR expression and inhibiting the JNK signaling pathway that promotes apoptosis (H. Liu et al., 2020).

Overall, the evidence is not clear: (1) the increased levels of D-serine and NMDAR hyperfunction may contribute to memory impairments and excitotoxicity observed in AD and/or (2) D-serine may be sufficiently potent to be neuroprotective by activating sNMDAR, but also are gentle enough to allow normal synaptic transmission and neurobehavioral improvement. Due to this controversy, there is no clinical trial testing the efficacy of D-serine on AD. Nevertheless, there is great consensus among all available studies: Aβ dysregulates astrocytic Ca^{2+}-signaling with consequent dysregulation of astrocytic gliotransmission.

2. Rationale and Aims

Even though new insight has been gained about the neurotoxic mechanisms and the clinical aspects of AD, the actual neuropathogenic processes remain unclear. Early stages of neurodegeneration are associated with morphological atrophy of astrocytes, which results in insufficient synaptic coverage, disruption of synaptic connectivity, unbalance in neurotransmitter homeostasis, and neuronal death through increased excitotoxicity. Aβ induces a Ca^{2+}-signaling dysregulation in astrocytes, which can trigger the abnormal Ca^{2+}- and SNARE-dependent release of gliotransmitters. In turn, this anomalous release of gliotransmitters can be linked to the increase in neuronal excitability that leads to the disruption of synaptic transmission and plasticity with consequent memory impairment. Thus, the main goal of this master thesis is to investigate how, in AD, changes in astrocyte-neuron signaling suppress synaptic plasticity mechanisms and contribute to deficits in learning and memory. To clarify this, a transgenic mice model (dn-SNARE) with a selective impairment in the astrocytic vesicular release of gliotransmitters will be used to investigate the impact of astrocytic SNARE-dependent signaling in synaptic mechanisms and cognitive functions. Moreover, despite many years of research in AD, results from animal models have presented variable results, and the existence of translatable models of human AD is limited. Therefore, we used an alternative model involving the production, *in vivo*, in the mouse hippocampus, of moderate levels of amyloid derivatives, resembling as closely as possible the pattern of expression observed in the hippocampus of human AD patients, to study the consequences of initial amyloid pathway engagement. To accomplish the proposed general aim, the following specific aims will be pursued:

1. Identify the role of the SNARE-dependent release of gliotransmitters in synaptic transmission and plasticity.
2. Determine the involvement of SNARE-dependent gliotransmission in synaptic alterations mediated by Aβ oligomers.
3. Evaluate the influence of SNARE-dependent gliotransmission on cognitive processing and electrophysiological activity in an AD model that mimics human APP processing.
4. Disclose the role of astrocytes for D-serine dynamics.
5. Unravel the protective effects of D-serine against Aβ induced synaptic toxicities.
6. Evaluate the impact of Aβ oligomers on glutamate release by astrocytes.

2. Materials and Methods

2.1. Genetic model: Transgenic dominant-negative SNARE (dn-SNARE) mice

All experimental procedures were conducted in accordance with the guidelines for the welfare of laboratory animals, with the guidelines of Directive 2010/63/EU, and the Portuguese Law (DL 113/213). For this project, the dominant-negative SNARE (dn-SNARE) mice model was used. The generation of dn-SNARE mice was performed as previously described by Pascual and his colleagues in 2005 (Pascual et al., 2005). In this strain, the SNARE domain of the synaptobrevin II (dn-SNARE) expression is conditionally suppressed in astrocytes, through a tet-Off expression system, allowing the study of SNARE-dependent gliotransmission. Briefly, the dn-SNARE mice and wild-type (Wt) littermates were obtained by crossing two founder transgenic mouse lines: hGFAP.tTA mice, where the expression of tetracycline transactivator (tTA) is driven by the astrocyte-specific human glial fibrillary acidic protein (hGFAP) promoter; and tetO.dnSNARE, in which the cytosolic portion of the SNARE domain of VAMP2/Synaptobrevin II (amino acids 1 to 96), as well as, the reporter gene for enhanced green fluorescence protein (EGFP) and β-galactosidase gene (LacZ) are co-expressed, in astrocytes, under the control of the tetracycline operator (tetO) (Pascual et al., 2005) (Figure 7). In the GFAP-positive astrocytes of these animals, the expression of dn-SNARE, LacZ, and EGFP can be suppressed by doxycycline (Dox) (Sigma-Aldrich, St. Louis, Missouri, EUA) administration in the drinking water (25 µL/mL). Thus, in the absence of Dox (Figure 7, B), tTA binds to the tetO and activates the transcription of the dn-SNARE, LacZ, and EGFP, blocking SNARE-dependent gliotransmitters release. On the other hand, in the presence of Dox in the drinking water, Dox binds to the tTA transgene, and therefore tTA cannot bind to the operator tetO, and the expression of dn-SNARE, LacZ and EGFP genes remains inactive (Figure 7, A) (Pascual et al., 2005).

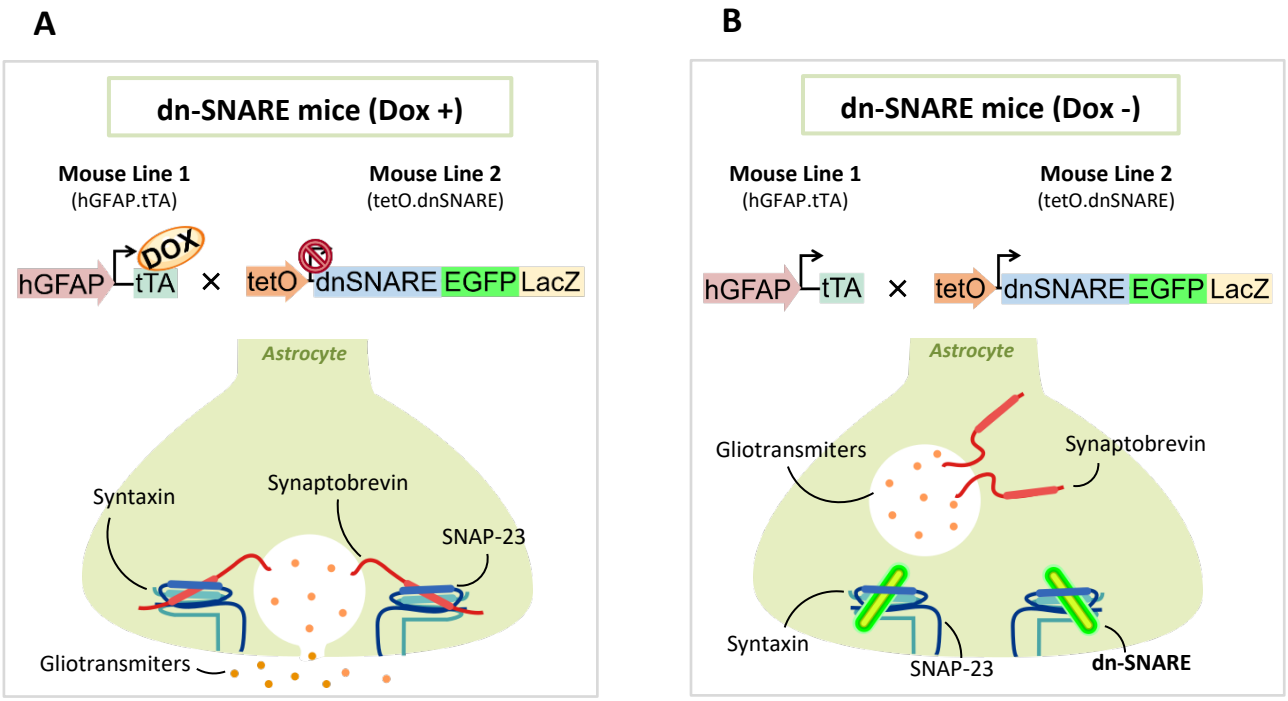

Figure 7: Schematic functioning of the transgenic dn-SNARE mice. The GFAP.tTA mice line contains the human astrocyte-specific glial fibrillary acidic protein (hGFAP) promoter that drives the expression of the tetracycline controlled transactivator protein (tTA), while the tetO.dnSNARE mice line contains a dn-SNARE domain, which corresponds to the cytosolic portion of synaptobrevin, and the enhanced green fluorescent protein (EGFP) reporter gene, regulated by a tetO operator promotor (tetO). **A.** Dox administration via drinking water leads to the inhibition of dn-SNARE domain transcription, leading to functional Ca^{2+}-dependent release of gliotransmitters. **B.** In the absence of Dox, the tetO will drive the expression of the dn-SNARE, and thus the mice have compromised astrocytic vesicular release.

2.1.1. Animal's genotyping

In the context of colony management, dn-SNARE and Wt littermates were identified through a genotyping process. Animals' genotype was assessed by polymerase chain reaction (PCR) of DNA extracted from the animal's tail or ear samples. First, to each sample (ear or tail patch) was added 100 µL of digestion buffer (100mM NaCl, 10mM TrisHCl, 25mM EDTA, 0.5% SDS), followed by 4 µL of 20 µg/mL proteinase K (Sigma-Aldrich, St. Louis, Missouri, EUA). The samples were left in a heating block at 55°C overnight for tissue dissociation. Next, samples were mixed using a vortex and centrifuged at 13000 rpm for 10 min. The supernatant was collected, transferred to a new tube, and 100 µL of isopropanol was added to induce DNA precipitation. Each tube was carefully flicked 4 to 5x until DNA precipitated, followed by centrifugation (13000 rpm for 10 min). Next, the supernatant was discarded, and the pellet was washed with 50 µL of ethanol 70%. The samples were then left

dry for 60-90 min at room temperature (RT). Lastly, DNA was eluted in 30 µL of H_2O miliQ for posterior DNA quantification using a NanoDrop 2000 (Thermo Scientific).

After DNA quantification, genotype was determined by PCR followed by electrophoresis, where Wt mice (negative for tTA and tetO), dn-SNARE mice (positive for both tTA and tetO), and mice expressing only single transgenes (GFAP-tTA or tetO.dnSNARE) were tested. HSF-1, a constitutive mouse gene was used as a positive control to confirm the identification of Wt mice. The dn-SNARE animals possess three bands with different sizes, namely at 200 bps, 380 bps and 500 bps, which corresponds to tTA, tetO and HSF-1 genes, respectively. Comparatively, Wt animals possess only one band at 500 bps (HSF-1), while hGFAP.tTA and tetO.dnSNARE mice possess two bands each (the positive control and the respective transgene). The primers used for the identification of the tTA, tetO and HSF-1 genes were the following: tTA forward – 5'-ACT CAG CGC TGT GGG GCA TT-3' and tTA reverse – 5'-GGC TGT ACG CGG ACC CAC TT-3'; tetO forward - 5'-CAA GCG CAA ATA CTG GTG GAA AA-3' and tetO reverse - 5'-GCG GAT CCA GAC ATG ATA AGA-3'; HSF-1 forward - TCT CCT GTC CTG TGT GCC TAG CM and HSF-1 reverse – 5'-CAG GTC AAC TGC CTA CAC AGA CC-3'. The PCR mix and the thermocycler parameters are presented in Table 1 and Table 2, respectively.

Table 1: PCR mix used for the genotyping of Wt and dn-SNARE animals.

PCR Reaction Mix	Volume/Sample
Dream Taq buffer $(NH_4)_2SO_4$ 10x	1 µL
dNTP mix (10 mM)	0,24 µL
Primer tTA forward (10 µM)	0,6 µL
Primer tTA reverse (10 µM)	0,6 µL
Primer tetO forward (10 µM)	0,6 µL
Primer tetO reverse (10 µM)	0,6 µL
Primer HSF-1 forward (10 µM)	0,4 µL
Primer HSF-1 reverse (10 µM)	0,4 µL
Dream Taq DNA Polymerase (1 µM)	0,3 µL
DMSO 99,9%	0,24 µL
RNase Free H2O	5,02 µL

Table 2: PCR conditions used for the genotyping of Wt and dn-SNARE animals.

PCR Reaction Mix	Temperature (ºC)	Duration (min)	
Initial Denaturation	95	2	
Denaturation	95	0.5	*35 cycles*
Annealing	59.1	0.5	
Extension	72	0.5	
Final Extension	72	10	
Hold	4	∞	

Amplified PCR products were separated on a 1% agarose gel prepared in Tris-Acetate-EDTA (TAE) (20 mM acetic acid, 40 mM Tris-base, 1mM EDTA), that was heated, before the addition of 8 µL of the DNA dye GelRed marker 1% (VWR, EUA). After agarose gel solidification, 2 µL of Running Buffer was added to each sample to increase the samples' molecular weight. Afterward, the DNA size marker (0,1 – 1 kb NZYDNA Ladder V, NZYTech) and the samples were loaded into the gel, and electrophoresis at 110 – 120 mV run for 1h30. Gel pictures were captured using a transilluminator (Chemidoc XRS+, Bio-Rad).

2.2. *In vivo* AAV-AD model

An *in vivo* model involving the production, in the mouse hippocampus, of moderate levels of amyloid derivatives, resembling as closely as possible the pattern of expression observed in the hippocampus of human AD patients was used to study astrocytes contribution to the initial amyloid pathway engagement (Audrain et al., 2016). Plasmid design and vector production were conceived by Prof. Nicole Déglon (Faculty of Biology and Medicine, Université de Lausanne). Briefly, the sequences of a double-mutant human APP751 cDNA containing the Swedish and London mutations, and a human PS1 cDNA containing the M146L mutation were cloned in an Adeno Associated Virus (AAV) 2 plasmid with CAG promoter to generate AAV2-CAG-PS1M146L (AAV-PS1) and AVV-CAG-APPSL + AAV2-CAG-PS1M146L (AAV-APP/PS1).

Before starting the surgical procedure, the surgical table was disinfected with 70% ethanol, and all the used tools were sterilized. All animals were weighed before surgery to allow valid control of post-surgical weight loss. Individually, each animal was placed in the isoflurane induction chamber until fully anesthetized with isofluorane, containing 2-3% O_2 (mice should no longer be responsive

to nociceptive stimuli, such as pinching the toes with forceps). To prevent hypothermia, animals were kept on top of heating pads (37ºC) during all the procedure time. After shaving the fur of the head, exposed skin was disinfected with Betadine® (Meda Pharmaceuticals, USA), and local anesthetic emla® cream (AstraZeneca, London, UK) was applied inside the ear canal to minimize pain or discomfort once the animal was placed in the stereotaxic apparatus with ear bars to stabilize the position of the head. Lacryvisc® ophthalmic gel (Alcon, Switzerland) was also applied to the eyes of the animal to prevent dehydration. General analgesic buprenorphine (0.016 mg/mL, in NaCl) was administrated subcutaneously (0.05 mg per kg of body weight). Next, animals were transferred to a stereotaxic apparatus (Stoelting, IL, USA). Using a scalpel, a longitudinal incision along the midline of the head was done to expose cranial sutures. Having bregma as a reference, the following coordinates were used for the site of injection: antero-posterior -2 mm, lateral ± 1 mm, and ventral -2 mm. A small hole was drilled in the skull, and 2 µL of viral preparation was injected into each site ($1.5x10^{11}$ vg/mL) of the hippocampi of both hemispheres at a rate of 0.2 µL/min, with a 10 µL 33-gauge Microliter Syringe (Hamilton Company, USA) and a Micro4TM MicroSyringe Pump Controller (World Precision Instruments, FL, USA). After removing the syringe, the skin of the animal was sutured with Silkam® 4/0 silk sutures (Braun, Germany), and Bepanthene® Plus (Bayer, Leverkusen, Germany) was applied on top of the sutures. Animals were maintained individually on recovery cages until regaining ambulatory ability. Animals were monitored frequently to ensure that they remained healthy during recovery. Six groups were designed, a non-injected control (non-injected Wt and dn-SNARE mice), Wt mice injected control (Wt injected with AAV-PS1), dn-SNARE injected control (dn-SNARE injected with AAV-PS1), and two APP-processing AD models (Wt injected with AAV-APP/PS1 and dn-SNARE injected with AAV-APP/PS1).

2.3. *Ex-vivo* electrophysiological recordings

The present protocols aimed to study the role of gliotransmission in synaptic transmission and plasticity. Accordingly, extracellular electrophysiological recordings were performed to evaluate the activity of a population of neurons that are in the vicinity of the recording electrode.

2.3.1. Preparation of acute hippocampal slices

For electrophysiological recordings, acute hippocampal slices from both Wt and dn-SNARE mice were prepared as previously described (Rei et al., 2020). Animals exclusively used in *ex vivo* were sacrificed by decapitation after cervical displacement and the brain was rapidly removed to isolate the hippocampus. The hippocampus was dissected in ice-cold artificial cerebrospinal fluid (aCSF) containing (in mM): 124 NaCl, 3 KCl, 1.2 NaH_2PO_4, 25 $NaHCO_3$, 2 $CaCl_2$, 1 $MgSO_4$ and 10 glucose, which was continuously oxygenated with 95% O_2 and 5% CO_2. The hippocampal slices were cut perpendicularly to the long axis of the hippocampus (400 µm thick) with a McIlwain tissue chopper and allowed to recover functionally and energetically for at least 1h in a resting chamber filled with continuously oxygenated aCSF, at RT, before being set up for electrophysiological recordings.

2.3.2. Drug treatment

After recovering functionally and energetically for at least 1h in a resting chamber filled with oxygenated aCSF at RT, hippocampal slices from Wt and dn-SNARE animals were treated with one of the following conditions before the electrophysiological recordings: control (no drug incubation) or pre-incubated for 3h with $A\beta_{1-42}$ oligomers (200 nM). D-serine (10 µM) or L-serine (10 or 50 µM) were tested by perfusing hippocampal slices already placed in the recording chamber at least 15 min before the LTP induction.

The chosen concentration for $A\beta_{1-42}$ oligomers (200 nM) used in this work was based on previous reports that have demonstrated that in the brain extracellular fluid under normal physiological conditions and in AD patients, Aβ is present at low nanomolar or high picomolar concentrations (Hu et al., 2009), and, on previous studies that have shown that 200 nM of oligomeric $A\beta_{1-42}$ can significantly inhibit LTP induction (Chen et al., 2000).

Furthermore, D-serine, a co-agonist of glutamate which acts on NMDAR (Coyle et al., 2020; Martineau et al., 2014), was previously described as able to fully rescue LTP suppression caused by clamping the intra-astrocyte Ca^{2+} concentration, at a concentration of 10 µM (Henneberger et al., 2010). Moreover, to gain further insight into the potential contribution of the astrocytes in D-serine release (using L-serine as a substrate), L-serine was applied in the perfusion bath with the same D-serine concentration (10 µM) and with a known concentration that rescues LTP in animals conditionally lacking PGDH in astrocytes (50 µM) (Le Douce et al., 2020).

2.3.3. Extracellular recordings of field excitatory postsynaptic potentials (fEPSPs) and Long-Term Potentiation (LTP) induction

Following the slice recovery time and, if applicable, the drug incubation period, hippocampal slices were transferred to a recording chamber for submerged slices (1mL capacity plus 5 mL dead volume) and were constantly superfused at a flow rate of 3mL/min with aCSF kept at 32ºC, gassed with 95% O_2 and 5% CO_2. Field excitatory postsynaptic potentials (fEPSPs) were recorded extracellularly by placing a microelectrode (4 to 8 MΩ resistance), filled with aCSF solution, in the *stratum radiatum* of the CA1 area. Stimulation was delivered through a bipolar concentric wire electrode fabricated from platinum/iridium wire (25 µm diameter, <800 kΩ impedance) positioned in the *Schaffer Collateral* (Figure 8, A).

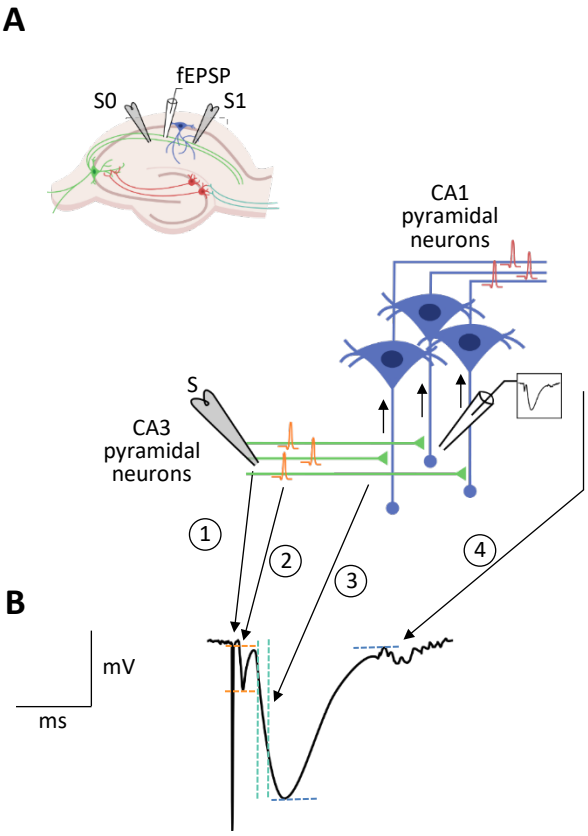

Figure 8: Schematic illustration of electrode positions in CA1 region of hippocampal slice and diagram of field excitatory postsynaptic potential (fEPSP). **A.** The stimulating electrodes are positioned in *the Schaffer Collateral* fibers arising from CA3 and the evoked field excitatory postsynaptic potentials (fEPSP) are recorded extracellularly by the recording electrode placed in the *stratum radiatum* of the CA1 area. **B.** The arrow in **(1)** is pointing to the stimulus artifact that results from the electrical stimulation of *Schaffer Collaterals*. This stimulation will induce the firing of action potential in all fibers surrounding the electrode that will propagate and reach the presynaptic terminal. This synchronous firing and propagation of action potentials will originate the presynaptic volley that follows the stimulus artifact in **(2)** and is measured between horizontal orange dotted lines. Synchronous release of neurotransmitters in the presynaptic terminals will result in activation of the respective postsynaptic receptors and the consequent synaptic

potential. The combination of synaptic potentials of the group of recorded postsynaptic neurons results in a **(3)** fEPSP (measured between the two vertical green dotted lines). The postsynaptic potential from each pyramidal cell will propagate through the dendrites and reach the soma. Here, synaptic potentials will be summated and, in case of reaching the threshold for activation of voltage-dependent sodium channels, it will fire an action potential. The sum of all action potentials from the group of pyramidal cells recorded will originate a population spike, as shown in **(4)** that is measured between blue horizontal dotted lines. *Adapted from Rombo, D., Doctoral Thesis, 2015*.

In the configuration shown in Figure 8, an extracellular recording electrode is placed among apical dendrites of CA1 pyramidal cells, and stimulating electrodes are positioned in the *Schaffer collaterals* to stimulate two separate input pathways. fEPSPs were evoked by the stimulation of the two different pathways of the *Schaffer collaterals* fibers at every 10s (rectangular pulses of 0.1ms duration). Averages of eight consecutive responses were continuously acquired using an Axoclamp-2B amplifier (Axon Instruments, Foster City, CA), digitized with the WinLTP program (Anderson and Collingridge, 2001) and quantified as the slope of the initial phase of the averaged fEPSPs (Figure 8, B). The stimulus intensity was adjusted at the beginning of the experiment to obtain an fEPSP slope close to 0.5 mV/ms, to evoke fEPSPs of amplitude about 50% of maximal amplitude with minimal contamination by a population spike. Each slice allows recordings from two independent pathways (S0 and S1, Figure 8, A). In any case, fEPSPs were recorded under basal stimulation conditions (standard stimulus intensity and frequency) and stability of fEPSP slope values was monitored for more than 20 min before starting the LTP protocol detailed below. Two or three slices per animal were tested in each experimental day (for different experimental conditions). Traces shown from representative experiments are composed by stimulus artifact, presynaptic fiber volley (PSFV), and fEPSP.

LTP was induced after obtaining a stable recording of the fEPSP slope for at least 30 min. A weak 4x4 θ-burst stimulation LTP-inducing protocol was used, consisting of 1 stimulus with 4 bursts (200 ms interburst interval) and with 4 pulses each (100 Hz each). θ-burst stimulation was used to elicit LTP since this pattern of stimulation is considered similar to what occurs physiologically in the hippocampus during episodes of learning and memory in living animals (Albensi et al., 2007). The intensity of the stimulus was never changed during the experimental data acquisition. The magnitude of LTP was quantified as the % change in the average slope of the fEPSP taken from 50-60 minutes after the induction of LTP in comparison to the average slope of the fEPSP measured during the 15-20 minutes before LTP induction.

2.4. Western blot

The Western blot (WB) technique was used to assess the levels of EGFP (dn-SNARE transgene reporter) and APP (human and total) proteins. After electrophysiological recordings, tissue homogenates from the remaining hippocampal slices were prepared. Samples were homogenized through sonication, in Radio Immuno Precipitation Assay lysis buffer (1% Nonidet® P40 Substitute [NP40], 50 mM Tris-HCl (pH 7.5), 150 mM NaCl, 5mM ethylenediamine tetra-acetic acid (EDTA), 0.1% sodium dodecyl sulphate (SDS) and 1% Triton X-100) containing one protease inhibitor cocktail tablet (Roche, Germany) for each 10 mL. Samples were then centrifuged at 13000g for 10 minutes at 4ºC, after which the supernatant was collected. Sample protein quantification was performed through Bradford assay and DCTM Protein Assay kit (Bio-Rad Laboratories, USA), with bovine serum albumin (BSA) as the standard. Absorbance was read at 750 nm, using an Infinite M200 multimode microplate reader (Tecan, Switzerland).

After quantification, samples were prepared for WB analysis, by adding 5 µL 6x sample buffer (36% glycerol, 12% SDS, 0.015% bromophenol blue, 720 mM dithiothreitol, 420 mM Tris pH 6.8) and then denatured (10 min, 95ºC), and stored at -20ºC until use. Proteins were separated by sodium dodecyl sulphate polyacrylamide gel electrophoresis (SDS-PAGE), in running buffer (0.1% SDS, 192 mM glycine, 25 mM Tris pH 8.3), at constant voltage (80-120 V), using 10% acrylamide/bis-acrylamide resolving gels (0.1% SDS, 0.1% ammonium persulfate (APS), 0.04% N,N,N',N'-tetramethylethane-1,2-diamine (TEMED), 375 mM Tris pH 8.8), and 5% acrylamide/bis-acrylamide stacking gels (0.1% SDS, 0.1% APS, 0.1% TEMED, 125 mM Tris pH 6.8), with 1.5 mm thickness. NZYColour Protein Marker II (NZYTech, Portugal) was used as a protein molecular weight marker.

Proteins were transferred to polyvinylidene difluoride membranes, soaked with methanol, within the transfer buffer (10% methanol, 192 mM glycine, 25 mM Tris pH 8.3), at constant amperage (350 mA, 1h15). After transfer, membranes were blocked with 3% BSA in Tris-buffered saline with Tween® 20 (TBS-T) (200 nM Tris base, 1.5 M NaCl, 0.1% Tween® 20, pH 7.6) for 1h at RT. After blockage, membranes were washed with TBS-T (3x 10 min) and incubated overnight with primary antibodies: anti-GFP rabbit polyclonal antibody, Alexa Fluor 488 (1:1000, Life Technologies, USA), anti-GAPDH mouse monoclonal antibody (1:5000, Life technologies, USA), anti-APP C-terminal rabbit polyclonal antibody (1:500, BioLegend, USA), and anti-6E10 mouse monoclonal antibody that recognizes the N-terminus and Aβ region of human APP (from now referred as human APP, 1:100, Biolegend, USA). After washing with TBS-T (3x 10 min), membranes were incubated, for 1h (RT),

with secondary antibodies: goat anti-mouse IgG-horseradish peroxidase-conjugated (Bio-Rad, USA) and goat anti-rabbit IgG-horseradish peroxidase-conjugated (Bio-Rad, USA) secondary antibodies (1:10 000). All primary and secondary antibodies were prepared in the blocking solution. After washing, proteins were revealed with ClarityTM Western ECL Substrate (Bio-Rad, USA), using ChemiDocTM XRS+ imaging system with Image LabTM software (Bio-Rad, USA). Band quantification was assessed using the Image Lab software (Bio-Rad, USA), and all the samples were normalized according to the loading control (GAPDH).

2.5. Immunofluorescence assays

To visualize the expression of APP (total and human) and the dn-SNARE transgene reporter (EGFP) together with its co-expression with astrocytic and neuronal markers, immunohistochemistry was performed in brain slices from mice non-injected and injected with AAV-PS1 or AAV-APP/PS1 (5 months after the viral injection). Animals were euthanized by cervical dislocation and immediate decapitation. The brains were removed, and one hemisphere was post-fixed by immersion in 4% PFA overnight at 4ºC. Hippocampal slices, to be used in electrophysiological recordings, were prepared form the other hemisphere. After a quick wash in PBS (phosphate-buffered saline, in mM: 137 mM NaCl, 2.7 mM KCl, 8 mM $Na_2HPO_4.2H_2O$, and 1.5 mM KH_2PO_4, pH 7.4), brains were immersed in a 15% sucrose (in a 50 mL tube) solution at 4ºC. When the brains moved to the bottom of the tube, they were changed to a 30% sucrose solution. Again, when precipitated to the bottom of the tube, the brains were transferred to a solution of 15% sucrose. After, coronal brain sections (40 µm thick) from the hemispheres, were obtained using a vibratome (Leica, Germany), and stored at 4ºC in PBS with 0.02% sodium azide until used.

The antibodies staining protocol started with three washes with PBS, 10 min each, followed by permeabilization for 30 min (RT) with 5 % Triton X-100 in PBS. Then, slices were rinsed in PBS and incubated with 10% fetal bovine serum (FBS) in PBS blocking solution (to reduce unspecific bounds) for 30 min at RT. After blocking, slices were incubated with the primary antibodies, diluted in the blocking solution, at 4ºC overnight: anti-GFAP rabbit polyclonal (1:750, Sigma-Aldrich, Germany), anti-APP C-terminal rabbit polyclonal antibody (1:500, BioLegend, USA), anti-6E10 mouse monoclonal antibody (1:100, Biolegend, USA) and anti-βIII tubulin rabbit monoclonal (1:500, Sigma-Aldrich, Germany). Next, brain slices were rinsed three times in PBS, and then incubated with the respective species-specific secondary antibodies: Alexa Fluor® 568 donkey anti-mouse and Alexa

Fluor® 568 donkey anti-rabbit (1:500, Invitrogen, USA) in PBS, during 2h, in the dark at RT. After rinsing the brain slices with PBS, the nucleic acids were stained with DAPI (4',6'-diamidino-2-phenylindole, 1:1000, Invitrogen, USA) for 7 min in the dark. After washing with PBS (3x 10 min), slices were mounted on microscope slides (SuperfrostTM Plus, ThermoFisher Scientific) with Mowiol (non-absorbing compound without autofluorescence and light scattering), and glass coverslips on top, and allowed to dry for at least 24h. Images of the CA3-CA1 hippocampal regions were captured using a Zeiss LSM 880 with Airyscan (Carl Zeiss, Germany) confocal point-scanning microscope, with 20x and 40x objectives, and analyzed by FIJI open-source software. Each set of images, of the same condition, is composed of 3-4 slices, separated from each other by 240 µm. The results presented will represent the injection site, following the coordinates.

2.6. FRET-base live-cell imaging in astrocytes

The present experiment was designed to assess if astrocytes release more glutamate in the presence of $A\beta_{1-42}$ oligomers. This protocol uses a fluorescence resonance energy transfer (FRET)-based glutamate biosensor, which senses glutamate by changing the ratio of FRET from cyan fluorescent protein (CFP) to yellow fluorescent protein (YFP) upon glutamate binding.

2.6.1. Primary cultures of astrocytes

Primary hippocampal- cortical astrocytes were obtained from 0-4 days old C57BL/6J pups (Charles River, Barcelona, Spain) of either sex following a standard protocol (Schildge et al., 2013). Pups were sacrificed by decapitation and the heads were sterilized by submersion in alcohol three times. The brains of the pups were dissected in PBS by removing the scalp covering the top part of the skull. A midline incision was made in the skull exposing the brain which was then dissected out by introducing a spatula between the cortex and olfactory bulbs separating them and sliding the spatula under the brain cutting the optical nerves and removing the brain from the skull. The cerebellum was removed, and the hemispheres were separated. The basal ganglia and meninges were removed, leaving only the cortex area and the hippocampus. The cortexes and hippocampus were then vigorously dissociated mechanically with a 10 mL pipette in 4.5 g/L glucose Dulbecco's Modified Eagles Medium (DMEM, Gibco, UK) supplemented with 10% (v/v) FBS (Gibco, UK), 0.01% antibiotic/antimycotic (100 U/mL penicillin, 0.25 µg/mL amphotericin B and 100 µg/mL

streptomycin (Sigma-Aldrich, Germany) solution and 0.01% glutamine (Gibco, UK) at 37 ^{o}C. The dissociated cells were filtered through a 230 µm pore mesh followed by a 70 µm mesh (BD Falcon, Belgium). After each filtration, the cells underwent two centrifugations at 200 g × 10 minutes at RT. After each centrifugation, the supernatant was discarded, and the pellet was resuspended in 10 mL of fresh DMEM supplemented medium. In the last centrifugation, the pellet was resuspended for the final volume of 8 mL supplemented medium for each cortex and plated in a T-75 flask coated with poly-D-lysine at a concentration of 10 µg/ml. Cultures were kept in an incubator with a humidified atmosphere (5% CO_2) at 37ºC and the medium was changed once a week. At 7 days in vitro, the T-75 flasks were agitated horizontally at 300 rpm for 6 hours to remove any contaminating microglia and oligodendrocyte precursor cells and thus obtain astrocytic-enriched cultures (Schildge et al., 2013). For live imaging, T-75 flasks were then replated in 35 mm µ-Dish (Ibidi GmbH, Germany) in a concentration that allows astrocytes to form a 70-80% confluent monolayer when plated. During incubation, cells were kept in a humified atmosphere (5% CO_2) at 37 ^{o}C. The culture medium was changed once or twice a week.

2.6.2. FRET biosensor for glutamate assay

The genetically encoded FRET-based biosensor pDisplay FLIPE-600nSurface biosensor (#13545, Addgene, UK) (Okumoto et al., 2005) responds to glutamate enabled quantitative imaging of the extracellular glutamate levels of individual living astrocytes and observation of glutamate levels regulation in response to changes in the environment of the cells, namely the presence of 200 nM $A\beta_{1-42}$ oligomers.

2.6.2.1. Growing of bacterial cultures

The plasmid-carrying E. *coli* colony (Addgene plasmid #13545; RRID: Addgene_13545, UK) was transferred with a sterile pipette tip to a 100 mL Erlenmeyer with 10 mL of Luria Broth medium (20mg/L) (Sigma-Aldrich, Germany) supplemented with 10 µL of 100 mg/mL carbenicillin. Carbenicillin, an ampicillin analog, inhibits the synthesis of the bacterial cell wall, which results in bacteria that are very structurally weak. In the hypotonic media, cells exposed to carbenicillin will swell and lyses (Ziervogel and Roux, 2013). Thus, for cells to survive, they must include a means to break down the carbenicillin. The plasmid has an additional gene coding for an enzyme, β-lactamase,

that is secreted by cells and in a local area will hydrolyze the carbenicillin. Therefore, only the bacteria that retained the plasmid can survive. After, the Erlenmeyer was incubated for 12–16 h at 37 °C with vigorous shaking.

2.6.2.2. Plasmid DNA purification from E. coli

For small-scale extraction of plasmid DNA from recombinant E. *coli* cells that were grown overnight, a Miniprep Kit (NZYTech, Portugal) was used according to the manufacturer's directions. Briefly, 2 mL of bacterial cells were pelleted by centrifugation at 13000 rpm for 1 min. Afterward, the supernatant was removed, and the pellet was resuspended in 250 µL of cell resuspension buffer by vigorous vortexing. Cells were lysed by adding 250 µL of plasmid lysis buffer followed by a RT incubation of 4 minutes. The lysate was neutralized by adding 300 µL of plasmid neutralization buffer and clarified by centrifuging at 13000 rpm for 5-10 min at RT. Then, the supernatant was transferred to the spin column and centrifuged for 1 min at 13000 rpm. The flow-through was discarded and the silica membrane was washed twice with 500 µL of plasmid wash buffer followed by a 1 min centrifugation at 13000 rpm. After, the silica membrane was dried by re-inserting the spin column into an empty 2 mL Eppendorf and centrifuging for 2 min at 13000 rpm. Lastly, the highly pure DNA was eluted by adding 30-50 µL DNA elution buffer to the center of the matrix and centrifuging for 1 min at 13000 rpm. The purified DNA was stored at -20ºC. To verify whether the received plasmid matches the expected sequence, the insert was identified by Sanger sequencing using the following appropriate primers (Figure 9): T7 promoter, forward primer 5'-TAATACGACTCACTATAGGG-3', that is upstream of the insert, and the BGH terminator, reverse primer 5'-TAGAAGGCACAGTCGAGG-3' that is in the terminal part of the insert. The sequencing result was analyzed in SnapGene Viewer and the sequences were verified in BLASTP and UniProt protein databases.

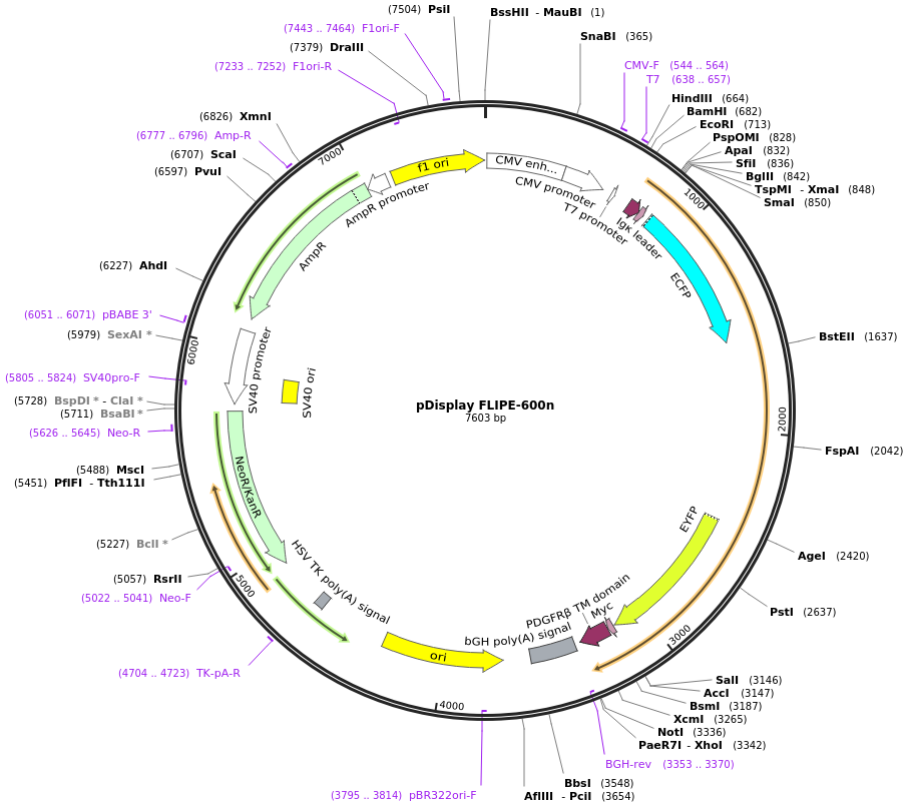

Figure 9: Vector Map of pDisplay FLIPE-600n: FLIPE insert (2400 bp) containing ECFP (N terminal on insert) and EYFP (C terminal on insert) sequences were cloned into pDisplay vector backbone in which the expression cassette contained an E. coli origin of replication (ori) and ampicillin resistance gene (AmpR) (Okumoto et al., 2005).

2.6.2.3. Fluorescence principles and FRET

FRET is a phenomenon of non-radiative energy transfer from a higher energy (more blue-shifted) donor fluorophore to a lower energy (more red-shifted) acceptor fluorophore, in which the transferred emission energy from the donor triggers fluorescence emission of the acceptor positioned typically within 1 to 10 nm (Carlson and Campbell, 2009; L. Liu et al., 2020). FRET can be directly detected using specific excitation wavelengths and filter sets to measure acceptor emission upon donor excitation (FRET intensity). A higher ratio of FRET to donor intensity is correlated with a higher FRET efficiency that, in turn, can be attributed to a shorter distance or more favorable relative orientation between the fluorophores, resulting in FRET increase (Carlson and Campbell, 2009).

In general, FRET-based biosensors commonly utilized to monitor cellular activity consist of the two fluorescent probes (donor and acceptor) fused to a central protein binding pocket which undergoes

a global structural rearrangement upon binding to its ligand (Okumoto et al., 2005). When cells transfected with FLIPE biosensor are excited at the optimal excitation wavelength of the donor, the ratio of acceptor emission over donor fluorescence intensity allows for the quantification of biosensor responses (L. Liu et al., 2020) (Figure 10, A and B). Among the variety of fluorescent proteins, the ECFP and EYFP pair is commonly used as a FRET pair due to the significant overlap between the emission spectrum of ECFP and the excitation spectrum of EYFP (L. Liu et al., 2020) (Figure 10, C).

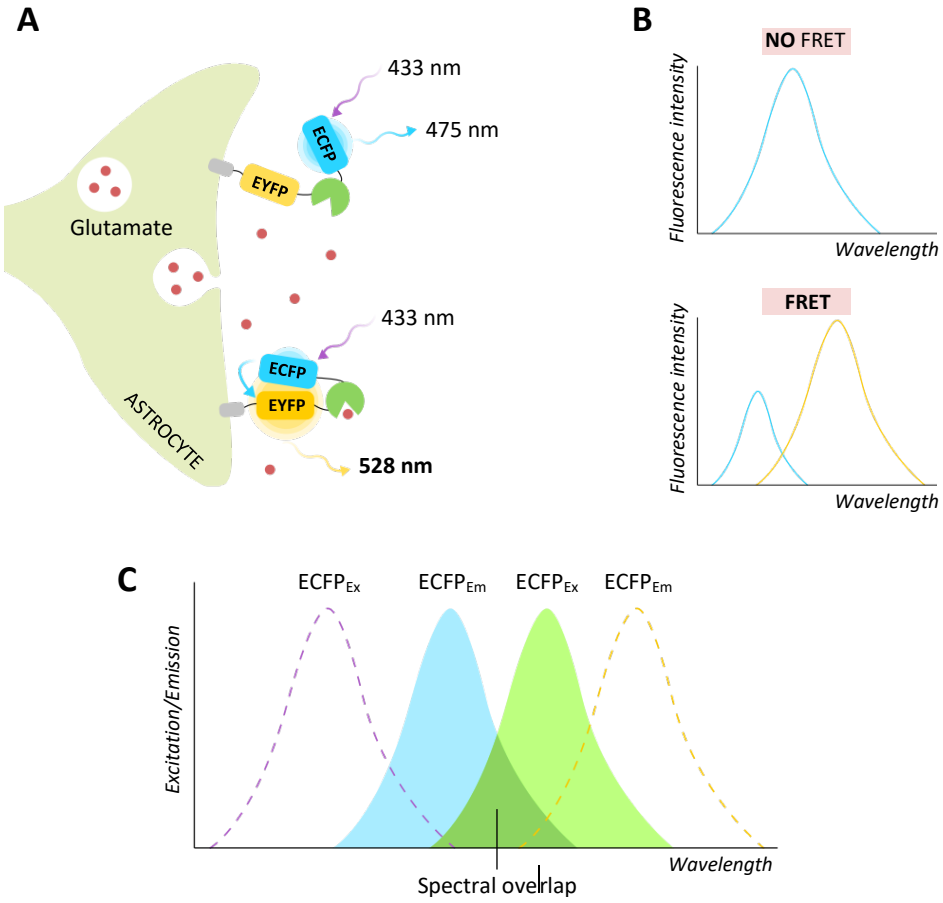

Figure 10: Characterization of a FRET-based biosensor for the quantification of glutamate released from cultured astrocytes. A. Schematic diagram of glutamate sensor displayed on astrocyte surface: the fluorescent proteins ECFP (blue) and EYFP (yellow) are fused to one of the lobes of the glutamate-binding protein YBEJ (green). In this FRET-based biosensor, ECFP acts as the donor and EYFP as the acceptor. When the two fluorophores are separated by a considerable distance, exposing the sample to light with the excitation frequency for ECFP results in an emission spectrum corresponding to ECFP only, with no contribution from the acceptor (EYFP). **B.** Upon glutamate binding (red), a conformational change brings the two lobes closer to each other and FRET can be observed in the microscope by excitation of ECFP (donor), which results in a nonradiative energy transfer from ECFP to the nearby EYFP acceptor, causing EYFP to emit at its emission wavelength. At the same time, due to the transfer of energy, emission from ECFP is

considerably reduced. **C.** Represents the excitation (Ex.) and emission (Em.) wavelength of ECFP and EYFP, as a FRET donor and acceptor, respectively. The emission wavelength of ECFP overlaps with the excitation wavelength of EYFP, enabling the energy transfer between donor and acceptor when their distance is less than 10 nm.

FRET was performed essentially as described (Socodato et al., 2020). First, astrocytes seeded in a 35 mm μ-Dish (Ibidi GmbH, Germany) were transfected with the plasmid encoding the FRET probe ECFP/EYFP. Lipofectamine™ 3000 was diluted in Opti-MEM medium and P3000™ reagent in accordance with manufacturers. Then, the plasmid DNA was diluted in the mix (1:1 ratio), allowed to incubate for 10-15 minutes at RT to form DNA-lipid complexes, and after was added to the astrocytes to allow particle-cell interaction. The probe was expressed for 16-24h. After that time, the medium was discarded, and the cells were gently washed with PBS. Then, 2 mL of imaging solution (for a volume of 100 mL: 820 mg of NaCl 140 mM, 37 mg of KCl 5 mM, 476 mg of HEPES 20 mM, 72 mg of glucose 4 mM, 41.6 mL of $MgCl_2$ 1 mM (stock solution at 2.4 M), 50 mL of $CaCl_2$ 2 mM (stock solution at 4 M) and 98.5 mL of ddH_2O) were added to each dish.

Cells were imaged with a Zeiss Cell Observer widefield fluorescence microscope controlled by ZEN software 3.0 with settings in accordance to (Socodato et al., 2020), using a 40x EC Plan-NeoFluar NA=0.75 objective, and filters for the donor channel (ECFP excitation and ECFP emission) and for the FRET channel (ECFP excitation and EYFP emission). Each FRET analysis started with a time-lapse of the baseline, with images acquired with 20 seconds of interval, followed by the addition of $A\beta_{1-42}$ oligomers (200 nM) and incubation for 30 minutes. Subsequently, images were collected for 5 minutes with an interval of 20 seconds. Images were processed in FIJI open-source software following (Socodato et al., 2020) guidelines.

2.7. Behavioral tests

Patients suffering from AD usually present memory deficits at the initial stages of the disease, which tend to aggravate along with the disease progression, namely due to compromised hippocampal function (Gold, 2009). Therefore, evaluation of behavioral paradigms, specifically regarding memory performance, was a crucial step in attempting to confirm our AAV-AD model as an *in vivo* model that mimics the early consequences of AD in terms of APP and APP cleavage products (Audrain et al., 2016). Accordingly, to tackle if changes in SNARE-dependent vesicular gliotransmitter release

from astrocytes contribute to deficits in learning and memory caused by APP-processing, different tests were carried out using Wt and dn-SNARE mice injected with AAV-PS1 and AAV-APP/PS1.

Cognitive functions are mainly dependent on the hippocampus (spatial learning and recognition tasks) or the prefrontal cortex (working memory tasks), thus the MWM, Barnes maze, Y-maze spontaneous alternation, and the OLT were performed to evaluate special learning, recognition memory, and working memory. Furthermore, to exclude an anxiety-like behavior phenotype that could bias the cognitive assessment, we performed the OFT which, in addition to providing a measure of anxiety-like behavior, also provides measures of motor and exploratory activity (Seibenhener and Wooten, 2015). All tests were performed during the light phase of the day. Before experimentation, mice were handled daily for at least 5 minutes, throughout one week, and habituation to testing rooms was performed before starting any behavior assessment for at least 30 minutes, with dim light and temperature conditions kept stable throughout the testing period. Furthermore, to diminish the likelihood of stress-induced by one test influencing the results of the following, resting periods were introduced wherever possible. A chronogram of behavioral testing procedures is described in Figure 11. To erase any olfactory clues, for every test and between each trial, the arena and/or objects were carefully cleaned with a 30% ethanol solution. In every test, the experimenter moved from the test zone to an independent zone separated by a curtain immediately after placing the animal in the corresponding apparatus. The animal's behavior was recorded and analyzed using the SMART®2.5 video tracking software (Panlab, Harvard Apparatus, Spain), with the dorsum of the animals as the reference point used for tracking. Besides, every test was also recorded using a Brio 4K Pro camera (Logitech, Lausanne, Switzerland), and the resulting videos were manually analyzed posteriorly, using the Solomon Coder beta version 17.03.22 (András Péter, Milan, Italy) behavior coding software.

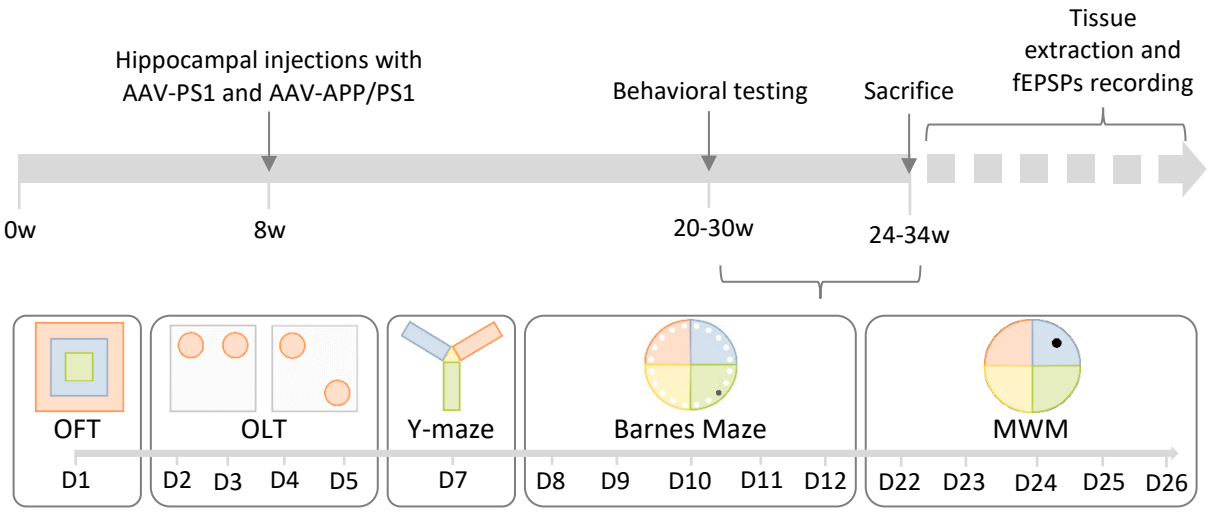

Figure 11: Experimental design. Wt and dn-SNARE mice were injected at 8 weeks old of age either with AAV-CAGPS1M146L (AAV-PS1 mice) or AVV-CAG-APPSL + AAV10-CAG-PS1M146L (AAV-APP/PS1 mice), and behavioral analyses were performed three months later. On D1 of behavioral experiments, mice were tested on OFT, which was also used as part of the first day of the habituation phase for the OLT test. Following the habituation phase (3 consecutive days), mice were exposed to a familiarization phase, and 24h after habituation spatial memory was evaluated. A resting day was taken and on D7 mice were tested for the Y-maze test. On D8, habituation to the Barnes maze was followed by an acquisition training phase of 4 consecutive days succeeded by a probe trial on D12. The animals were given 10 days of rest before starting the MWM. The MWM task was performed for one habituation day, followed by four consecutive days of training, and a probe trial was conducted 24h after the last training trial. At the end of the behavioral experiments, the animals were sacrificed for tissue collection and fEPSP recordings.

2.7.1. Open-field test

The OFT is a behavioral paradigm that allows the evaluation of spontaneous and anxious-like behavior, and exploratory and motor activity based on the natural aversion of rodents towards unknown, open and bright spaces, and the conflict between that aversion and the drive towards exploration (Seibenhener and Wooten, 2015). The testing apparatus (Figure 12) consisted of an empty enclosing white box (50 x 50 x 40 cm), virtually divided into three concentric square zones, respectively designated peripheral (PZ), intermediate (IZ) and central zone (CZ), at a similar distance from each other. Each animal was placed individually in the center of the OFT arena and allowed to freely explore it for 10 minutes, after which they were returned to their home cage. Locomotor activity within the first 5 minutes was evaluated by calculating the average velocity (expressed as cm/s) and total distance traveled (expressed as cm). Rearing frequency (standing on the hindlimbs

and scanning the environment from an elevated perspective) was used to measure exploratory behavior considering its relevance as a marker of behavioral responses to environmental novelty (Lever et al., 2006; Sturman et al., 2018). Moreover, to evaluate the anxious-like behavior of these mice, the time spent in the center was assessed (Seibenhener and Wooten, 2015; Sturman et al., 2018).

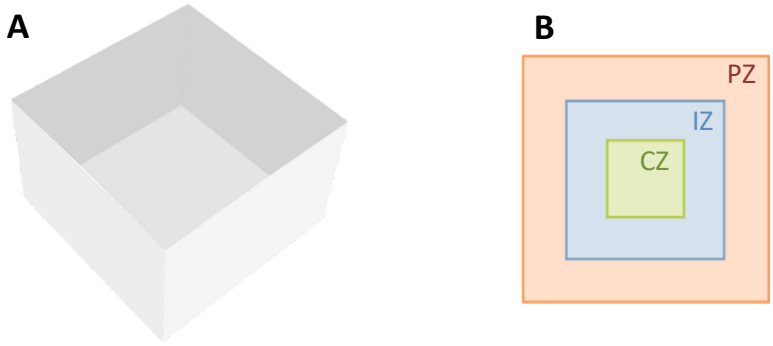

Figure 12: Schematic representation of the OFT. **(A)** The OFT arena consisted of an empty white acrylic square box (50 x 50 x 49 cm), divided in three virtual concentric squares: **(B)** a peripheral (PZ), an intermediate (IZ), and a central zone (CZ) defined by the tracking software, at a similar distance from each other

2.7.2. Y-maze spontaneous alternation

The Y-maze spontaneous alternation test was implemented to evaluate spatial working memory function (and hence intact prefrontal cortical functions), by taking advantage of the willingness of rodents to explore new environments (Brodziak et al., 2014; Kraeuter and Guest, 2019). The Y-maze apparatus consisted of three identical arms (15 cm L x 5 cm W x 12 cm H), (labeled “A”, “B”, and “C”), converging to an equal angle. Visual cues were placed on the walls at the end of two arms of the maze (horizontal black stripes and green dots), to aid the animals in remembering which arms had already been visited (Figure 13, A). Without prior habituation, each mouse was placed at the end of one arm, facing away from the center, and allowed to freely move through the maze for 8 minutes. An entry was considered valid when all four limbs of the animal were within the arm, and a correct alternation was denoted as consecutive entries in three different arms (Gold et al., 2013) (Figure 13, B). To exemplify, an animal performed a total of six entries, in the following sequence: A-B-C-B-A-A. Thus, A-B-C, B-C-B, C-B-A, B-A-A, A-A- and A- were all the actual number of alternations, from which two were considered correct (A-B-C and C-B-A) (Gold et al., 2013). Moreover, the percentage of correct spontaneous alternation was calculated as the number of alternations, divided by the total of arm entries minus 2, and then multiplied by 100 (Gold et al., 2013). In

addition, the total number of arm entries was used as a measure of locomotor activity. The number and sequence of arm entrances were recorded manually.

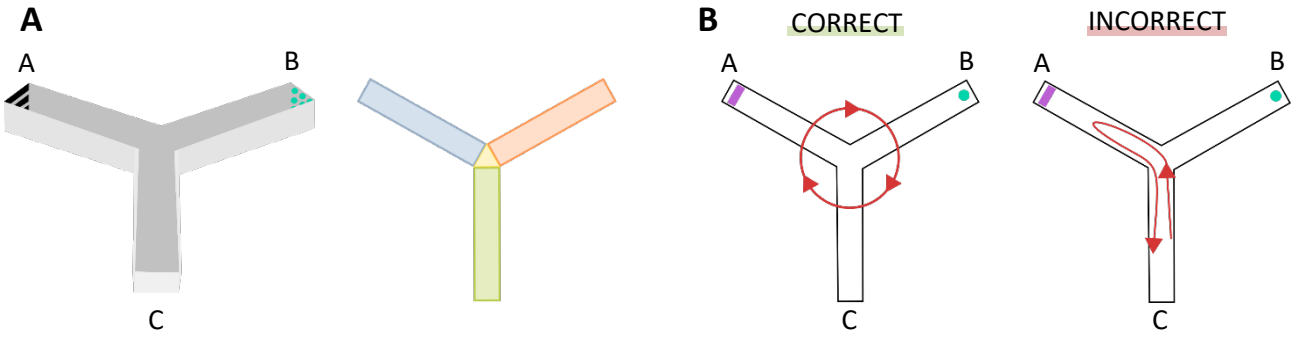

Figure 13: Schematic representation of the Y-maze continuous spontaneous alternation task. (A) Continuous spontaneous alternation task was conducted in the Y-maze apparatus that consists of three white, opaque, and identical arms mounted in the shape of a "Y at a 120° angle from each other, and with visual cues placed on the walls at the end of two arms. **(B)** Schematic illustration showing examples of a correct and an incorrect alternation in the Y-maze test.

2.7.3. Object Location Task

The OLT is divided into three phases and provides a measure of hippocampus-dependent spatial memory (Denninger et al., 2018). This task relies on the spontaneous tendency of animals', previously exposed to two identical objects, to prefer to explore an object in a novel location than explore the non-displaced object. The objects consisted of two lidded golden goblets (base of 5 cm in diameter, 13 cm in height) that were attached to the bottom of the box. The objects were used interchangeably as familiar and novel objects.

In the habituation phase (3 consecutive days) (Figure 14, A), each mouse freely explored the empty OFT arena for 10 minutes. In the familiarization phase, in the fourth day (Figure 14, B), each mouse was presented with the two to-be-familiarized objects (object A and A'), in randomized corners, for 5 minutes. The mouse was then removed from the arena for an inter-trial interval (ITI) of 24h, and one of the objects was moved. After 24h, the mouse was reintroduced to the arena for the test phase (Figure 14, C) and allowed to freely explore for 5 minutes the previously experienced objects, but one was in the same location (object A), and the other was in a new location (object A').

Total exploration time (s) of both objects in the familiarization or test phase was used as a measure of the exploratory drive. Besides, exploration time (%) of both objects in the test phase was used to

validate if both objected, even though indistinguishable, were equally appealing. The novelty discrimination index, assessed in the test phase, was calculated as a measure of relative novelty preference, by dividing the time spent exploring the novel object minus the time spent exploring the familiar object by the total time spent exploring both objects. Animals with hippocampal lesions have impaired spatial contextual learning and consequently demonstrate no preference for objects in the novel location, while animals with a normal hippocampal function will spend more time investigating the moved object (Denninger et al., 2018). Data were obtained by manually recording the time (seconds) that a mouse spent exploring the objects individually. Exploration was scored whenever the animal touched an object with its forepaws and/or bit, sniffed, reared, or climbed towards the object, unless the attention of the animal appears to be somewhere other than the object.

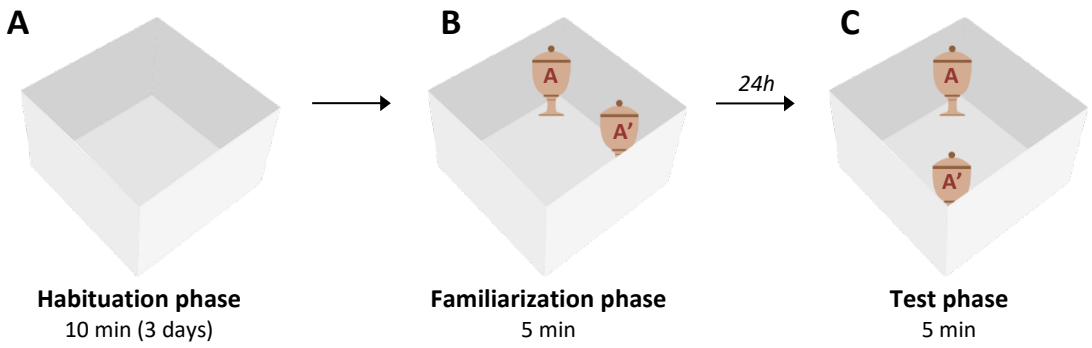

Figure 14: Diagram of OLT tasks. Experimental timeline for OLT: (**A**) OF testing arena without objects for habituation session for three days, (**B**) followed by a single session of familiarization, on the next day, in which two identical objects were presented to the animals for 5 minutes. (**C**) Following a 24h delay, one of the familiar objects was placed in a novel location at testing (5 minutes).

2.7.4. Barnes Maze

The Barnes maze is a dry-land hippocampal-dependent test where animals learn the relationship between distal cues in the surrounding environment and a fixed escape location (Malikowska-racia et al., 2018; Pitts, 2018). The test was conducted in an elevated circular platform with 20 evenly spaced holes around the perimeter, and a small dark recessed box (escape box) located under one of them, while the remaining 19 holes were left empty (Figure 15, A). Visual extra-maze cues were pictures of colored geometric figures with a contrasting background, that remained unaltered for the habituation, acquisition, and probe trial phases. Both loud white noise (70 dB) and bright light

and open spaces are aversive to rodents, thus serving as motivating factors to induce escape behavior. The experimental setup and corresponding procedures for testing and analysis were adapted from Pitts, 2018 and Malikowska-racia et al. 2018.

On the first day of the test (habituation phase, Figure 15, B), mice were individually placed in a cylindrical black start chamber located in the middle of the circular maze. Ten seconds later the mouse was released from the cylindrical black start chamber, the light was turned on, the white noise was played through a loudspeaker, and the animal was gently guided to the escape box where it remained for the next 2 minutes with the lights and noise turned off.

Immediately after the habituation, for four days each mouse was subjected to four trials daily with 15 minutes intervals between each trial. At the start of each trial, each mouse was placed in the start chamber in the center of the arena. After 10 seconds, the start chamber was lifted the light and white noise were turned on, and the mouse was allowed to explore the maze for 180 seconds. The trial concludes when the mouse enters the escape box or 3 minutes elapses. If an animal failed to find the escape tunnel within the 3 minutes, it was guided towards it. Immediately after the mouse entered the box, the light and noise were turned off and the mouse was allowed to stay in the box for 1 minute. During this phase, the number of incorrect holes checked prior to locating the box (primary errors), the latency to locate (primary latency) the escape box (primary latency), the distance traveled (path length) prior to locating the escape box, and speed velocity were measured. In addition, the location of the first hole checked relative to the escape box was tracked, and the values range from 0 (target hole) to 9/-9 and opposite (directly opposite the target hole) (Figure 15 B). The search strategy was classified as direct for 3 or fewer primary errors and primary hole distance, corrected when the animal navigates to a distal region of the target, re-angulates and make a direct movement towards the escape box, serial for trials in which mice spent the majority of the time on the periphery performing systematic hole searches in a clockwise or counterclockwise manner, or random for other searches (Figure 15, C) (Illouz et al., 2016; Pitts, 2018). On day 5, 24h after the final session of acquisition training, the assessment of reference short-term memory was conducted by a probe trial in which the escape tunnel was removed from the apparatus (Figure 15, B). Each mouse was placed in the center of the apparatus inside the cylindrical black start chamber for 10 seconds. After its removal, the mouse was allowed to explore the maze for 90 seconds. For the probe trial, the percentage of time spent in target and nontarget zones were recorded, along with the number of nose pokes in each hole.

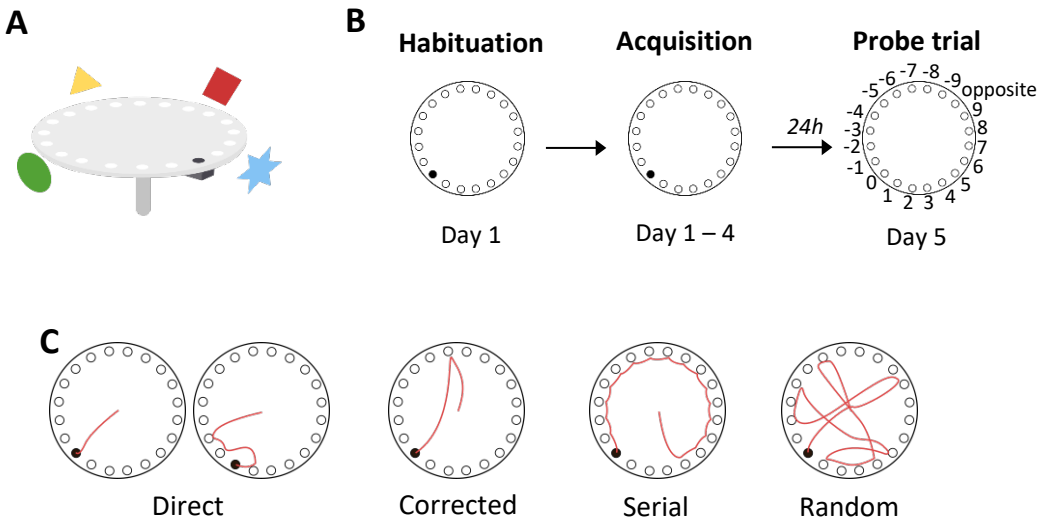

Figure 15: Schematic representation of Barnes Maze test. (A) Diagram of Barnes maze apparatus. **(B)** Schematic outline of full behavioral paradigm. Mice were submitted to the habituation phase, followed by the acquisition phase (four series of four-trial daily training). On the day after the last training day, the animals were tested for task retrieval (90 s probe trial). **(C)** Search strategies used by mice to locate the hidden escape box were classified as direct, that reflects the optimal acquisition of the target's location, corrected, that reflects a slightly lower efficiency, as the animal makes a minor correction in the trajectory towards the target, serial, that reflects a systematic non-spatial method of enhancing the probability of finding the target, and random searches that reflect no acquisition of the target location.

2.7.5. Morris Water Maze

The MWM is a test of spatial learning for rodents that relies on distal cues to navigate from start locations around the perimeter of an open swimming arena to locate a submerged escape platform. It is strongly correlated with hippocampal synaptic plasticity and NMDAR function (Vorhees and Williams, 2006). The test was conducted under dim light in a dark circular pool (110 cm diameter) filled with water at RT. Imaginary lines were dividing the tank into four quadrants, one of which contains a circular and adaptable platform, with a diameter of 8 cm (Figure 16, A). To increase the contrast to detect the mice, water was made opaque with the addition of non-toxic white paint. After each trial, mice were placed in their cages under a heat lamp to prevent hypothermia.

During the habituation day, each mouse should learn that the final goal is to reach the platform and remain there. The habituation consisted of two trials, starting with the platform centered in the pool above the water and each mouse was required to complete 1 minute on the platform (Figure 16, B). This same process was performed in a second trial, with the difference of the platform being placed

1 cm under the surface of the water. In case an animal jumps into the water, it would be manually guided back until completed 1 minute on the platform.

During the learning phase, the protocol consisted of a hippocampal-dependent task whose goal was to assess the ability of mice to learn the position of the hidden platform kept always in the same position. Extrinsic visual cues (square, triangle, horizontal stripes and cross with different colors) were placed outside the pool walls and the platform was hidden 1 cm below the surface at the center of the quadrant. The starting point was randomized between trials and was never on the same quadrant of the platform, nor on its interactions with neighbor quadrants. For instance, if the platform was placed on the first quadrant (Q1), the starting point was not 1, 1/2 nor 4/1 (Figure 16, A). Four consecutive trials, separated by approximately 30 seconds intervals, were performed on each mouse per day (Figure 16, B) (Sardinha et al., 2017). At each trial, the animal was placed in the pool facing the maze wall and oriented to each of the extrinsic cues in random order, and allowed to explore and reach the platform within 60 seconds. Once the platform was found, the mouse was allowed to stay there for 30 seconds. However, if the platform was not found by the end of 60 seconds, the mouse was manually guided to the platform for 30 seconds. Distances swum of each animal to reach the platform was registered to evaluate the learning progression during this phase. Therefore, animals with shorter distance swam display better reference memory. Besides, since the formation of spatial memory in the WMW depends on the function of the hippocampus in rodents, the strategy performed by the animals in each trial was evaluated and classified in spatial hippocampus-dependent search strategies (direct finding, approaching target and self orienting) and random hippocampus-independent search strategies (random searching, circling and thigmotaxis) (Graziano et al., 2003) (Figure 16, C).

The probe test was performed on the last day, consisting of a single trial in which the platform was removed, and the mouse swam freely for 60 seconds. Results concerning learning and memory performance during this phase are presented as time spent in the correct quadrant (%) and the number of crossings of the platform zone of each animal.

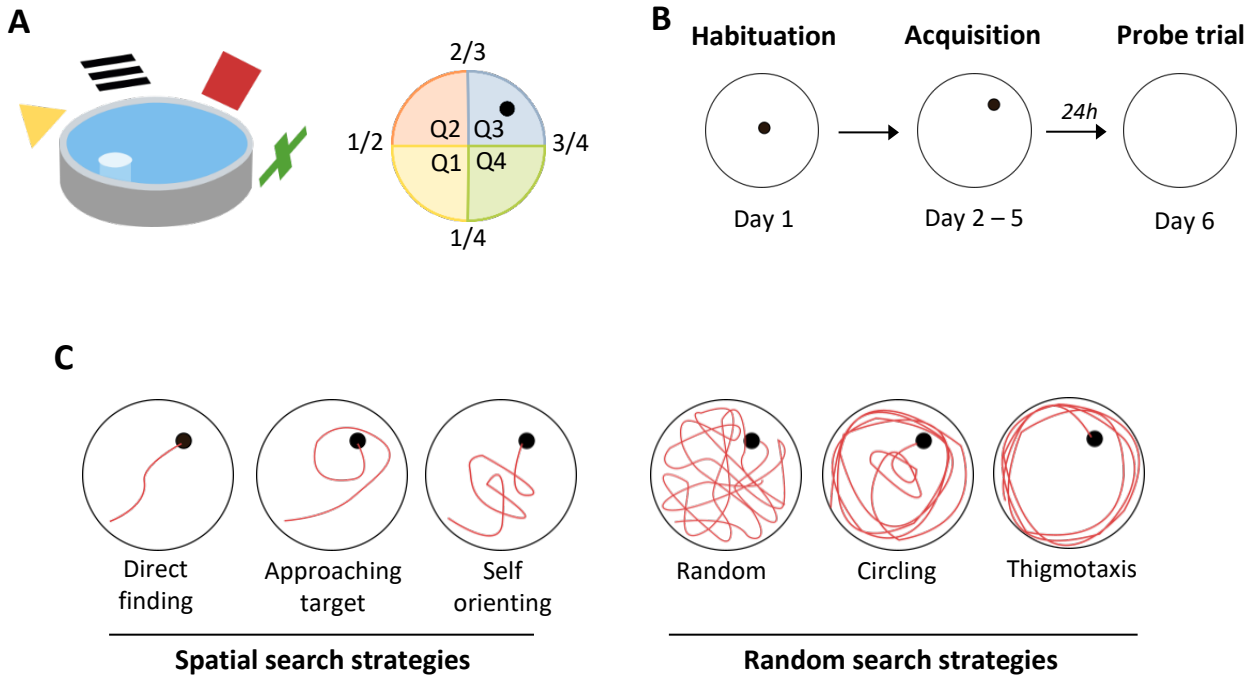

Figure 16: Schematic representation of the MWM test. A. Schematic representation of the MWM with virtual quadrants (Q1-4). **B.** Initial visible platform trial, followed by a central hidden platform trial were conducted as a means of habituation. After, mice are trained to navigate to a platform located below the water's surface for four days. In a subsequent probe trial, the platform is removed and the animals' memory is evaluated by their swimming persistence in the surroundings of the previous platform location. **C.** Search strategies were categorized in spatial hippocampus-dependent search strategies (direct finding, approaching target and self orienting), that rely on distal cues to locate the escape platform, and random hippocampus-independent search strategies (random searching, circling and thigmotaxis).

3. Results

3.1. Role of astrocytic signaling in the modulation of synaptic plasticity, and cognitive functions

To assess the contribution of astrocytes to synaptic plasticity, and learning and memory processes, the transgenic dn-SNARE mice with selectively impaired SNARE complex-dependent gliotransmitter release from astrocytes and their respective controls were used (Pascual et al., 2005). Accordingly, fEPSPs were recorded in hippocampal CA1-CA3 synapses and θ-burst stimulation was used to induce LTP to evaluate synaptic plasticity.

3.1.1. Validation of the dn-SNARE mouse model

Despite being a widely used model, the effectiveness of dn-SNARE mouse model as a good model to study SNARE-dependent vesicular release of astrocytic gliotransmitters was questioned (Fujita et al., 2014). Although efforts have been made to produce evidence to support this model (Lalo et al., 2021b; Pascual et al., 2005; Sardinha et al., 2017; Sultan et al., 2015), we performed complementary experiments to revalidate the dn-SNARE mouse model, and thus highlight astrocytes contribution to neurotransmission through SNARE-dependent release of gliotransmitters.

3.1.1.1. Transgene detection and quantification

As previously described, dn-SNARE animals are equipped with Lac-Z, EGFP, and dn-SNARE genes on their astrocytes, and when Dox is removed, they start to express the dn-SNARE domain. Since dn-SNARE protein levels are hard to detect in brain samples, as the available antibodies detect equally both exogenous and endogenous forms of synaptobrevin II, dn-SNARE transgene protein levels were indirectly screened by EGFP quantification, since EGFP levels are directly correlated with the dn-SNARE transgene expression (Sardinha et al., 2017). The results indicate that the transgene is specific for dn-SNARE mice (Wt: 0.03±0.01, n=10; dn-SNARE: 1.77±0.21, n=14; ***p≤0.001; Figure 17, A), supporting the genotyping data. Moreover, it was also observed that GFP has a variable expression across dn-SNARE animals (Figure 17, B).

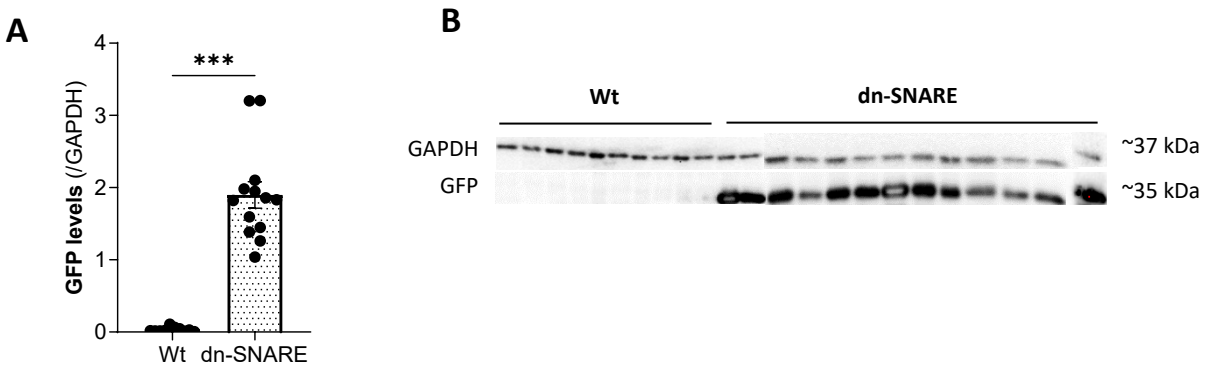

Figure 17: Quantification of the transgene reporter GFP in the hippocampus of Wt and dn-SNARE mice. A. Histogram shows membrane intensity of the ratio of GFP/GAPDH (n=10-14). **B.** Western-blots of hippocampal slices tissue samples from dn-SNARE and Wt mice depict immunoreactive bands for EGFP (~35 kDa) and GAPDH (loading control; ~37 kDa). All values are presented as mean ± S.E.M. from *n* independent observations. Statistical significance was assessed by unpaired t-test.

3.1.1.2. Immunofluorescence analysis

To verify astrocyte specificity of transgene expression, immunofluorescence staining was conducted on brain slices containing the hippocampus from Wt and dn-SNARE mice. Taking advantage of the innate EGFP fluorescence, antibodies to label astrocytic or neuronal markers were used to appraise co-localization.

Immunohistochemical analysis confirmed that EGFP co-localizes with GFAP-positive astrocytes in the dorsal CA1 area of dn-SNARE mice and is absent in the dorsal CA1 region of Wt mice hippocampus (Figure 18 A, B). Moreover, to support astrocyte specificity and to exclude the neuronal expression of the dn-SNARE transgene, immunostainings with βIII-tubulin, that stains neurites, was performed. The staining failed to show overlap between EGFP and βIII-tubulin at the CA1 area of dn-SNARE animals (Figure 18, C). Therefore, combined with previous reports (Halassa et al., 2009; Pascual et al., 2005; Sardinha et al., 2017), these results support astrocyte-specific dn-SNARE expression and exclude the potential neuronal expression of dn-SNARE transgene.

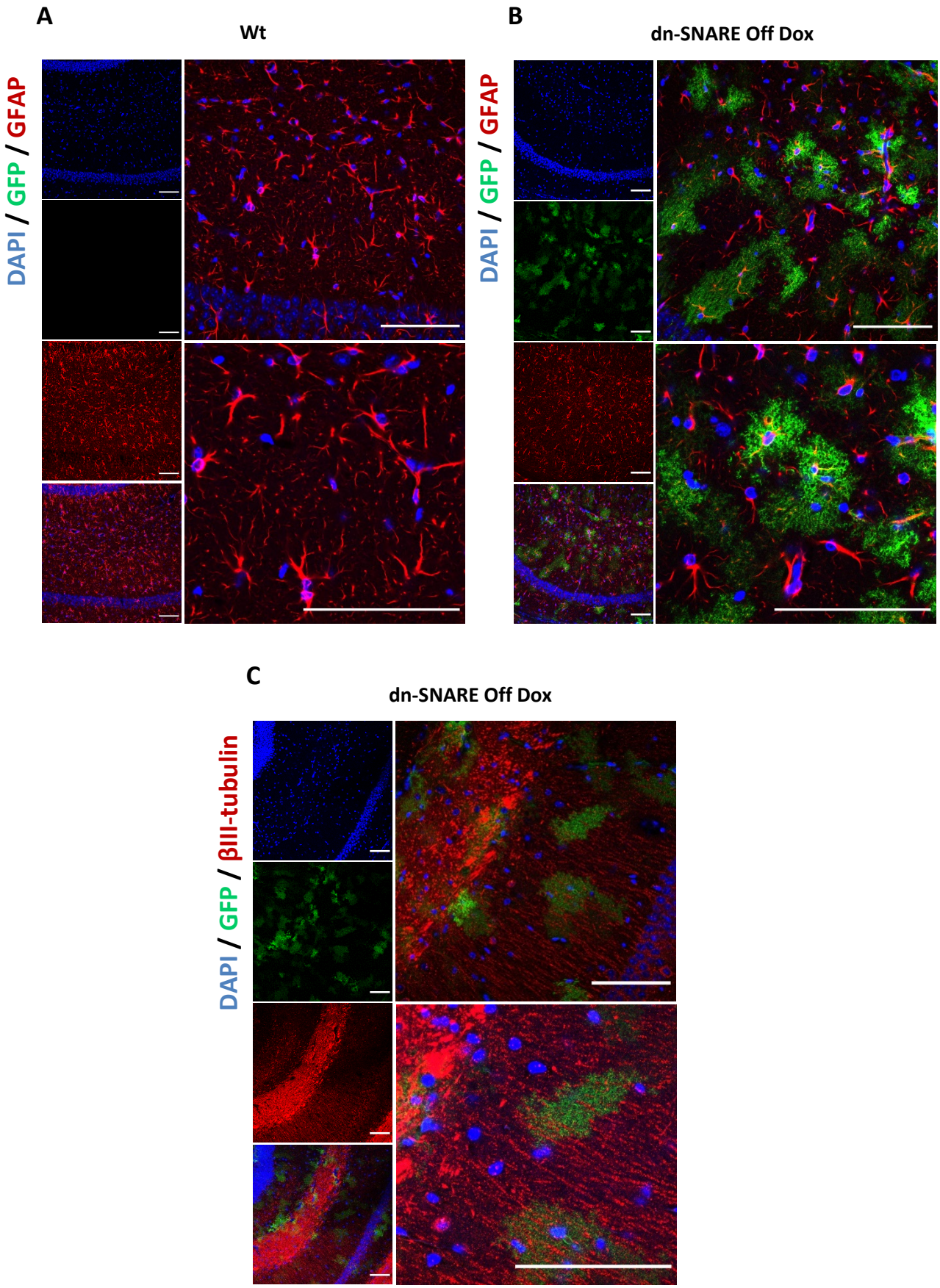

Figure 18: dn-SNARE transgene expression is astrocyte-specific. Representative confocal images of **(A)** GFP reporter transgene (green) with GFAP (red) and DAPI (blue) in the dorsal CA1 of Wt mice, of **(B)** GFP reporter transgene (green)

with GFAP (red) and DAPI (blue) in the dorsal CA1 of dn-SNARE mice, and **(C)** GFP reporter transgene (green) with βIII-tubulin (red) and DAPI (blue) in the dorsal CA1 of dn-SNARE mice. Scale bars = 100 µm.

3.1.2. Electrophysiological testing of dn-SNARE mice: Synaptic plasticity

To study the role of SNARE-dependent gliotransmission in hippocampal synaptic plasticity, LTP at CA3-CA1 synapses was elicited by delivering a weak θ-burst (4x) stimulation protocol to hippocampal slices from Wt and dn-SNARE mice. All dn-SNARE animals used in this thesis had Dox removed from the diet, at 4 weeks of age, to induce the expression of the dn-SNARE transgenes.

Weak θ-burst stimulation of hippocampal slices from Wt mice leads to an initial enhancement of the fEPSP slope followed by a decrease and stabilization period. At the end of the recording interval (50-60min after θ-burst), fEPSP slope values remained higher than before θ-burst stimulation (55.82±3.22%, n=9, Figure 19 A and B). In dn-SNARE animals, where the SNARE-dependent release of gliotransmitters was selectively compromised, the LTP magnitude was 34.48±6.02% (n=10, Figure 19 B), corresponding to an increase, when compared to pre-θ-burst values. Statistical analysis was applied and LTP magnitude is significantly smaller in dn-SNARE mice in comparison to Wt mice (**p≤0.01, Figure 18 A and B).

Overall, these results are indicative of an astrocytic regulation, through SNARE-dependent release of gliotransmitters, of the strength of long-term forms of synaptic plasticity, as previously reported in the literature (Pascual et al., 2005).

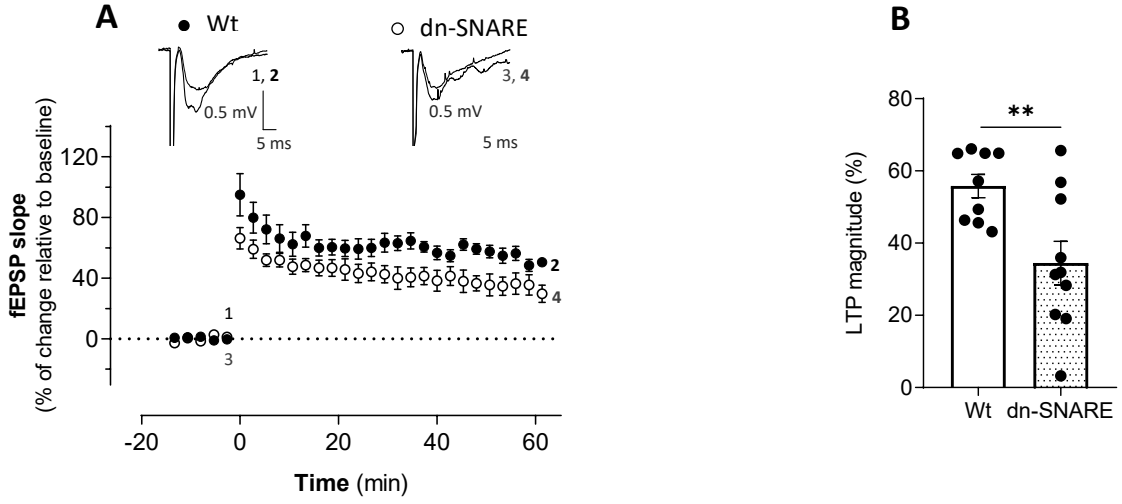

Figure 19: SNARE-dependent gliotransmission modulates LTP. (**A).** Represents the time course of averaged normalized changes in fEPSP slope after delivery of a weak θ-burst (4x4) to hippocampal slices from Wt (n=9) and dn-SNARE (n=10)

mice (8–12 weeks). The ordinates represent normalized fEPSP slopes, where 0% corresponds to the average five slopes recorded before θ-burst stimulation and the abscissa represents the time that averages begun. On top are shown the corresponding representative traces of fEPSPs recorded before (thin line) and 58-60 min after (bold line) θ-burst stimulation. Each trace is the average of eight consecutive responses obtained from slices from Wt and dn-SNARE mice and is composed by the stimulus artifact, followed by the presynaptic fiber volley and the fEPSP. Scale bar: 5 ms (horizontal), 0.5 mV (vertical). **(B).** Comparison of the magnitude of LTP (change in fEPSP slope at 50-60 min) induced by weak θ-burst stimulation obtained in the experiments illustrated in (A). LTP magnitude was quantified as the % of the change in fEPSP slope recorded at the 50–60 min after LTP induction, in comparison to the average slope of the baseline fEPSP. All values are presented as mean ± standard error of mean (S.E.M.) from *n* independent observations. Statistical significance was assessed by paired t-test.

3.2. The role of SNARE-dependent gliotransmitters release Aβ-mediated toxicity on hippocampal synaptic plasticity

To investigate the role of SNARE-dependent gliotransmission upon Aβ-mediated effect on synaptic plasticity, the transgenic dn-SNARE mice and their respective controls were used. Accordingly, LTP at CA3-CA1 synapses was elicited by delivering θ-burst stimulation protocol to hippocampal slices from Wt and dn-SNARE mice incubated with $A\beta_{1-42}$ oligomers (200 nM) for 3h. The θ-burst stimulation of hippocampal slices from Wt mice incubated with $A\beta_{1-42}$ oligomers led to an initial increase of the fEPSP slope followed by a progressive decrease towards pre-θ-burst levels, reaching a value below the baseline values at the end of the LTP recording period ($Wt_{Control}$: 55.82±3.22%, n=9; $Wt_{A\beta}$: -9.87±6.52%, n=7; ***p≤0.001, Figure 20 A, C). Nonetheless, when the same paradigm of weak θ-burst stimulation was applied in slices incubated with $A\beta_{1-42}$ oligomers (200 nM) from dn-SNARE mice, LTP magnitude increased when compared to pre-θ-burst values, and no significant differences were found between hippocampal slices from dn-SNARE mice incubated or not with $A\beta_{1-42}$ oligomers (dn-$SNARE_{Control}$: 34.48±6.02%, n=10; dn-$SNARE_{A\beta}$: 24.62±4.11%, n=8; p>0.05, Figure 20 B, C). Therefore, $A\beta_{1-42}$ oligomers can impair LTP only in animals with functional gliotransmission, thus suggesting a critical role of SNARE-dependent gliotransmission upon Aβ-triggered synaptic plasticity deficits.

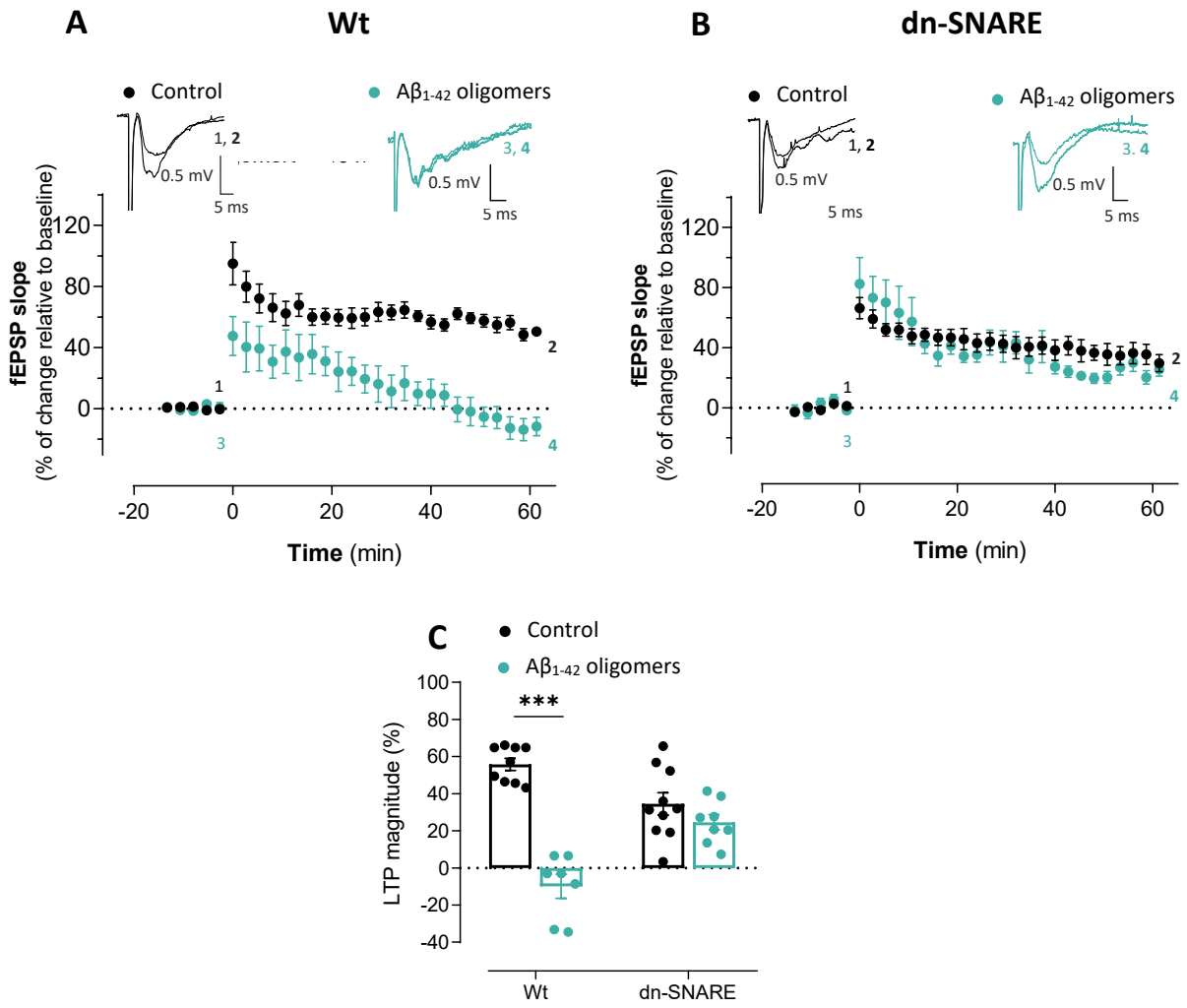

Figure 20: Blocking SNARE-dependent gliotransmission reverts LTP impairment mediated by Aβ$_{1-42}$ oligomers. (A) Averaged time courses changes in fEPSP slope induced by a θ-burst stimulation in Wt mice hippocampal slices without (n=9) or with a pre-exposure for 3 h to aCSF solution containing 200 nM Aβ$_{1-42}$ (n=7). Tracings from representative experiments are shown to top; each tracing is the average of eight consecutive responses obtained before (1 and 3) and 50–60 min after (2 and 4) LTP induction. Tracings are composed of the stimulus artifact, followed by the pre-synaptic volley and the fEPSP. Scale bar: 5 ms (horizontal), 0.5 mV (vertical). **(B)** Averaged time courses changes in fEPSP slope induced by a θ-burst stimulation in dn-SNARE mice hippocampal slices without (n=10) or with a pre-exposure for 3 h to aCSF solution containing 200 nM Aβ$_{1-42}$ (n=8). Tracings from representative experiments are shown to top; each tracing is the average of eight consecutive responses obtained before (1 and 3) and 50–60 min after (2 and 4) LTP induction. Tracings are composed of the stimulus artifact, followed by the pre-synaptic volley and the fEPSP. Scale bar: 5 ms (horizontal), 0.5 mV (vertical). **(C)** Histograms depicting LTP magnitude (change in fEPSP slope at 46–60 min) induced by θ-burst stimulation in the presence and absence of Aβ$_{1-42}$ for Wt and dn-SNARE pretreated slices. All values are presented as mean ± S.E.M. from *n* independent observations. Statistical significance was assessed by Two-way ANOVA followed by Holm-Sidak's *post hoc* test for multiple comparisons.

3.3. Astrocytes as the main source of D-serine

D-serine, synthesized from L-serine (that shuttles to neurons from astrocytes) is a well-established sNMDAR co-agonist that lacks robust evidence of its primary source (Coyle et al., 2020). Thus, to investigate the role of astrocytic D-serine in synaptic plasticity, the transgenic dn-SNARE mice with selectively impaired Ca^{2+}-dependent gliotransmission from astrocytes and their respective controls were used. Accordingly, fEPSPs were recorded and θ-burst stimulation was used to induce LTP to evaluate synaptic plasticity in the presence of D-serine (10 μM) and L-serine (10 and 50 μM).

3.3.1. Synaptic plasticity: Wt and dn-SNARE hippocampal slices perfused with D-serine

To unveil, the effects of D-serine (NMDAR co-agonist) upon synaptic plasticity, LTP at CA3-CA1 synapses was elicited by delivering a weak θ-burst stimulation protocol to hippocampal slices from Wt and dn-SNARE mice after D-serine perfusion. Weak θ-burst stimulation of hippocampal slices from Wt mice perfused with 10μM of D-serine at least 15 minutes prior to recordings lead to an initial enhancement of the fEPSP slope followed by a decrease and stabilization period, reaching similar values to the control condition at the end of the LTP recording period ($Wt_{Control}$: 55.82±3.22%, n=9; $Wt_{D\text{-}serine}$: 43.95±9.45%, n=9; $p>0.05$, Figure 21 A, C). When the same paradigm of θ-burst stimulation was applied after perfusion of D-serine in slices from dn-SNARE mice, the LTP magnitude increased when compared to pre-θ-burst values, reaching higher values than the control dn-SNARE 50-60 min after LTP induction ($dn\text{-}SNARE_{Control}$: 34.48±6.02%, n=10; $dn\text{-}SNARE_{D\text{-}serine}$: 53.05±8.60%, n=6, $p>0.05$, Figure 21 B, C). Therefore, D-serine shows a tendency to potentiate LTP only in animals with compromised gliotransmission, to values similar to controls, thus, suggesting a role of astrocytic SNARE-dependent exocytosis in the release of D-serine.

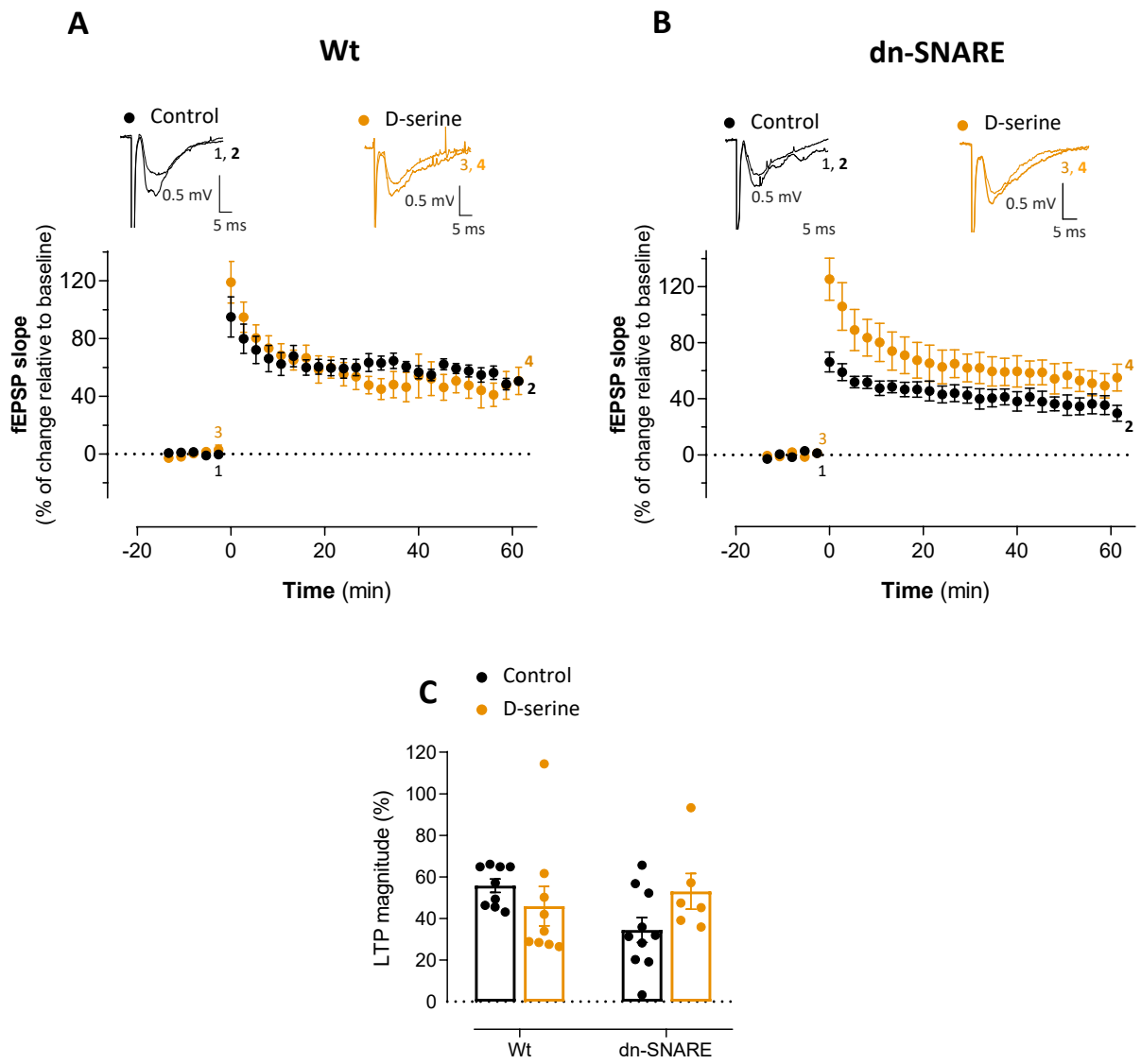

Figure 21: D-serine tends to increase LTP only in animals with compromised gliotransmission: (A) Averaged time courses changes in fEPSP slope induced by a θ-burst stimulation in Wt mice perfused with D-serine (n=9) and the respective controls (n=9). Tracings from representative experiments are shown to top; each tracing is the average of eight consecutive responses obtained before (1 and 3) and 50–60 min after (2 and 4) LTP induction. Tracings are composed of the stimulus artifact, followed by the pre-synaptic volley and the fEPSP. Scale bar: 5 ms (horizontal), 0.5 mV (vertical). **(B)** Averaged time courses changes in fEPSP slope induced by a θ-burst stimulation in dn-SNARE mice perfused with D-serine (n=6) and the respective controls (n=10). Tracings from representative experiments are shown to top; each tracing is the average of eight consecutive responses obtained before (1 and 3) and 50–60 min after (2 and 4) LTP induction. Tracings are composed of the stimulus artifact, followed by the pre-synaptic volley and the fEPSP. Scale bar: 5 ms (horizontal), 0.5 mV (vertical). **(C)** Histograms depicting LTP magnitude (change in fEPSP slope at 46–60 min) induced by θ-burst stimulation in the presence and absence of D-serine for Wt and dn-SNARE perfused slices. All values are presented as mean ± S.E.M. from *n* independent observations. Statistical significance was assessed by Two-way ANOVA followed by Holm-Sidak's *post hoc* test for multiple comparisons.

3.3.2. Synaptic plasticity: Wt and dn-SNARE hippocampal slices perfused with L-serine

To unravel the source of D-serine, hippocampal slices from Wt and dn-SNARE mice were perfused with 10 µM and 50 µM of L-serine to assess its effect in synaptic plasticity. Thereby, LTP at CA3-CA1 synapses was elicited by delivering a weak θ-burst (4x) stimulation protocol.

Weak θ-burst stimulation of hippocampal slices from Wt mice perfused with 10 or 50 µM of L-serine at least 15 minutes prior to recordings lead to an initial enhancement of the fEPSP slope followed by a decrease and stabilization period, reaching similar values to the control condition at the end of the LTP recording period ($Wt_{Control}$: 55.82±3.22%, n=9; $Wt_{L\text{-}serine10\mu M}$: 31.94±4.78%, n=6; $Wt_{L\text{-}serine50\mu M}$: 42.92±11.14%, n=7; p>0.05 Figure 22 A, C). Notably, in hippocampal slices from dn-SNARE mice, where the SNARE-dependent release of gliotransmitters was selectively compromised, LTP magnitude increased when compared to pre θ-burst values with both L-serine concentrations, reaching similar values to the control condition 50-60 min after LTP induction (dn-$SNARE_{Control}$: 34.482±6.015%, n=10; dn-$SNARE_{D\text{-}serine10\mu M}$: 25.093±9.796%, n=8; dn-$SNARE_{D\text{-}serine50\mu M}$: 42.922±11.136%, n=6; p>0.05, Figure 22 B, C). Thus, since in animals with compromised gliotransmission different effects were obtained using D-serine and L-serine (D-serine precursor), these data evidence the importance of astrocytic SNARE-dependent exocytosis in the release of D-serine.

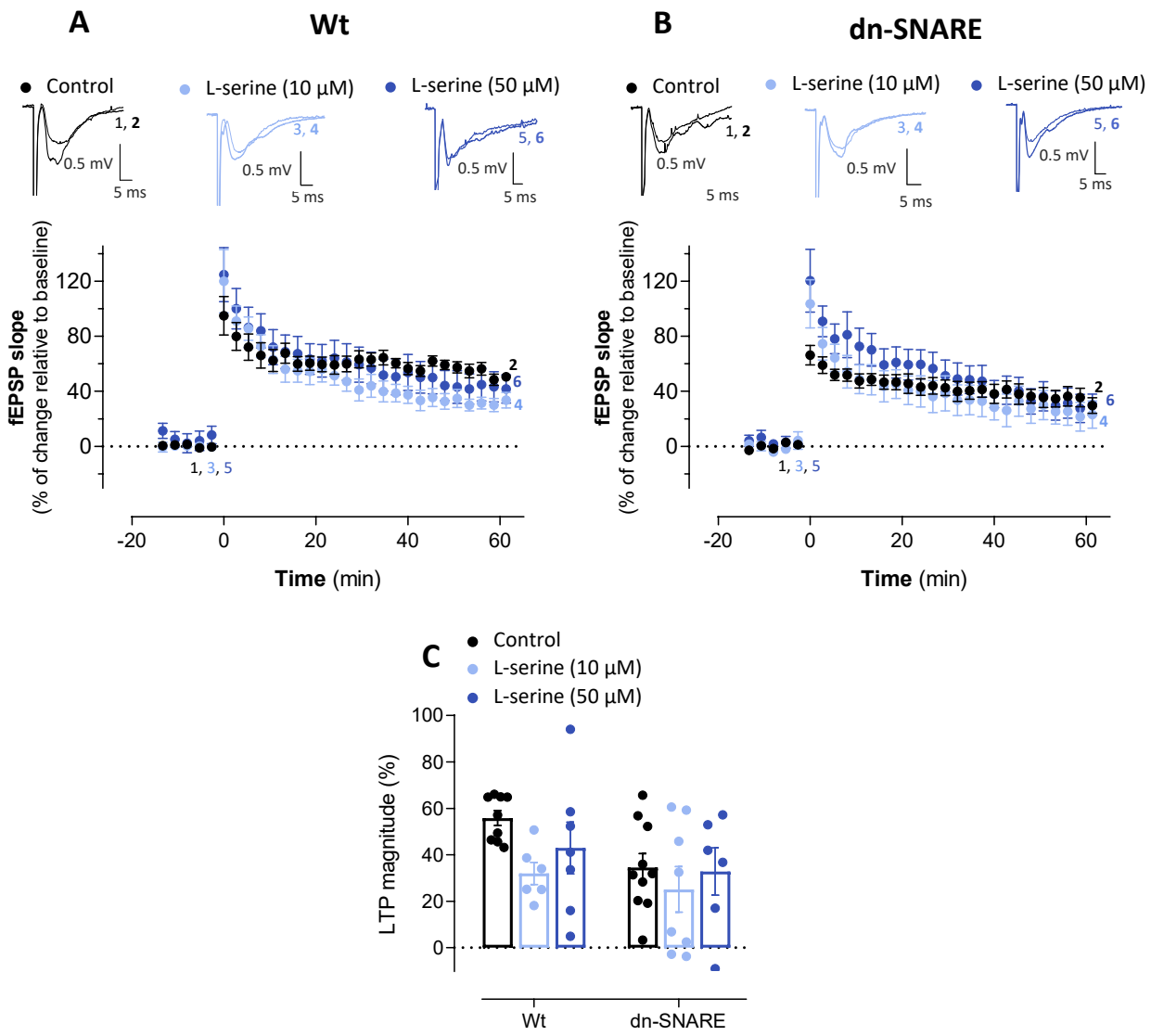

Figure 22: L-serine does not alter LTP in animals with compromised gliotransmission. (A) Averaged time courses changes in fEPSP slope induced by a θ-burst stimulation in Wt mice perfused with 10 µM (n=6) or 50 µM of L-serine (n=7), and the respective controls (n=9). Tracings from representative experiments are shown to top; each tracing is the average of eight consecutive responses obtained before (1, 3 and 5) and 50–60 min after (2, 4 and 6) LTP induction. Tracings are composed of the stimulus artifact, followed by the pre-synaptic volley and the fEPSP. Scale bar: 5 ms (horizontal), 0.5 mV (vertical). **(B)** Averaged time courses changes in fEPSP slope induced by a θ-burst stimulation in dn-SNARE mice perfused with 10 µM (n=8) and 50 µM of L-serine (n=6), and the respective controls (n=10). Tracings from representative experiments are shown to top; each tracing is the average of eight consecutive responses obtained before (1, 3 and 5) and 50–60 min after (2, 4 and 6) LTP induction. Tracings are composed of the stimulus artifact, followed by the pre-synaptic volley and the fEPSP. Scale bar: 5 ms (horizontal), 0.5 mV (vertical). **(C)** Histograms depicting LTP magnitude (change in fEPSP slope at 46–60 min) induced by θ-burst stimulation obtained in the experiments illustrated in (A) and (B). All values are presented as mean ± S.E.M. from *n* independent observations. Statistical significance was assessed by Two-way ANOVA followed by Holm-Sidak's *post hoc* test for multiple comparisons.

3.4. LTP-impairment triggered by Aβ-oligomers was rescued by supplying exogenous D-serine

Considering that Aβ accumulation dysregulates astrocytes and that underactivation of sNMDAR suppresses the induction of LTP, hippocampal slices from dn-SNARE mice (with impaired gliotransmission) and their respective controls were perfused with D-serine, after exposure to $A\beta_{1-42}$ oligomers, to test whether sNMDAR activation, by D-serine, can rescue the aberrant engagement of synaptic mechanisms triggered by Aβ. Thereby, LTP at CA3-CA1 synapses was elicited by delivering a weak θ-burst (4x) stimulation protocol to hippocampal slices from Wt and dn-SNARE mice after $A\beta_{1-42}$-oligomers (200 nM) pre-treatment for 3h with posterior D-serine (10 µM) perfusion.

Weak θ-burst (4x4) stimulation applied in hippocampal slices from Wt mice exposed to $A\beta_{1-42}$ oligomers and perfused with D-serine led to an increase of fEPSP slope 50-60 min after LTP induction in comparison to pre-θ-burst values ($Wt_{Control}$: 55.82±3.22%, n=9; $Wt_{A\beta}$: -9.87±6.52%, n=7, ***p≤0.001; $Wt_{A\beta+D\text{-}serine}$: 34.91±9.97%, n=8, p>0.05; Figure 23 A, C), which corresponds to a significant increase of LTP when compared with the presence of Aβ1-42 oligomers alone (** p≤0.01, Figure 23 A, C). Moreover, when the same paradigm of weak θ-burst stimulation protocol was applied in hippocampal slices derived from dn-SNARE mice, LTP magnitude slightly increased when compared to control and $A\beta_{1-42}$ oligomers alone ($dn\text{-}SNARE_{Control}$: 34.49±6.02%, n=10; $dn\text{-}SNARE_{A\beta}$: 24.62±4.11%, n=8; $dn\text{-}SNARE_{A\beta+D\text{-}serine}$: 48.90±14.97%, n=5; p>0.05, Figure 23 B, C).

Therefore, these results demonstrate that even though $A\beta_{1-42}$ oligomers can impair LTP in animals with functional gliotransmission, D-serine appears to have a benefic effect in LTP rescue. Besides, LTP magnitude in significantly improved in hippocampal slices from dn-SNARE mice exposed to $A\beta_{1-42}$ oligomers and D-serine compared to Wt treated with $A\beta_{1-42}$ oligomers (***p≤0.001, Figure 23 C), which suggests that modulation gliotransmission (by potentially blocking glutamate release) and supplementing D-serine may be advantageous in AD.

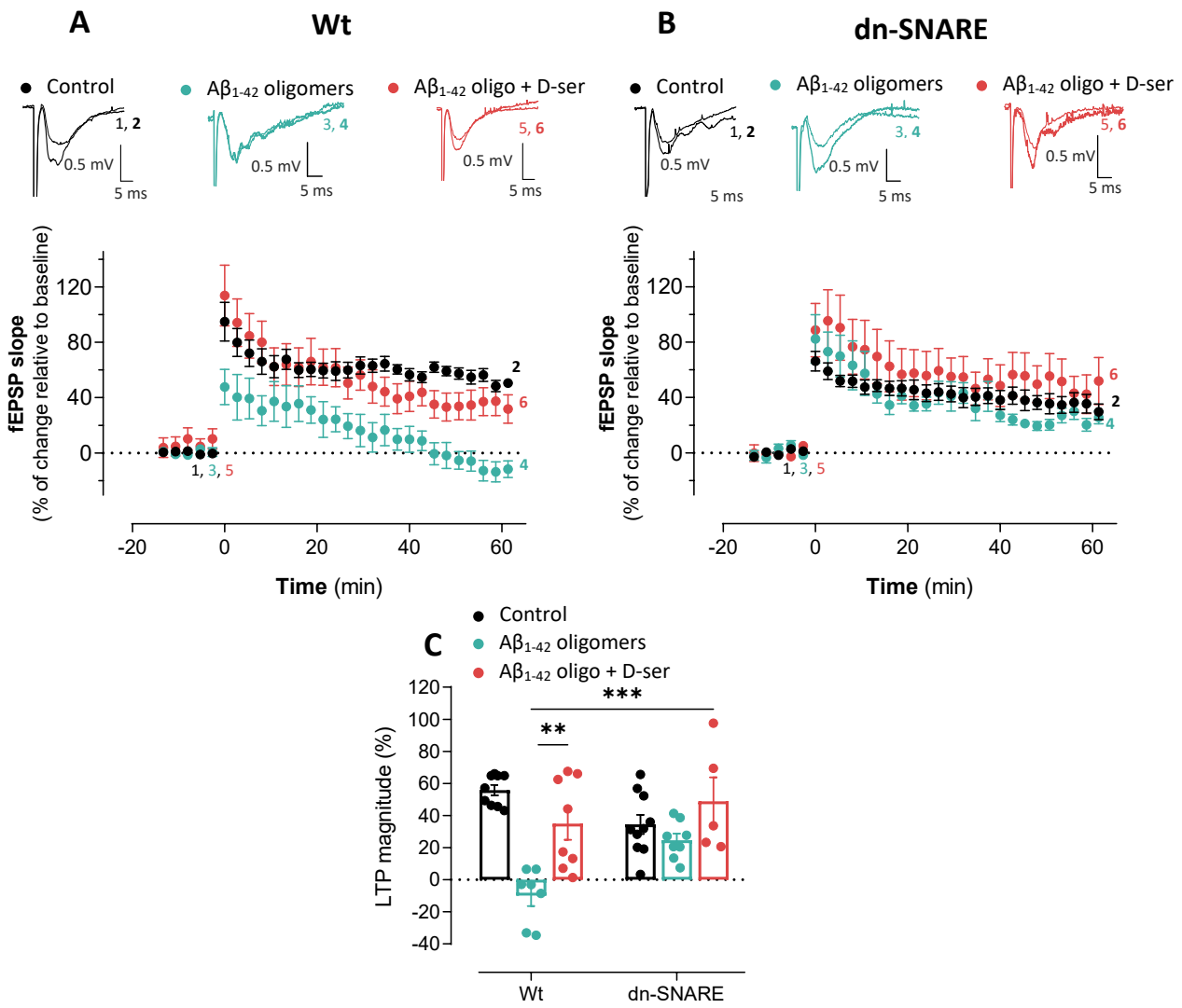

Figure 23: D-serine rescues the deficit of Aβ-induced LTP. (A) Averaged time courses changes in fEPSP slope induced by a θ-burst stimulation in Wt mice pre-treated with $A\beta_{1\text{-}42}$ oligomers alone (n=6), with both with $A\beta_{1\text{-}42}$ oligomers and D-serine (n=8) and the respective controls (n=9). Tracings from representative experiments are shown to top; each tracing is the average of eight consecutive responses obtained before (1, 3 and 5) and 50–60 min after (2, 4 and 6) LTP induction. Tracings are composed of the stimulus artifact, followed by the pre-synaptic volley and the fEPSP. Scale bar: 5 ms (horizontal), 0.5 mV (vertical). **(B)** Averaged time courses changes in fEPSP slope induced by a θ-burst stimulation in dn-SNARE mice pre-treated with $A\beta_{1\text{-}42}$ oligomers alone (n=8), with both with $A\beta_{1\text{-}42}$ oligomers and D-serine (n=5) and the respective controls (n=10). Tracings from representative experiments are shown to top; each tracing is the average of eight consecutive responses obtained before (1, 3 and 5) and 50–60 min after (2, 4 and 6) LTP induction. Tracings are composed of the stimulus artifact, followed by the pre-synaptic volley and the fEPSP. Scale bar: 5 ms (horizontal), 0.5 mV (vertical). **(C)** Histograms depicting LTP magnitude (change in fEPSP slope at 46–60 min) induced by θ-burst stimulation obtained in the experiments illustrated in (A) and (B). LTP magnitude was quantified as the % of change in fEPSP slope recorded at the 50–60 min after LTP induction, in relation to the average slope of the baseline fEPSP. All values are presented as mean ± S.E.M. from *n* independent observations. Statistical significance was assessed by Two-way ANOVA followed by Holm-Sidak's *post hoc* test for multiple comparisons

3.5. The role of SNARE-dependent gliotransmitters release in Alzheimer's disease: memory and learning impairment

To unravel the implication of astrocyte-derived gliotransmitters to cognitive deficits in AD, we aimed to recapitulate *in vivo* features that are suspected to account for triggering AD. Thus, two-month-old Wt and dn-SNARE mice were injected into the hippocampus with AAV-based transfer of human mutant APP and PS1 genes, to mimic *in vivo* APP processing closer to the human situation in AD (Audrain et al., 2016). In this set of experiments, AAV-PS1 injection will function as the disease control (Wt-PS1 and dn-SNARE-PS1) and AAV-APP/PS1 injection (Wt-APP/PS1 and dn-SNARE-APP/PS1) will work as the APP-mediated AD condition. Three months after injections, all groups of animals were submitted to different behavior tests, including the OFT, Y-maze, OLT, Barnes Maze, and MWM. Afterward, fEPSPs were recorded and θ-burst stimulation was used to induce LTP and evaluate synaptic plasticity of Wt and dn-SNARE injected with AAV-PS1 or AAV-APP/PS1.

3.5.1. Validation of the AD model: Western blot quantification

To validate the generated AAV vectors encoding human mutant full-length PS1M146L (AAV-PS1) and human mutant APPSL (AAV-APP), only AAV-APP/PS1 mice should show exogenous human APP expression in the hippocampus (Audrain et al., 2016).

Unexpectedly, western blot analysis of whole hippocampus revealed that the human APP transgene expression was undetectable in the hippocampus of injected Wt ($Wt_{Non\text{-}injected}$: 0.42±0.02, n=3; $Wt_{AAV\text{-}PS1}$: 0.18±0.01, n=3; $Wt_{AAV\text{-}APP/PS1}$: 0.28±0.07, n=4; $p>0.05$, Figure 24 A, B) nor dn-SNARE animals (dn-$SNARE_{AAV\text{-}PS1}$: 0.20, n=1; dn-$SNARE_{AAV\text{-}APP/PS1}$: 0.18±0.05, n=2; Figure 24 A, B).

By contrast, considering previous reports (Audrain et al., 2016), it was anticipated that the total amount of APP (exogenous human + endogenous murine forms) did not differ between non-injected Wt and Wt injected with AAV-PS1 or AAV-APP/PS1 (and similar for dn-SNARE). The results revealed that mice injected with AAV-APP/PS1 have slightly increased expression of total APP when compared to the respective genotype control group (Wt – $Wt_{Non\text{-}injected}$: 0.37±0.03, n=3; $Wt_{AAV\text{-}PS1}$: 0.49±0.07; $Wt_{AAV\text{-}APP/PS1}$: 0.53±0.05, n=4, $p>0.05$; dn-SNARE – dn-$SNARE_{AAV\text{-}PS1}$: 0.27, n=1; dn-$SNARE_{AAV\text{-}APP/PS1}$: 0.35, n=1; Figure 24 C). Together, the results suggest that the anti-human APP antibody failed to show protein expression in the WB, and that AAV-APP/PS1 injection shows a tendency to increase APP levels in the hippocampus.

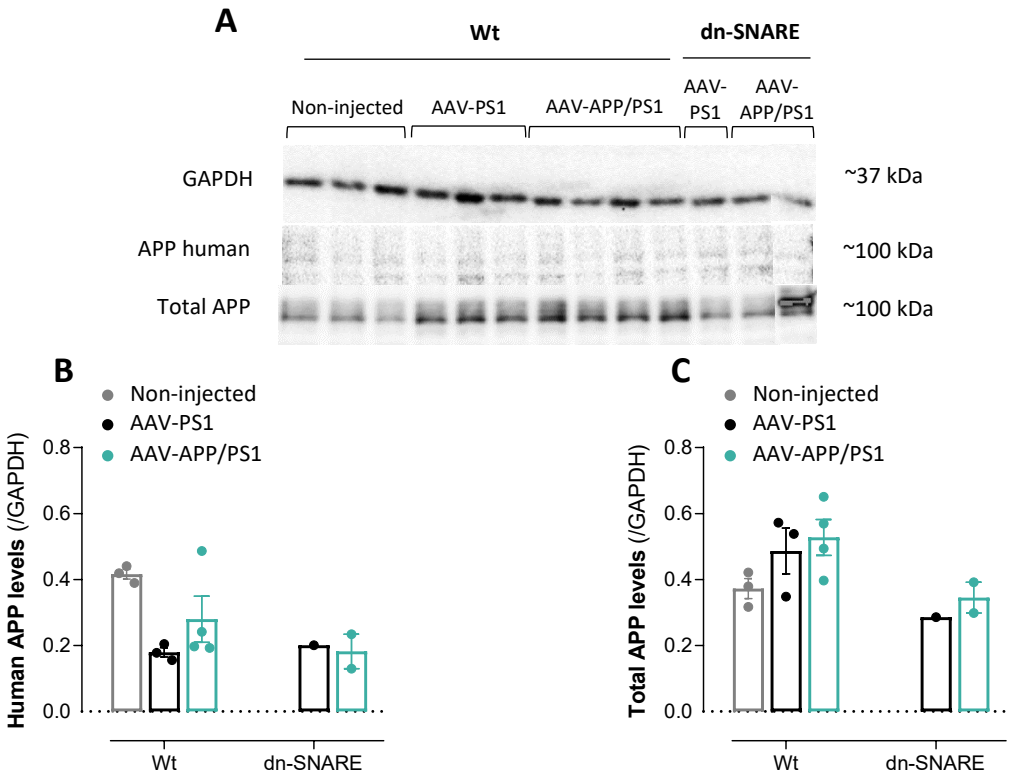

Figure 24: Quantification of human APP and total APP expression in the hippocampus of Wt and dn-SNARE mice 3 months after AAV-PS1 and AAV-APP/PS1 injections. (A) Wester-blots showing the expression of human APP (6E10 antibody, ~100 kDa), total APP (APP C-terminal antibody, ~100 kDa) and GAPDH (loading control; ~37 kDa). **(B)** Histogram of the gel represented in (A), showing membrane intensity of the ratio of human APP/GAPDH from non-injected Wt mice (n=3), Wt injected with AAV-PS1 (n=3), Wt injected with AAV-APP/PS1 (n=4), dn-SNARE injected with AAV-PS1 (n=1) and dn-SNARE injected with AAV-APP/PS1 (n=3). **(C)** Histogram of the gel represented in (A), showing membrane intensity of the ratio of total APP/GAPDH from non-injected Wt mice (n=3), Wt injected with AAV-PS1 (n=3), Wt injected with AAV-APP/PS1 (n=4), dn-SNARE injected with AAV-PS1 (n=1) and dn-SNARE injected with AAV-APP/PS1 (n=3). All values are presented as mean ± S.E.M. from *n* independent observations. Statistical significance was assessed by Two-way ANOVA followed by Holm-Sidak's *post hoc* test for multiple comparisons.

3.5.2. Validation of the AD model: Immunofluorescence analysis

To monitor vector-mediated human APP and total APP expression, immunofluorescence staining was conducted on brain slices containing the hippocampus from Wt (non-injected and injected with AAV-PS1 or AAV-APP/PS1) and dn-SNARE mice (injected with AAV-APP/PS1). Fluorescence intensity was quantified in the dorsal hippocampus in two CA1 and CA2 layers: *stratum pyramidale*, which contains the cell bodies of the excitatory pyramidal neurons, and in the *stratum radiatum*, which contains the *Schaffer collaterals* projections and the synapses that are potentiated in the LTP (Temido-Ferreira et al., 2019).

3.5.2.1. Human APP immunostaining

AAV vectors encoding human mutant full-length PS1M146L (AAV-PS1) and human mutant APPSL (AAV-APP/PS1) were injected bilaterally into the hippocampus of eight-week-old Wt and dn-SNARE mice. AAV 2/1 displays strong neuronal tropism and negligible transduction of glial cells and limited spread within the CNS (Haery et al., 2019; Perez et al., 2020). Therefore, it was expected that mice injected with co-injection of AAV-CAG-PS1M146L and AAV-CAG-APPSL vector (Wt and dn-SNARE AAV-APP/PS1) exhibited human APP expression.

In the CA1 region of the hippocampus, in the *stratum pyramidale*, human APP expression was only detectable on Wt AAV-APP/PS1 ($Wt_{Non\text{-}injected}$: 1.09, n=1; $Wt_{AAV\text{-}PS1}$: 0.55, n=1; $Wt_{AAV\text{-}APP/PS1}$: 67.53, n=1; dn-$SNARE_{AAV\text{-}APP/PS1}$: 0.90, n=1; Figure 25 A.1). However, in the CA1 *stratum radiatum* layer, Wt and dn-SNARE AAV-APP/PS1 exhibited similar fluorescence intensity values ($Wt_{Non\text{-}injected}$: 0.00, n=1; $Wt_{AAV\text{-}PS1}$: 0.56, n=1; $Wt_{AAV\text{-}APP/PS1}$: 58.68, n=1; dn-$SNARE_{AAV\text{-}APP/PS1}$: 67.41, n=1; Figure 25 A.2). Nonetheless, in the CA2 region of the hippocampus, where the AAV generators describe AAV almost exclusive transduction (Audrain et al., 2016), in the *stratum pyramidale*, human APP expression was the highest in Wt AAV-APP/PS1, followed by dn-SNARE AAV-APP/PS1, and almost unmeasurable in Wt non-injected and Wt AAV-PS1 ($Wt_{Non\text{-}injected}$: 1.73, n=1; $Wt_{AAV\text{-}PS1}$: 5.54, n=1; $Wt_{AAV\text{-}APP/PS1}$: 87.56, n=1; dn-$SNARE_{AAV\text{-}APP/PS1}$: 73.71, n=1; Figure 25 B.1). In the CA2 *stratum radiatum* layer, Wt AAV-APP/PS1 showed the highest human APP expression, followed by dn-SNARE AAV-APP/PS1 ($Wt_{Non\text{-}injected}$: 0.00, n=1; $Wt_{AAV\text{-}PS1}$: 7.03, n=1; $Wt_{AAV\text{-}APP/PS1}$: 136.51, n=1; dn-$SNARE_{AAV\text{-}APP/PS1}$: 18.67, n=1; Figure 25 B.2). In Figure 25 C is represented the staining using the human APP specific antibody (6E10, red). The present experience served as a complement of the WB analysis (in which no human APP was detected). The results suggest that human APP is exclusively expressed in AAV-APP/PS1 injected mice and tends to be slightly more expressed in Wt rather than in animals with compromised gliotransmission.

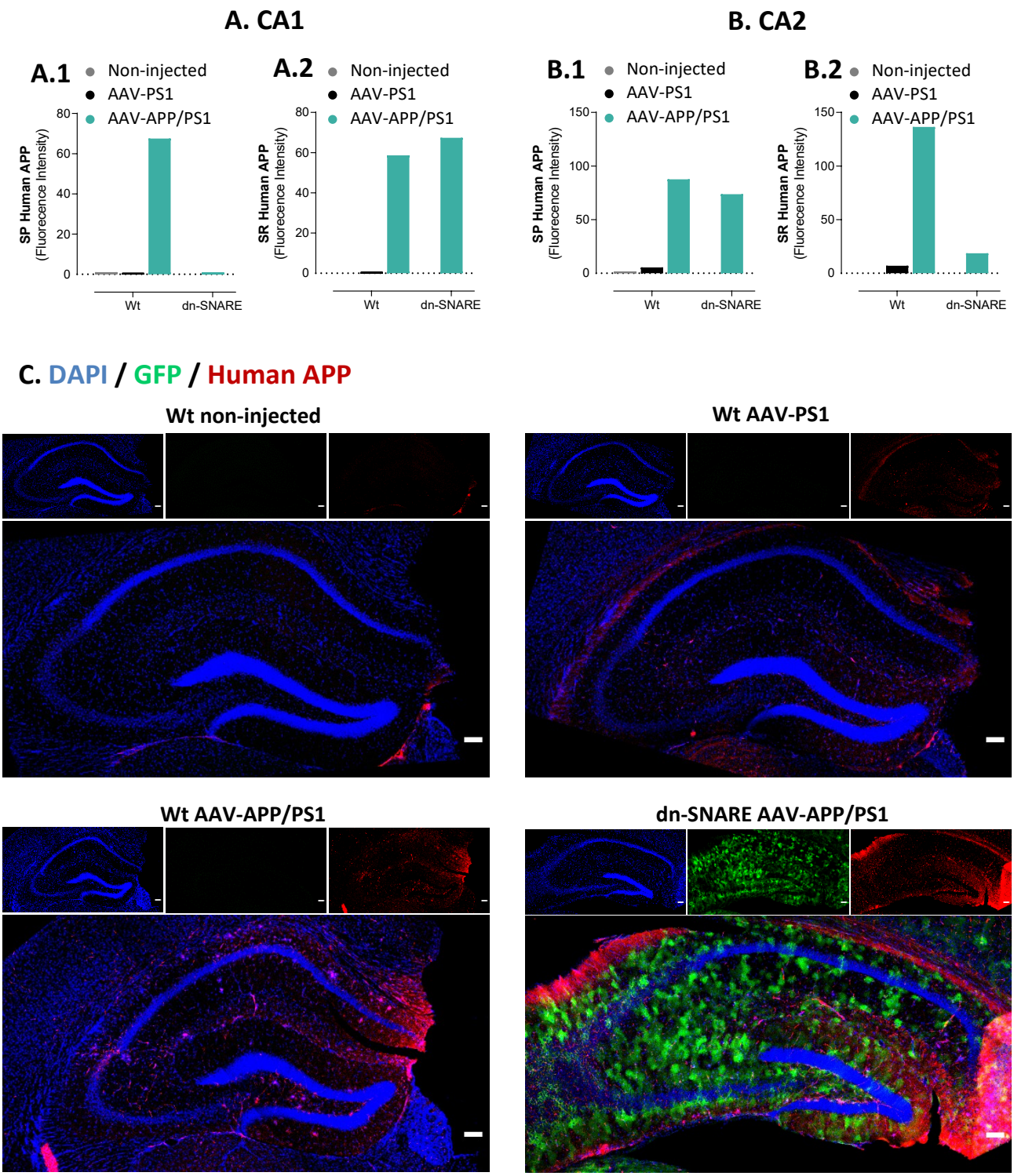

Figure 25: Human APP expression in hippocampal slices of Wt and dn-SNARE animals three months after AAV-PS1 and APP/PS1 injection. (A) Mean fluorescence intensity of human APP (anti-6E10 antibody) in the *stratum pyramidale* (SP) **(A.1)** and *stratum radiatum* (SR) **(A.2)** layers of CA1 hippocampal region. **(B)** Mean fluorescence intensity of human APP (anti-6E10 antibody) in the *stratum pyramidale* (SP) **(B.1)** and *stratum radiatum* SR) **(B.2)** layers of CA2 hippocampal region. **(C)** Representative confocal images stained with DAPI (blue), GFP reporter transgenes (green), and human APP (red) in the dorsal hippocampus of Wt non-injected, Wt AAV-PS1, Wt AAV-APP/PS1, and dn-SNARE AAV-APP/PS1 mice. N=1 Scale bars = 100 µm.

3.5.2.2. Total APP immunostaining

APP is a transmembrane protein that in physiological conditions appears to be essential for the regulation of several cellular functions (Gralle and Ferreira, 2007). However, alternative amyloidogenic processing of APP releases potentially Aβ neurotoxic species prone to aggregation, that are centrally implicated in the pathogenesis of AD (Gralle and Ferreira, 2007). Hence, APP in the dorsal CA1 and CA2 was quantified at the end of the behavioral analysis when the animals were sacrificed.

In the CA1 region of the hippocampus, in the *stratum pyramidale*, APP expression was mostly detectable on Wt AAV-APP/PS1 ($Wt_{Non\text{-}injected}$: 8.35, n=1; $Wt_{AAV\text{-}PS1}$: 5.64, n=1; $Wt_{AAV\text{-}APP/PS1}$: 2864.42, n=1; dn-$SNARE_{AAV\text{-}APP/PS1}$: 15.48, n=1; Figure 26 A.1). Contrarily, in the CA1 *stratum radiatum* layer, dn-SNARE AAV-APP/PS1 showed the highest APP expression levels ($Wt_{Non\text{-}injected}$: 1.43, n=1; $Wt_{AAV\text{-}PS1}$: 0.20, n=1; $Wt_{AAV\text{-}APP/PS1}$: 9.17, n=1; dn-$SNARE_{AAV\text{-}APP/PS1}$: 54.24, n=1; Figure 26 A.2). In the CA2 region of the hippocampus, where the AAV generators describe AAV almost exclusive transduction (Audrain et al., 2016), in the *stratum pyramidale*, APP expression was the highest, by a great amount, in Wt AAV-APP/PS1, followed by dn-SNARE AAV-APP/PS1, and almost undetectable in Wt non-injected and Wt AAV-PS1 ($Wt_{Non\text{-}injected}$: 0.01, n=1; $Wt_{AAV\text{-}PS1}$: 0.10, n=1; $Wt_{AAV\text{-}APP/PS1}$: 5244.47, n=1; dn-$SNARE_{AAV\text{-}APP/PS1}$: 153.23, n=1; Figure 26 B.1). In the CA2 *stratum radiatum* layer, Wt AAV-APP/PS1 and dn-SNARE AAV-APP/PS1 showed similar APP expression levels, while Wt non-injected and Wt AAV-PS1 did not exhibit APP detectable expression ($Wt_{Non\text{-}injected}$: 0.11, n=1; $Wt_{AAV\text{-}PS1}$: 0.12, n=1; $Wt_{AAV\text{-}APP/PS1}$: 56.79, n=1; dn-$SNARE_{AAV\text{-}APP/PS1}$: 59.91, n=1; Figure 26 B.2). Furthermore, Figure C suggests that Wt AAV-APP/PS1 and dn-SNARE AAV-APP/PS1 exhibit increased APP clusters spread all over the hippocampus. Nevertheless, CA1 Wt AAV-APP/PS1 pyramidal neurons are strongly stained for AAP C-terminal, while in dn-SNARE injected with AAV-APP/PS1, the blockade of vesicular gliotransmitter release in astrocytes decreases APP in neural cell-bodies rich areas in comparison to Wt in the same conditions. Besides, these data corroborate the western-blot results and indicate that AAV-APP/PS1 increases overall APP levels.

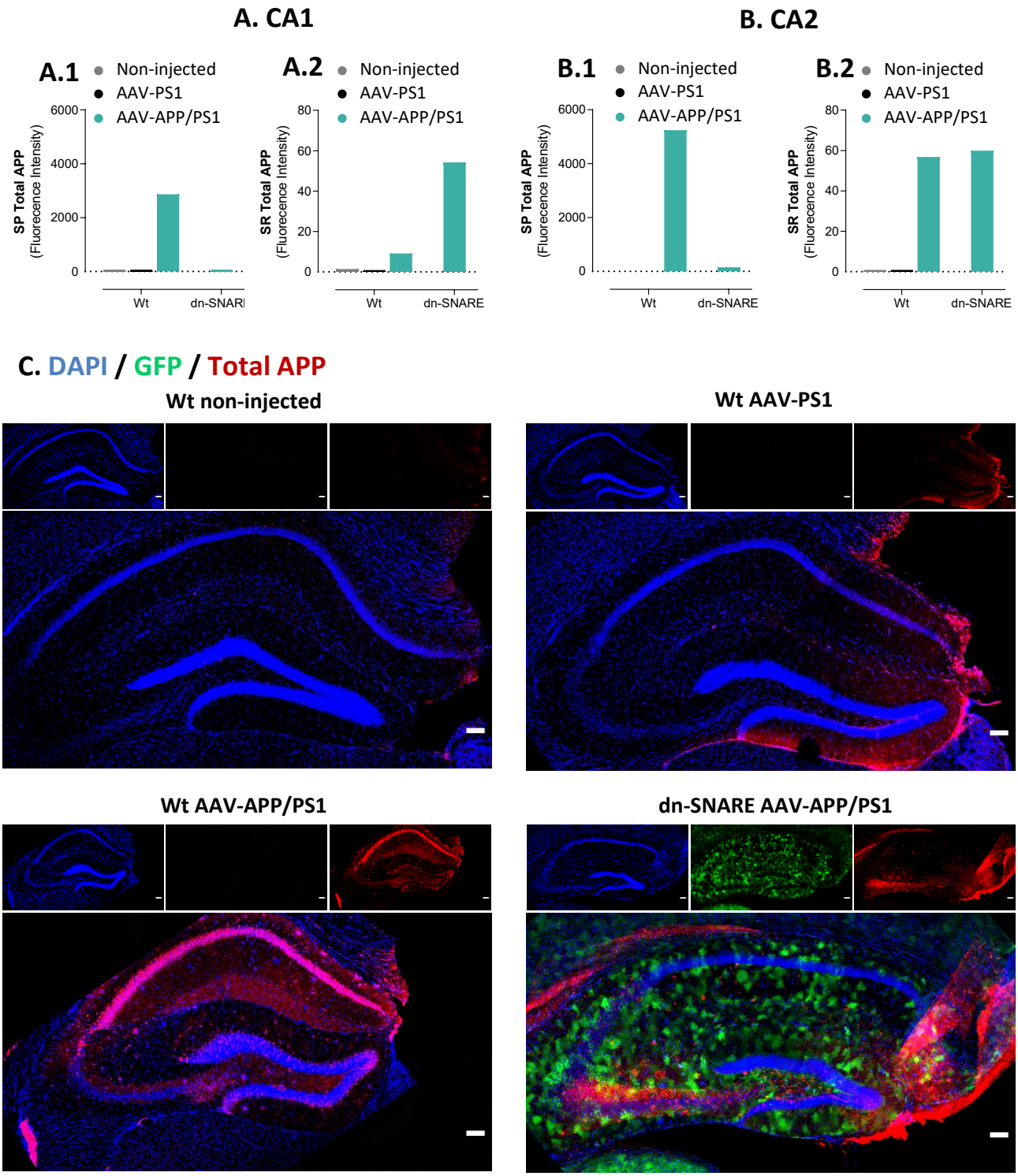

Figure 26: Total APP expression in hippocampal slices of Wt and dn-SNARE animals three months after AAV-PS1 and APP/PS1 injection. (A) Mean fluorescence intensity of total APP (anti-APP C-terminal antibody) in the *stratum pyramidale* (SP) **(A.1)** and *stratum radiatum* (SR) **(A.2)** layers of CA1 hippocampal region. **(B)** Mean fluorescence intensity of human APP (anti-APP C-terminal antibody) in the *stratum pyramidale* (SP) **(B.1)** and *stratum radiatum* (SR) **(B.2)** layers of CA2 hippocampal region. **(C)** Representative confocal images stained with DAPI (blue), GFP reporter transgenes (green), and total APP (red) in the dorsal hippocampus of Wt non-injected, Wt AAV-PS1, Wt AAV-APP/PS1, and dn-SNARE AAV-APP/PS1 mice. N=1 Scale bars = 100 µm.

3.5.3. Behavioral analysis

3.5.3.1. Open-Field Test

The spontaneous locomotor activity, exploratory behavior, and possible anxiogenic-like behavior of Wt and dn-SNARE animals (non-injected, injected with AAV-PS1 or AAV-APP/PS1) was analyzed in the OFT (Figure 27 A). No motor abnormality was detected, since the six groups travelled similar distances ($Wt_{Non\text{-}injected}$: 2183.41±274.59, n=5; $Wt_{AAV\text{-}PS1}$: 2195.93±144.72, n=5; $Wt_{AAV\text{-}APP/PS1}$: 2485.48±297.80, n=5; dn-$SNARE_{Non\text{-}injected}$: 2012.43±276.91, n=7; dn-$SNARE_{AAV\text{-}PS1}$: 1758.02±156.25, n=7; dn-$SNARE_{AAV\text{-}APP/PS1}$: 1901.18±201.862 cm, n=5; $p<0.05$; Figure 27 B) at similar velocities ($Wt_{Non\text{-}injected}$: 9.11±1.29, n=5; $Wt_{AAV\text{-}PS1}$: 9.03±0.73, n=5; $Wt_{AAV\text{-}APP/PS1}$: 11.75±1.25, n=5; dn-$SNARE_{Non\text{-}injected}$: 8.76±1.24, n=7; dn-$SNARE_{AAV\text{-}PS1}$: 7.85±0.77, n=7; dn-$SNARE_{AAV\text{-}APP/PS1}$: 6.77±0.82 cm/s, n=5; $p<0.05$; Figure 27 C). The exploratory behavior is unaffected by AAV-PS1 and AAV-APP/PS1 injection ($Wt_{Non\text{-}injected}$: 30.40±4.19, n=5; $Wt_{AAV\text{-}PS1}$: 24.00±1.95, n=5; $Wt_{AAV\text{-}APP/PS1}$: 29.20±7.76, n=5; dn-$SNARE_{Non\text{-}injected}$: 27.57±3.65, n=7; dn-$SNARE_{AAV\text{-}PS1}$: 27.29±4.46, n=7; dn-$SNARE_{AAV\text{-}APP/PS1}$: 22.604.19, n=5; $p<0.05$; Figure 27 D). Additionally, no significant differences were observed in regards of thigmotaxic behaviors ($Wt_{Non\text{-}injected}$: 25.02±10.02, n=5; $Wt_{AAV\text{-}PS1}$: 19.28±2.69, n=5; $Wt_{AAV\text{-}APP/PS1}$: 13.96±2.19, n=5; dn-$SNARE_{Non\text{-}injected}$: 19.66±3.43, n=7; dn-$SNARE_{AAV\text{-}PS1}$: 12.97±2.57, n=7; dn-$SNARE_{AAV\text{-}APP/PS1}$: 36.62±8.28 s, n=5; $p<0.05$; Figure 27 E). Accordingly, mice of the six groups performed similarly in all the OFT parameters, suggesting that the AD-like APP processing does not interfere with mice's emotional state nor their motor function.

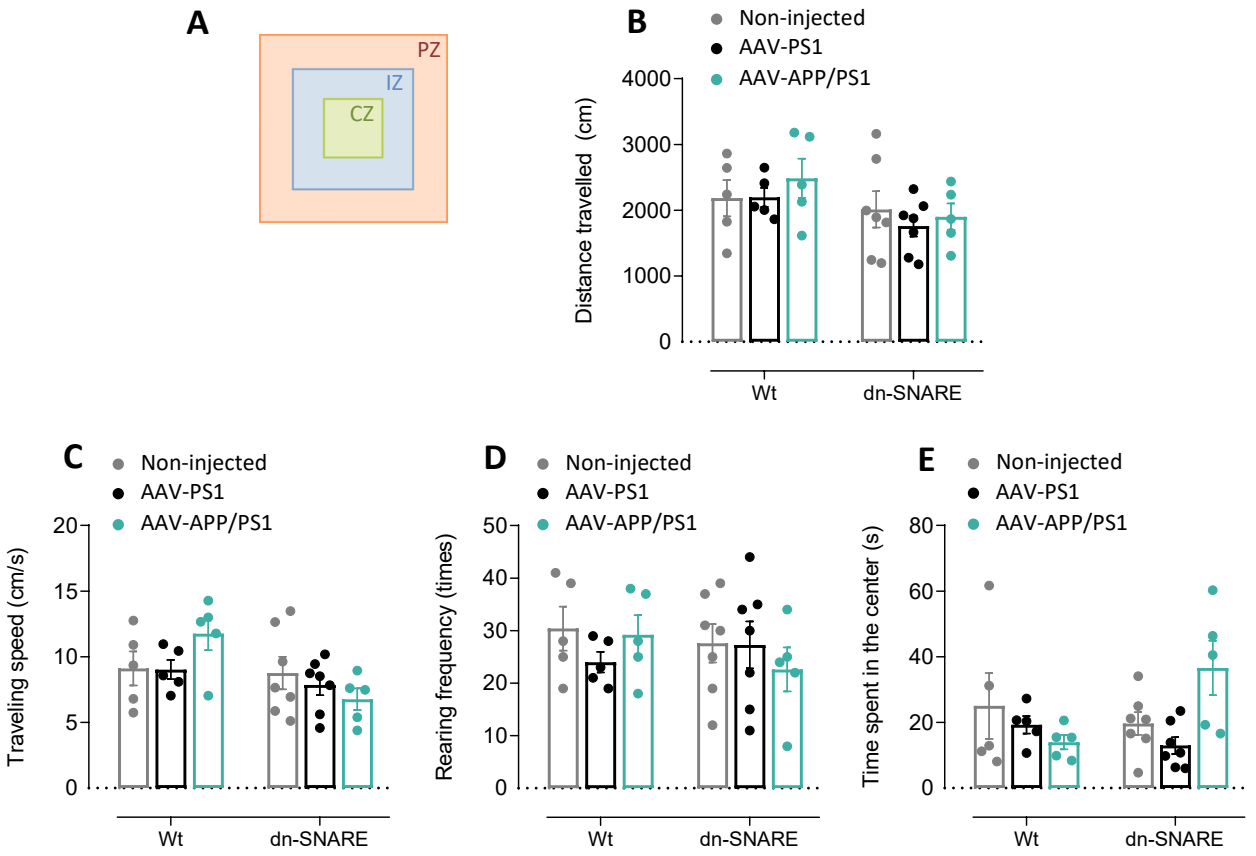

Figure 27: Assessment of motor function, exploration, and anxious-like behaviors by OFT of Wt and dn-SNARE mice 3 months after AAV-APP/PS1 and AAV-PS1 injections. **(A)** OFT scheme. The variables recorded from non-injected, AAV-PS1 and AAV-APP/PS1 Wt and AAV-PS1and AAV-APP/PS1 dn-SNARE mice during OFT were: general motor function, by determining **(B)** the total distance (cm) and **(C)** average velocity (cm/s) between three virtual concentric squares, delimiting the periphery, the center and an intermediate zone; **(D)** rearing, a variant of exploratory behavior in which the animal stands on its hind legs; and anxiety levels by **(E)** measuring the time spent in the center of the apparatus. All values are presented as mean ± S.E.M., n=5-7 per group, from n independent observations. Statistical significance was assessed by Two-way ANOVA followed by Holm-Sidak's *post hoc* test for multiple comparisons.

3.5.3.2. Y-maze spontaneous alternation

Spatial working memory was appraised by performing Y-maze spontaneous alternation test (Figure 28 A). While the animals freely explored the apparatus, no differences were observed in arm entries between the five groups (Wt –$Wt_{Non\text{-}injected}$: 33.00±7.10, n=3, $Wt_{AAV\text{-}PS1}$: 33.33±2.60, n=3, $Wt_{AAV\text{-}APP/PS1}$: 42.00±7.87, n=4; dn-SNARE – $dn\text{-}SNARE_{AAV\text{-}PS1}$: 26.00, n=1, $dn\text{-}SNARE_{AAV\text{-}APP/PS1}$: 29.00±4.00, n=2; Figure 28 B). Moreover, the percentage of spontaneous arm alternations was similar between the five groups (Wt – $Wt_{Non\text{-}injected}$: 59.00±4.97%, n=3, $Wt_{AAV\text{-}PS1}$: 60.70±1.93%, n=3, $Wt_{AAV\text{-}APP/PS1}$: 57.70±4.00%, n=4; dn-SNARE – $dn\text{-}SNARE_{AAV\text{-}PS1}$: 70.83%, n=1, $dn\text{-}SNARE_{AAV\text{-}APP/PS1}$: 56.80±8.42%

n=2; Figure 28 C). Thus, these data suggest that amyloid processing of APP does not affect spatial working memory and that the function of the prefrontal cortex remains intact in this AD model.

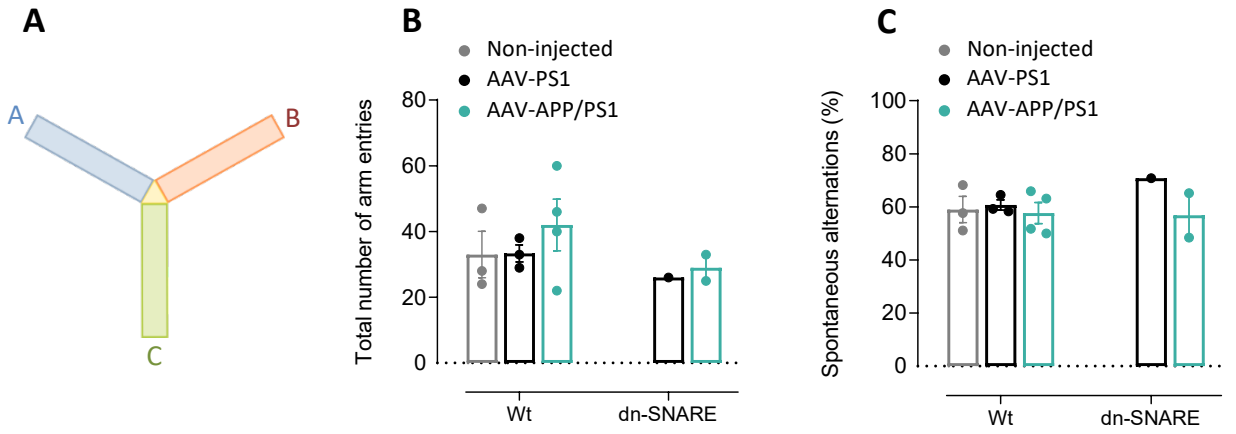

Figure 28: Y-maze spontaneous alternation to evaluate spatial working memory performance of Wt and dn-SNARE mice 3 months after AAV-APP/PS1 and AAV-PS1 injections. Spatial working memory was analyzed by Y-maze test **(A)**, by measuring the **(B)** total arm entries and **(C)** correct arm alternation (% spontaneous alternation) in a continuous spontaneous alternation task. All values are presented as mean ± S.E.M., n=1-4 per group, from *n* independent observations. Statistical significance was assessed by Two-way ANOVA followed by Holm-Sidak's *post hoc* test for multiple comparisons.

3.5.3.3. Object location test

The OLT relies on the principle of rodent predisposition to explore novelty. In this case using two identical objects that were first presented during a training phase and, after an ITI of 24h one of these objects was moved (Figure 29 A). Thus, animals with hippocampal impairment have compromised spatial contextual learning and consequently demonstrate no preference for objects in the novel location (Denninger et al., 2018).

During training phase, animals from the six groups showed no preference for either of the identical two objects that they were being familiarized with, validating that object A and object A' were equally appealing (data not shown). The novel location discrimination index indicates no major differences between the six groups (Wt – $Wt_{Non\text{-}injected}$: 0.15±0.20, n=5, $Wt_{AAV\text{-}PS1}$: 0.07±0.15, n=5, $Wt_{AAV\text{-}APP/PS1}$: 0.04±0.04, n=5, p>0.05; dn-SNARE – $dn\text{-}SNARE_{Non\text{-}injected}$: 0.17±0.07 n=7, $dn\text{-}SNARE_{AAV\text{-}PS1}$: 0.10±0.10, n=7, $dn\text{-}SNARE_{AAV\text{-}APP/PS1}$: 0.03±0.20, n=5, p>0.05; Figure 29 B). Although these results propose that astrocytic gliotransmission does not play a role in hippocampus-dependent spatial

memory, the results are not conclusive, considering that control animals (Wt non-injected) have not learned to proficiency execute the test, which invalidates OLT results.

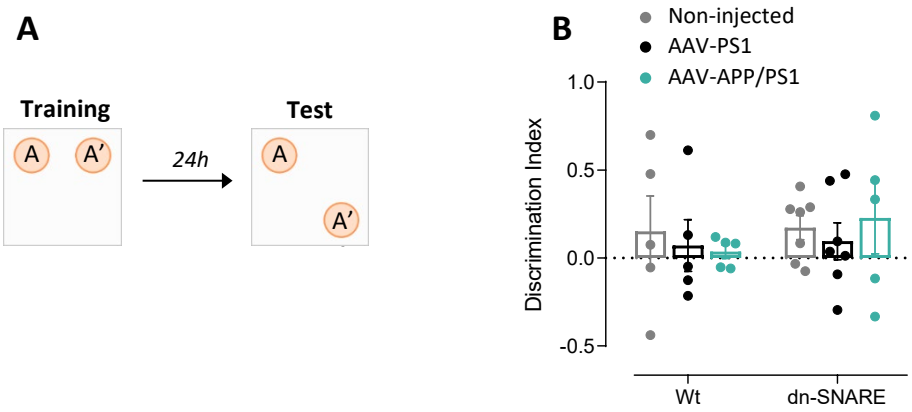

Figure 29: Spatial memory performance, in OLT, of Wt and dn-SNARE mice 3 months after AAV-PS1 and AAV-APP/PS1 injection. (A) For OLT mice were given training with two identical objects (object A and A'). For retention testing 24h later, one object was in the familiar location (object A), and one was placed in a novel location (object A'). **(B)** During the test phase, relative preference for the novel location (discrimination index) were calculated. All values are presented as mean ± S.E.M., n=5-7 per group, from *n* independent observations. Statistical significance was assessed by Two-way ANOVA followed by Holm-Sidak's *post hoc* test for multiple comparisons.

3.5.3.4. Barnes Maze

Wt and dn-SNARE mice injected with AAV-PS1 or AAV-APP/PS1 performed the Barnes Maze test, 3 months after AAV injections, to evaluate hippocampal-dependent spatial learning and reference memory. Briefly, the animals learned the relationship between distal cues in the surrounding environment and a fixed escape location (Pitts, 2018). This test comprises a four-day acquisition phase, where the ability of the animals to learn the location of a hidden escape box is evaluated, followed by a probe test on the fifth day, where the escape box is removed and the ability of the animals to recall its previous location is appraised (Pitts, 2018).

Starting with the results of Wt mice, it was anticipated that Wt AAV-APP/PS1 animals, as a consequence of the cognitive deficits mediated by the APP-processing, exhibited a less accentuated learning curve, compared to the control groups. However, this expected difficulty to find the target hole is only notorious on the last day of acquisition, given that the animals took longer to find the escape box ($Wt_{Non\text{-}injected}$ – Day 1: 44.50±8.41, Day 2: 42.21±9.69, Day 3: 41.21±17.58, Day 4: 16.04±2.17 s, n=3; $Wt_{AAV\text{-}PS1}$ – Day 1: 84.46±9.52, Day 2: 70.42±23.08, Day 3: 31.08±10.50, Day 4: 15.21±4.79 s, n=3, p>0.05; $Wt_{AAV\text{-}APP/PS1}$ – Day 1: 79.75±8.83, Day 2: 52.88±24.46, Day 3: 34.84±13.58,

Day 4: 36.88±8.65 s, n=4; p>0.05, Figure 30 A.1). Additionally, the number of incorrect holes checked before locating (primary errors) the escape box is also an indicator of spatial learning. However, there was no marked decrease in the number of primary errors in any group of Wt animals ($Wt_{Non\text{-}injected}$ – Day 1: 5.50±0.76, Day 2: 6.50±0.90, Day 3: 8.00±1.82, Day 4: 6.83±0.58, n=3, p>0.05; $Wt_{AAV\text{-}PS1}$ – Day 1: 6.667±0.220, Day 2: 7.083±2.171, Day 3: 7.417±1.294, Day 4: 917±1.158, n=3, p>0.05; $Wt_{AAV\text{-}APP/PS1}$ – Day 1: 9.12±0.42, Day 2: 5.75±0.86, Day 3: 7.19±1.55, Day 4: 8.00±1.68, n=4, p>0.05; Figure 30 A.2). Along with latency and errors, distance traveled prior to locating the escape box (path length) in each trial is also a sensitive measure of learning (Pitts, 2018). Therefore, it was expected that lesions in the hippocampus lead to deficits in the performance of the task, which translates into an increased distance traveled to the target hole. Even so, all groups of animals show a decrease in the distance traveled to the target over time, which indicates that the Wt animals of the three groups learned the location of the escape box ($Wt_{Non\text{-}injected}$ – Day 1: 156.26±24.64, Day 2: 163.09±19.86, Day 3: 187.93±73.50, Day 4: 105.60±10.88 cm, n=3; $Wt_{AAV\text{-}PS1}$ – Day 1: 182.88±54.19, Day 2: 216.45±89.37, Day 3: 152.51±26.89, Day 4: 89.30±14.96 cm, n=3, p>0.05; $Wt_{AAV\text{-}APP/PS1}$ – Day 1: 330.54±45.43, Day 2: 226.82±98.78, Day 3: 140.31±52.80, Day 4: 170.48±33.60 cm, n=4, p>0.05; Figure 30 A.3). Moreover, the three Wt groups slightly increased their speed over time ($Wt_{Non\text{-}injected}$ – Day 1: 6.46±0.62, Day 2: 6.08±0.20, Day 3: 5.54±0.23, Day 4: 6.60±0.49 cm/s, n=3; $Wt_{AAV\text{-}PS1}$ – Day 1: 4.08±0.28, Day 2: 4.64±0.48, Day 3: 7.17±1.80, Day 4: 8.08±1.70 cm/s, n=3, p>0.05; $Wt_{AAV\text{-}APP/PS1}$ – Day 1: 4.32±0.27, Day 2: 4.78±0.59, Day 3: 5.84±0.80, Day 4: 6.69±0.98 cm/s, n=4 p>0.05; Figure 30 A.4). The evolution in the type of strategies used to find the escape box (Figure 30 A.5), suggests that only the control Wt (non-injected and injected with AAV-PS1) completely abandoned the random strategy. But curiously, over time, the non-injected Wt used a less hippocampal-dependent strategy (serial), while Wt AAV-PS1 and AAV-APP/PS1 adopted similar strategies, using approximately 50% of the trials a hippocampus-dependent strategy (direct and corrected) and 50% a non-hippocampal-dependent strategy.

Further, regarding the results obtained by dn-SNARE, both dn-SNARE AAV-PS1 and dn-SNARE AAV-APP/PS1 learned to follow the external cues to locate the escape box ($dn\text{-}SNARE_{AAV\text{-}PS1}$ – Day 1: 79.63, Day 2: 113.75, Day 3: 14.13, Day 4: 11.13 s, n=1; $dn\text{-}SNARE_{AAV\text{-}APP/PS1}$ – Day 1: 87.63±55.13, Day 2: 58.94±42.19, Day 3: 27.81±4.31, Day 4: 13.38±0.38 s, n=2; Figure 30 B.1). However, on the second acquisition day, the dn-SNARE AAV-PS1 animal had some difficulty in the task and took longer to find the target hole, even though it recovered on the third day. The learning curve of

control dn-SNARE AAV-PS1 reflects that the animal has learned where the escape box was located, since it has a progressive decrease of primary errors. Nevertheless, the learning curve from dn-SNARE AAV-APP/PS1 animals is straight and does not reflect learning (dn-SNARE$_{AAV\text{-}PS1}$ – Day 1: 6.75, Day 2: 8.75, Day 3: 3.25, Day 4: 1.75, n=1; dn-SNARE$_{AAV\text{-}APP/PS1}$ – Day 1: 7.75±2.00, Day 2: 6.38±2.63, Day 3: 5.63±0.13, Day 4: 6.13±2.13, n=2, Figure 30 B.3). Both groups greatly reduced the distance traveled until they found the escape box (dn-SNARE$_{AAV\text{-}PS1}$ – Day 1: 310.92, Day 2: 444.91, Day 3: 61.14, Day 4: 43.60 cm, n=1; dn-SNARE$_{AAV\text{-}APP/PS1}$ – Day 1: 352.91±164.05, Day 2: 283.86±208.21, Day 3: 94.22±11.10, Day 4: 90.20±16.55cm, n=2; Figure 30 B.3), which suggests that both the dn-SNARE AAV-PS1 and AAV-APP/PS1 learned target localization. Moreover, both dn-SNARE groups slightly increased their speed over time (dn-SNARE$_{AAV\text{-}PS1}$ – Day 1: 3.78, Day 2: 3.32, Day 3: 5.97, Day 4: 4.73 cm/s, n=1; dn-SNARE$_{AAV\text{-}APP/PS1}$ – Day 1: 4.04±0.86, Day 2: 4.21±0.08, Day 3: 6.48±1.09, Day 4: 6.49±1.95 cm/s, n=2; Figure 30 B.4). The progressive evolution in the type of strategies used to find the escape box (Figure 30 B.5), suggests that over time dn-SNARE AAV-PS1 increases the use of hippocampal-dependent strategy (direct), although both groups of dn-SNARE animals stopped using the random strategy on the third day. Besides, dn-SNARE AAV-APP/PS1 used the serial strategy more often than dn-SNARE AAV-PS1.

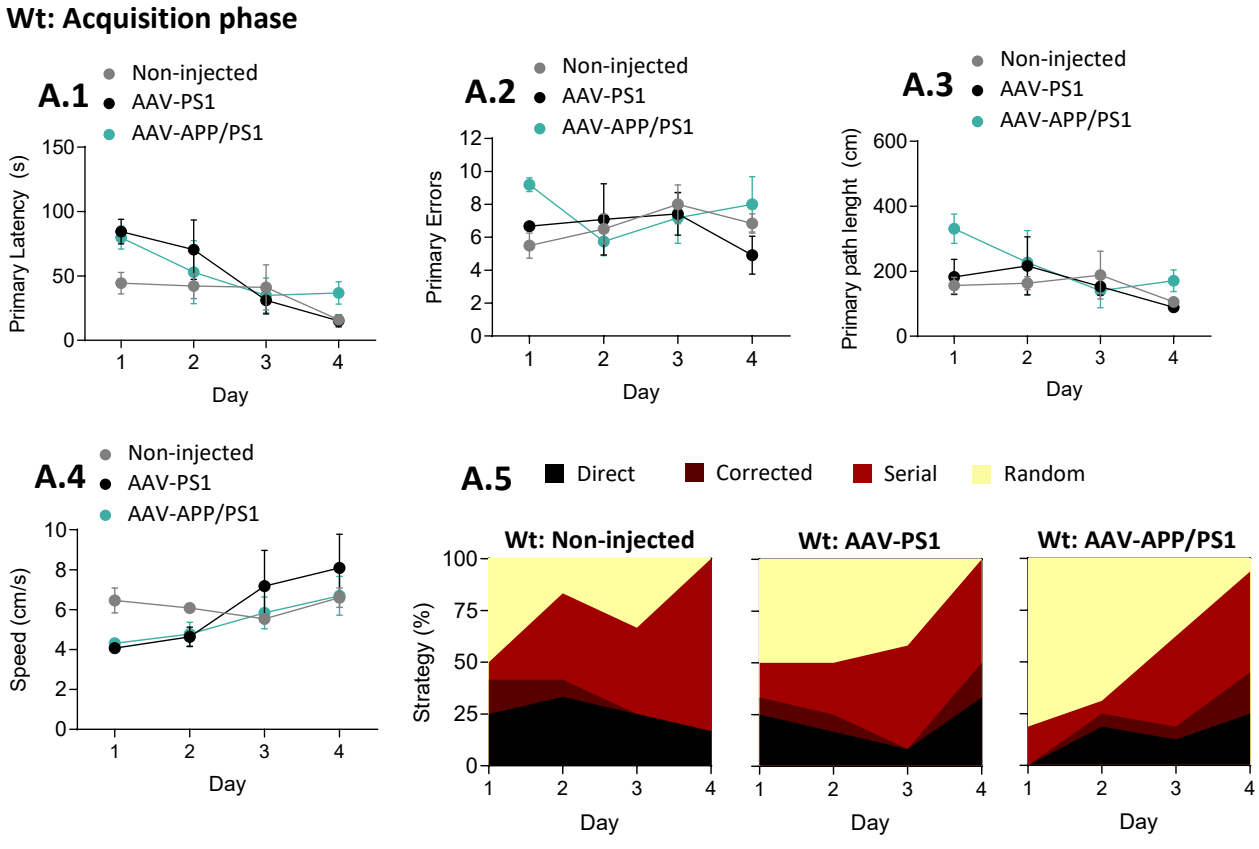

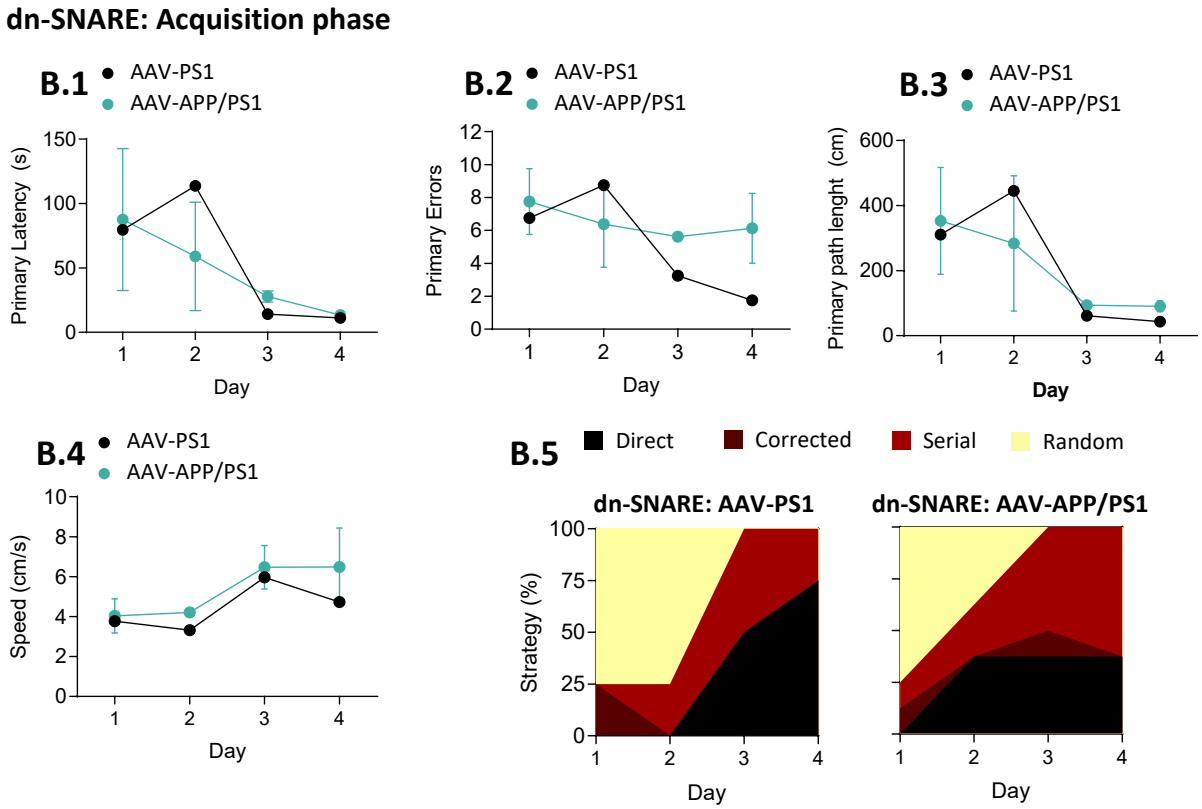

Figure 30: Learning performance in the Barnes Maze test of Wt and dn-SNARE mice 3 months after AAV-PS1 and AAV-APP/PS1 injection. Behavioral performance and navigation strategies during the acquisition of spatial reference memory in the Barnes maze. Mice learn to escape from an aversive (open, illuminated, and elevated) environment by following spatial cues and locating an escape hole. After four navigation trials, mice learn the location of the escape hole and were evaluated the **(A and B.1)** latency to locate (primary latency) the escape box, **(A and B.2)** number of incorrect holes checked prior to locating the escape box (primary errors), **(A and B.3)** the distance traveled prior to locating the escape box (primary distance), **(A and B.4)** average moving speed and **(A and B.5)** search strategy (direct, corrected, serial and random). All values are presented as mean ± S.E.M., n=1-4 per group, from *n* independent observations. Statistical significance was assessed by Two-way ANOVA followed by Holm-Sidak's *post hoc* test for multiple comparisons.

During the probe test it was expected that animals with impaired long-term memory performance exhibited difficulty in remembering the location of the target hole area, having a similar amount of nose poke rates in every zone. In Wt animals, nose poke rates look identical between the target and the other 19 holes, which is suggestive that none of the Wt groups had learned the location of the hidden escape hole ($Wt_{Non\text{-}injected}$: 3.33±0.67, n=3; $Wt_{AAV\text{-}PS1}$: 3.67±0.33, n=3, p>0.05; $Wt_{AAV\text{-}APP/PS1}$: 2.75±0.95, n=4, p>0.05; Figure 31 A). On the other hand, dn-SNARE AAV-APP/PS1 performed similarly to Wt animals. Curiously, dn-SNARE AAV-PS1 had the worst performance among all groups and were very persistent in the adjacent holes ($dn\text{-}SNARE_{AAV\text{-}PS1}$: 2.00, n=1; $dn\text{-}SNARE_{AAV\text{-}APP/PS1}$:

3.50±0.50, n=2; Figure 31 B). Overall, since that control animals (Wt non-injected) have not learned to execute the test and did not exhibit the expected performance, the results suggest that Barnes Maze may not be sensitive enough to detect slight alteration in the hippocampus.

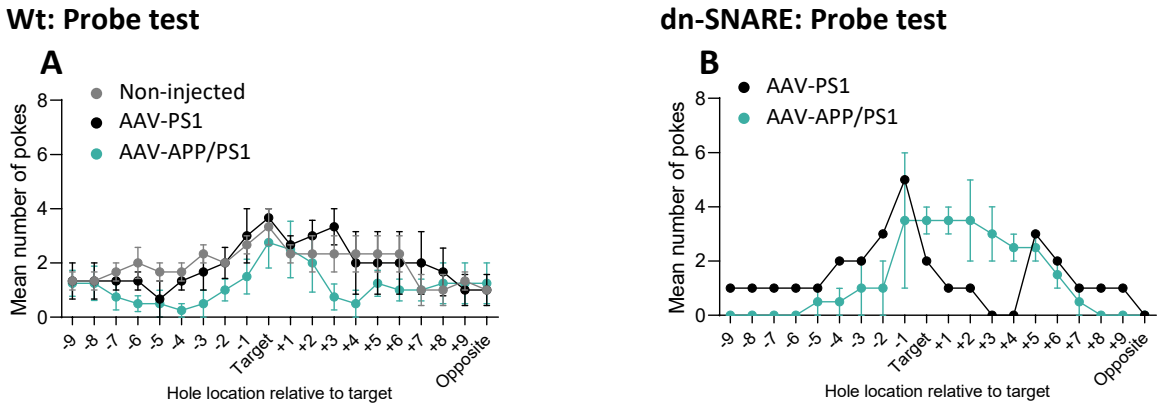

Figure 31: Spatial learning evaluation on probe trial from Barnes Maze test of Wt and dn-SNARE mice 3 months after AAV-PS1 and AAV-APP/PS1 injection. In the probe trial, in which the escape hole is not present, spatial memory was evaluated by the number of nose poke in Wt **(A)** and dn-SNARE **(B)** animals. All values are presented as mean ± S.E.M., n=1-4 per group, from *n* independent observations. Statistical significance was assessed by Two-way ANOVA followed by Holm-Sidak's *post hoc* test for multiple comparisons.

3.5.3.5. Morris Water Maze

The MWM tests hippocampal-dependent spatial learning and reference memory in mice (Vorhees and Williams, 2006). 24h after the last trial on the fourth day, mice must fulfill a probe trial, in which the platform was removed. Several variables were accounted for, including the distances swum, the swimming velocity, the time spent at the correct quadrant, and the number of times the animal crosses the platform location.

During the acquisition phase, Wt animals, in all experimental conditions, similarly decreased their swimming distance to reach the target platform, suggesting that the three animal groups improved their performance by learning the platform location ($Wt_{Non\text{-}injected}$ – Day 1: 511.49±10.71, Day 2: 292.64±55.50, Day 3: 160.82±80.06, Day 4: 228.07±75.35 cm, n=3; $Wt_{AAV\text{-}PS1}$ – Day 1: 526.47±97.50, Day 2: 300.60±101.99, Day 3: 221.62±74.89, Day 4: 124.48±60.01cm, n=3, p>0.05; $Wt_{AAV\text{-}APP/PS1}$ – Day 1: 652.51±134.14, Day 2: 315.13±97.31, Day 3: 199.77±51.65, Day 4: 175.13±94.68cm, n=4, p>0.05; Figure 32 A.1). Moreover, the Wt animals speed was constant over the days of acquisition, and similar between each other ($Wt_{Non\text{-}injected}$ – Day 1: 17.73±0.91, Day 2: 17.68±1.80, Day 3: 16.07±1.55, Day 4: 16.74±1.68 cm/s, n=3; $Wt_{AAV\text{-}PS1}$ – Day 1: 18.73±1.56, Day 2: 20.32±0.83, Day 3:

19.01±1.32, Day 4: 20.10±3.62 cm/s, n=3, p>0.05; $Wt_{AAV\text{-}APP/PS1}$ – Day 1: 17.95±0.64, Day 2: 22.51±1.33, Day 3: 20.81±0.33, Day 4: 18.50±1.88 cm/s, n=4, p>0.05; Figure 32 A.2), however, non-injected Wt were slightly slower than the injected mice. Furthermore, the control Wt AAV-PS1 used more goal-oriented strategies during the last acquisition day than the Wt AAV-APP/PS1 mice (Figure 32 A.3). Strangely, one of the non-injected animals had a lot of difficulty in performing the tasks on the last acquisition day, which resulted in an overall increase in distance swam, and a decrease in hippocampal-dependent strategies used to find the platform within Wt non-injected group.

Regarding dn-SNARE animals' results, even though dn-SNARE AAV-APP/PS1 exhibited difficulty finding the platform on the third day, the animals recovered on the fourth day, swimming for a similar time when compared to dn-SNARE AAV-PS1. The difficulty presented by the dn-SNARE AAV-APP/PS1 on the third day is reflected in an increase in the distance swam by the animals, which was recovered on the last day of training, in which the dn-SNARE AAV-APP/PS1 swam virtually the same distance as the dn-SNARE AAV-PS1 ($dn\text{-}SNARE_{AAV\text{-}PS1}$ – Day 1: 570.87, Day 2: 241.00, Day 3: 130.11, Day 4: 207.24 cm, n=1; $dn\text{-}SNARE_{AAV\text{-}APP/PS1}$ – Day 1: 575.81±142.29, Day 2: 310.11±28.05, Day 3: 470.65±6.35, Day 4: 186.51±36.29 cm, n=2; Figure 32 B.1). Besides, the speed of the dn-SNARE animals was constant over the days of acquisition, but dn-SNARE APP/PS1 were slower than dn-SNARE AAV-PS1 ($dn\text{-}SNARE_{AAV\text{-}PS1}$ – Day 1: 15.90, Day 2: 18.46, Day 3: 19.48, Day 4: 18.11 cm/s, n=1; $dn\text{-}SNARE_{AAV\text{-}APP/PS1}$ – Day 1: 13.45±2.34, Day 2: 12.78±1.54, Day 3: 13.05±2.72, Day 4: 16.19±0.08 cm/s, n=2, Figure 32 B.2). Dn-SNARE AAV-APP/PS1 used >50% of the time cue-based strategies that rely on the hippocampus (Figure 32 B.3), suggesting that AAV-APP/PS1 injection does not affect dn-SNARE hippocampus function.

In the probe test, all animals spent similar amount of time in the target quadrant ($Wt_{Non\text{-}injected}$: 27.27±3.21%, n=3; $Wt_{AAV\text{-}PS1}$: 31.82±1.91%, n=3; $Wt_{AAV\text{-}APP/PS1}$: 26.05±4.17%, n=4; $dn\text{-}SNARE_{AAV\text{-}PS1}$: 28.76%, n=1; $dn\text{-}SNARE_{AAV\text{-}APP/PS1}$: 27.52±3.26%, n=2; Figure 32 C.1). Wt AAV-APP/PS1 crossed within the platform border less than half of the times than Wt controls ($Wt_{Non\text{-}injected}$: 3.67±1.20, n=3; $Wt_{AAV\text{-}PS1}$: 4.67±2.03, n=3; $Wt_{AAV\text{-}APP/PS1}$: 1.75±1.03, n=4; Figure 32 C.2, p>0,05), which suggests that Wt AAV-APP/PS1 are aware of the existence of the platform, but their long-term memory acuity may be impaired. Conversely, dn-SNARE do not appear to be as affected by AAV-APP/PS1 injection, whereas the decrease in time spent in the correct quadrant and platform crosses relative to control is less contrasting than the difference between Wt animals ($dn\text{-}SNARE_{AAV\text{-}PS1}$: 4.00, n=1; $dn\text{-}SNARE_{AAV\text{-}APP/PS1}$: 2.50±0.50, n=2; Figure 32 C.2). In summary, AD-like APP processing mainly affects

Wt animals rather than animals with compromised gliotransmission, suggesting a critical role of astrocytes and gliotransmitters in the early stage of AD.

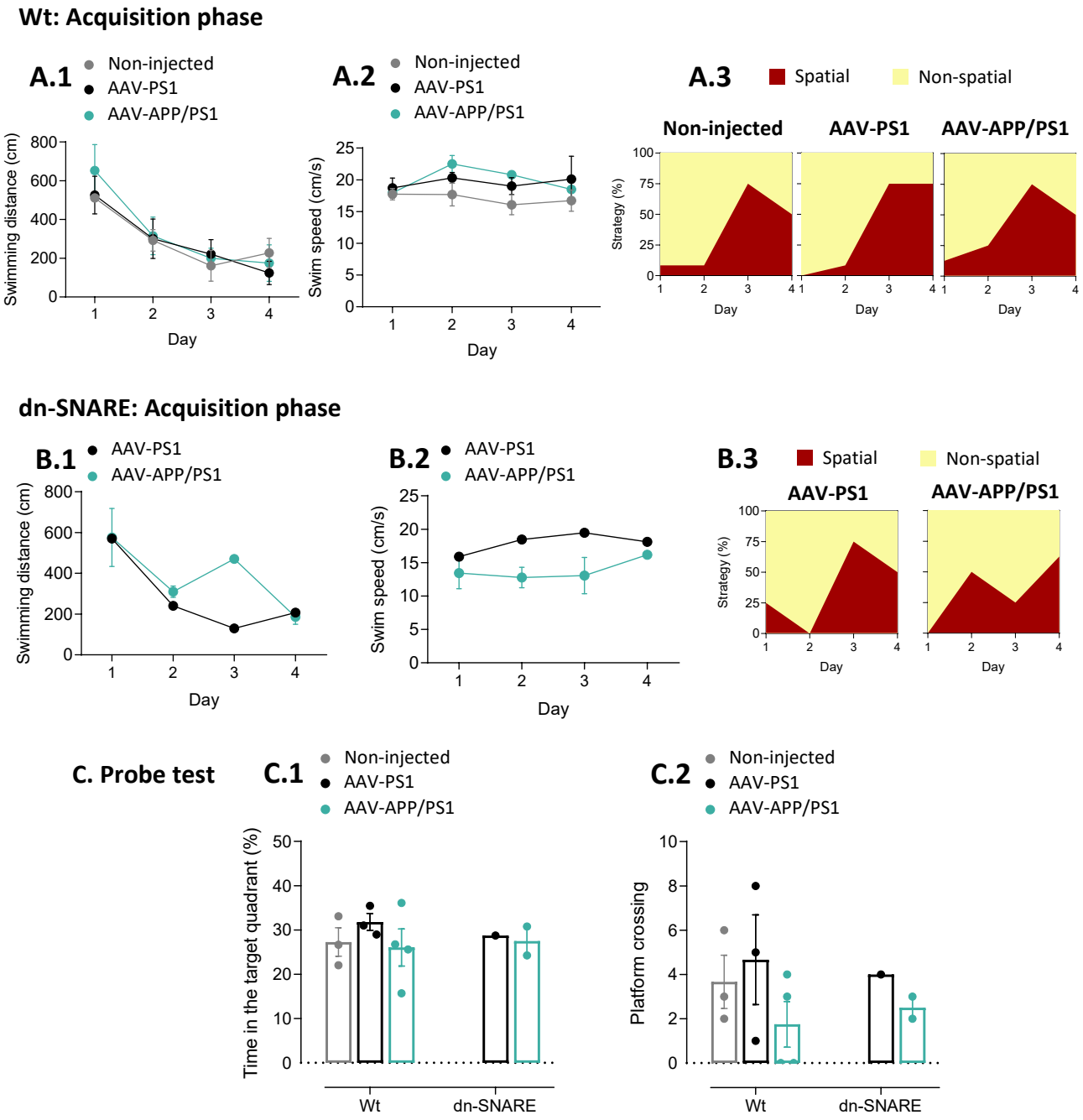

Figure 32: Learning performance in the MWM test of Wt and dn-SNARE mice 3 months after AAV-PS1 and AAV-APP/PS1 injection. For the MWM, during the four days of the acquisition phase, each animal was required to reach a platform placed in a specific quadrant. For each trial were evaluated the distances swum of each animal to reach the platform, **(A.1, Wt and B.1, dn-SNARE)**, the average swimming speed **(A.2, Wt and B.2, dn-SNARE)** and the search strategy (hippocampal-dependent: spatial, or independent: non-spatial, **A.2, Wt and B.2, dn-SNARE**). After completing the hidden-platform training phase, a probe trial, in which the platform was removed, was conducted 24h following the

last training trial. The performance on the probe test was evaluated in terms of **(A)** time spent in the correct quadrant and **(B)** the number of times the animals crossed the area where the platform had previously been located. All values are presented as mean ± S.E.M., n=1-4 per group, from *n* independent observations. Statistical significance was assessed by Two-way ANOVA followed by Holm-Sidak's *post hoc* test for multiple comparisons.

3.5.4. Long-term potentiation of AAV-PS1 or AAV-APP/PS1 injected dn-SNARE and Wt mice

To explore implications of AAV-APP/PS1 injection in synaptic plasticity, LTP at CA3-CA1 synapses was elicited by delivering a weak θ-burst (4x) stimulation protocol to hippocampal slices from Wt and dn-SNARE mice injected with AAV-PS1 or AAV-APP/PS1, after the behavioral tests.

Weak θ-burst stimulation of hippocampal slices from Wt non-injected or injected with AAV-PS1 lead to an initial enhancement of the fEPSP slope followed by a decrease and stabilization period, and 50-60min after θ-burst remained higher than before θ-burst stimulation ($Wt_{Non\text{-}injected}$: 13.09±3.49%, n=3; $Wt_{AAV\text{-}PS1}$: 9.41±3.62%, n=2, Figure 33 A, C). Contrarily, weak θ-burst stimulation of hippocampal slices from Wt AAV-APP/PS1 mice lead to an initial increase of the fEPSP slope followed by a progressive decrease towards pre-θ-burst levels, reaching values below the baseline at the end of the LTP recording period ($Wt_{AAV\text{-}APP/PS1}$: -5.61±7.49 %, n=3, Figure 33 A, C). Nonetheless, when the same paradigm of weak θ-burst stimulation protocol was applied in a slice of dn-SNARE AAV-PS1 and AAV-APP/PS1, it resulted in an initial enhancement of the fEPSP slope that decreased and stabilized at higher values than the pre-θ-burst (dn-$SNARE_{AAV\text{-}PS1}$: 26.32%, n=1; dn-$SNARE_{AAV\text{-}APP/PS1}$: 45.183%, n=1, Figure 33 B, C). These results suggest that *in vivo* amyloid APP processing closer to the human situation in AD, induces a trend towards a decrease in LTP magnitude following θ-burst stimulation, only in Wt animals. Therefore, proposes a fundamental role of SNARE-dependent gliotransmission on AD synaptic plasticity deficits, suggesting that modulation of astrocytes may be beneficial in AD cases.

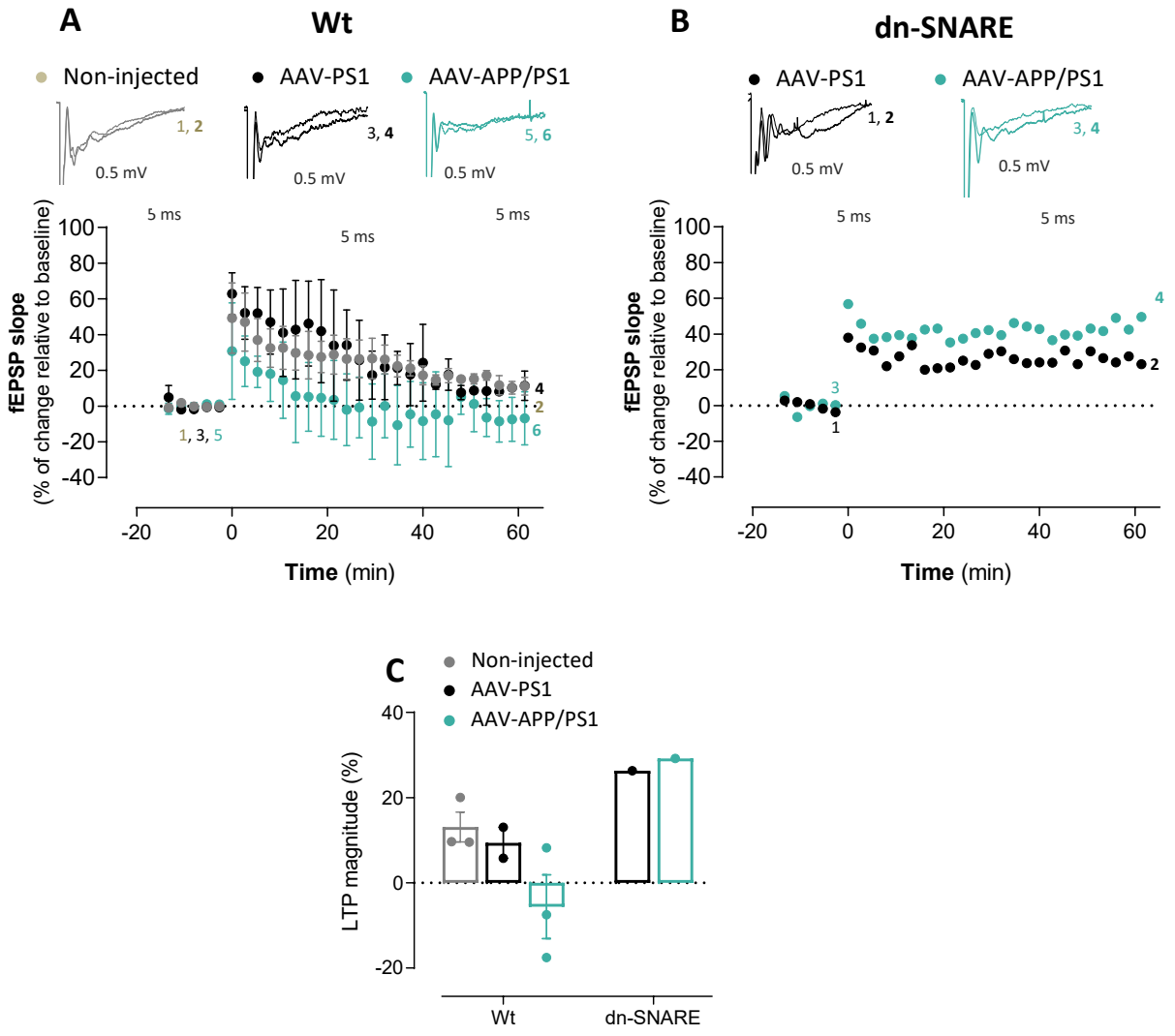

Figure 33: Synaptic plasticity changes in LTP in Wt and dn-SNARE mice three months after AAV-PS1 or AAV-APP/PS1 injection. (A) Averaged time courses changes in fEPSP slope induced by a θ-burst stimulation in hippocampal slices from Wt non-injected (n=3) and injected with AAV-PS1 (n=2) or AAV-APP/PS1 (n=3). Tracings from representative experiments are shown to top; each tracing is the average of eight consecutive responses obtained before (1,3 and 5) and 50–60 min after (2, 4 and 6) LTP induction. Tracings are composed of the stimulus artifact, followed by the pre-synaptic volley and the fEPSP. Scale bar: 5 ms (horizontal), 0.5 mV (vertical). **(B)** Averaged time courses changes in fEPSP slope induced by a θ-burst stimulation in hippocampal slices from dn-SNARE injected with AAV-PS1 (n=1) or AAV-APP/PS1 (n=1). Tracings from representative experiments are shown to top; each tracing is the average of eight consecutive responses obtained before (1 and 3) and 50–60 min after (2 and 4) LTP induction. Tracings are composed of the stimulus artifact, followed by the pre-synaptic volley and the fEPSP. Scale bar: 5 ms (horizontal), 0.5 mV (vertical). **(C)** Histograms depicting LTP magnitude (change in fEPSP slope at 46–60 min) induced by θ-burst stimulation from the conditions represented in (A) and (B). All values are presented as mean ± S.E.M. from *n* independent observations.

3.6. $A\beta_{1-42}$-oligomers increase glutamate release by astrocytes

In the tripartite synapse context, astrocytes can respond to neural activity and release several gliotransmitters, for instance, glutamate, which in turn modulate LTP by the activation of glutamate receptors, such as AMPAR, NMDAR, and mGluR, expressed both in pre- and postsynaptic neurons (Araque et al., 1998a). Aβ can increase glutamate release from neurons and astrocytes, resulting in the abnormal high extracellular levels of glutamate, which in turn activate eNMDAR (Talantova et al., 2013). Likewise, a proof-of-concept experiment was conducted using a FRET-based glutamate sensor (FLIPE-600n), whose structure is based on the ligand-binding site of glutamate receptors, to monitor glutamate release from primary cultures of astrocytes acutely exposed to oligomeric $A\beta_{1-42}$. In such sensor, an increase in FRET to donor fluorescence ratio indicates an increase in the release of glutamate (Okumoto et al., 2005; Socodato et al., 2020).

As shown in the panels and graph (Figure 34), the change in FRET/Donor ratio, reflecting glutamate release concentration, is increased after bath application of 200 nM $A\beta_{1-42}$ oligomers (Control: 1.03±0.02, n=2; After $A\beta_{1-42}$ oligomers: 1.14±0.13, n=2; Figure 34). Therefore, these results confirm that acute exposure to $A\beta_{1-42}$ oligomers induces astrocytic glutamate release.

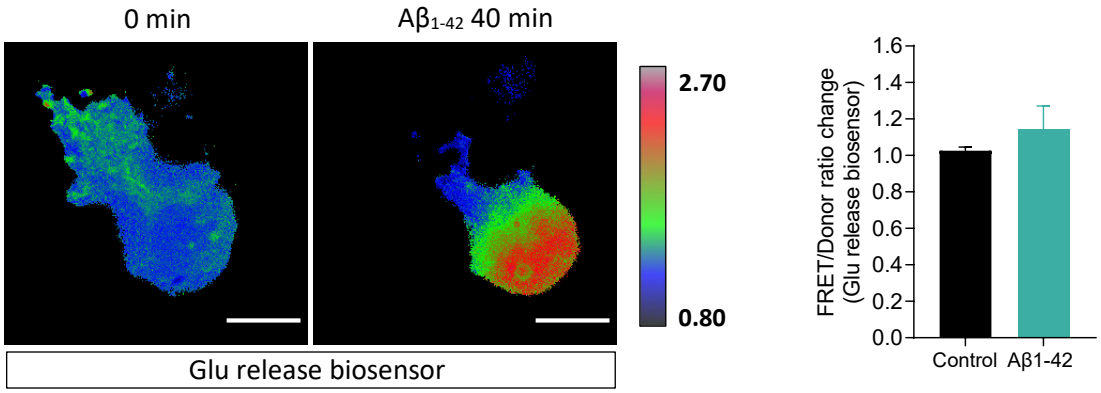

Figure 34: $A\beta_{1-42}$ oligomers induce an increase in glutamate release by astrocytes. Primary hippocampal and cortical astrocytes from Wt mice expressing the FRET-based glutamate biosensor (FLIPE) recorded in saline (0 min) and at the end of 200 nM $A\beta_{1-42}$ oligomers treatment. The figures show fluorescence change in FRET/Donor ratio in the beginning and at the end of the experiment. Scale bars, 10µm. The graph (mean ± S.E.M) show FRET/Donor ratio changes for the FLIPE biosensor (normalized at 0 min) before and after $A\beta_{1-42}$ oligomers exposure (n=2 cells pooled across 1 experiment).

4. Discussion

4.1. The dn-SNARE mice model

The perception of the role of astrocytes in brain function is a highly debated topic. There is growing evidence that astrocytes can receive, integrate and respond to neural activity, by increasing the metabolic support of neurons and modulating synaptic transmission via release of gliotransmitters, by Ca^{2+}-mediated signaling that ultimately leads to SNARE-dependent exocytosis (Araque et al., 2014; Halassa et al., 2009; Lalo et al., 2014; Pascual et al., 2005). In 2005, the dn-SNARE mouse model was described (Pascual et al., 2005) as a model to elucidate the importance of vesicular gliotransmission, considering that these animals express the dominant-negative domain (cytosolic portion) of vesicular SNARE protein VAMP2/synaptobrevin2, in which the redundant expression of dn-SNARE competes with endogenous VAMP2, compromising astrocytic exocytosis (Pascual et al., 2005). Nonetheless, Fujita and collaborators questioned the mouse model validity and suggested that neuronal populations may also express small quantities of the transgene, and thus results obtained with this mouse line may account for neuron-specific, rather than astrocyte-specific effects (Fujita et al., 2014). Hence, we performed complementary sets of experiments to validate the dn-SNARE model as a good model to dissect the role of astrocyte-derived signaling, and therefore emphasize the evidence for a role of vesicular gliotransmitter release in astrocyte-neuron interactions.

To support astrocyte specificity and to exclude the neuronal expression of dn-SNARE transgenes, double immunostainings were performed against the GFAP astrocytic marker and the neuronal-specific β-III tubulin that stains neuronal cell bodies, dendrites, axons, and axonal termination (Geisert and Frankfurter, 1989) and by taking advantage of the natural fluorescence of the dn-SNARE reporter (EGFP). Our results do not support Fujita et al. 2014 conclusions that demonstrate that most NeuN-positive neurons in the cortex and hippocampus also exhibit low to moderate levels of EGFP: first, in our results, the typical astrocyte bushy morphology is observed in EGFP labeled structures (Lalo et al., 2021b; Pascual et al., 2005; Sardinha et al., 2017; Sultan et al., 2015), and second, dn-SNARE reporter gene, EGFP, strongly co-localize with the astrocytic marker GFAP, but fails to show colocalization with the neuronal marker (as also shown by Sardinha et al. 2017). Furthermore, it was previously reported that EGFP staining and relative levels are correlated with dn-SNARE expression, since mice that express higher levels of dn-SNARE, also express higher levels of EGFP mRNA, which in turn translates into increased EGFP levels in those mice (Sardinha et al.,

2017). Thus, we screened by WB the transgenic protein levels in the hippocampus (brain region analyzed in the electrophysiology experiments), based on relative reporter EGFP levels. We observed (Figure 17) that EGFP has a variable expression in the hippocampus, across dn-SNARE animals. The variable transgene expression observed among different animals may be caused by biological factors that affect gene regulation, for instance, the epigenetic state of a gene, which sums from the DNA methylation status, nucleosome assembly, and posttranslational histone modifications (Jong et al., 2021).

Considering that dn-SNARE protein expression modulates the level of exocytosis blockade (Sardinha et al., 2017), it is expected that dn-SNARE animals exhibit variability regarding synaptic plasticity and behavioral performance. The incomplete inhibition of glial exocytosis could explain the diverse LTP magnitudes observed in Figure 19, and why some dn-SNARE animals are so similar to Wt animals. Moreover, LTP magnitude is significantly smaller in comparison to Wt mice (Figure 19), which is an indication that astrocytes regulate the strength of synaptic plasticity. This LTP impairment closely agrees with previous data on the major role of astrocytes in the release of glutamate (Zhang et al., 2004) and D-serine (Sultan et al., 2015), which can regulate synaptic plasticity, by activating NMDARs and thus enhancing LTP induction (Pascual et al., 2005). Besides, other gliotransmitters can also modulate LTP by different pathways, as is the case of ATP that can also be released by SNARE-dependent mechanisms (Lalo et al., 2014). Furthermore, it would be of interest to explore if the levels of the dn-SNARE protein expression are correlated with the degree of impairment in synaptic plasticity, considering that it is a mechanism dependent on exocytotic release from astrocytes.

Considering that mood and locomotor alterations could condition the execution of specific tests, basal anxiety, locomotor activity, and exploratory behavior were measured using the OFT. From our observations, no differences were seen between Wt and dn-SNARE mice (Figure 27, grey bars), a result that follows previous studies that suggested that dn-SNARE expression does not affect locomotor activity (Hines et al., 2013), exploratory paths and stops (Clasadonte et al., 2013), and rearing number (Sardinha, V. Doctoral Thesis, 2017), which, overall, support the exclusion of a depressive-like phenotype and locomotor problems in this mouse model.

Having established that impaired gliotransmission does not influence locomotor, exploratory and anxious behavior, and therefore compromised gliotransmission would not impact the motivation to perform further tests, we aimed to characterize Wt and dn-SNARE mice in what concerns to their learning and memory abilities. Spatial recognition memory was assessed by OLT, by displacing one

of two objects to the opposite side of the box, in a second trial with 24h delay. The Wt animals did not perform the test as expected, suggesting that the test is not working, and the animals failed to learn the test correctly (Figure 29, grey bars). A previous study suggested that mice are not able to distinguish a familiarized object in a new location without extra-field cues, but can recognize a novel object on the test trial without extra-field cues (Murai et al., 2007). Since the OLT is a task that takes advantage of a mouse's innate tendency to explore novel objects in their environment but relies on spatial memory, maybe the plain white open-field arena with only external cues from the room was not sufficient for the mice to spatially orient themselves during the OLT. Therefore, symbolic spatial cues should be incorporated into the arena wall or extra-field, to serve as spatial landmarks or reference points (Denninger et al., 2018). Thus, in the future, further optimizations of OLT will be performed and the NOR test will also be conducted. The NOR test is identical to the OLT until the test phase when one of the objects is replaced by a novel object instead of one object being moved to a new location, and it evaluates non-spatial learning of object identity, which relies on multiple brain regions (Denninger et al., 2018). Additionally, further behavioral tests will also be included to elucidate the influence of astrocytes in complex cognitive functions, such as the Y-maze spontaneous alternation test, to evaluate spatial working memory, and the MWM, to assess long-term spatial memory. Our results complement the existing evidence, and clearly show that the deficit in the synaptic plasticity in dn-SNARE mice can be solely attributed to the impairment of astroglial exocytosis.

4.2. Role of gliotransmission in $A\beta_{1-42}$ effects in synaptic plasticity

While AD manifests as a synaptic abnormality early on, little is known about the contribution of astrocytes to its pathogenesis. To address this gap, we used dn-SNARE transgenic mice, where SNARE-dependent gliotransmission was selectively disrupted, and incubated hippocampal slices, together with the respective controls, with $A\beta_{1-42}$ oligomers for 3h. We found that selectively compromising gliotransmission prevents $A\beta_{1-42}$ oligomers-mediated LTP deficits (Figure 20), suggesting that gliotransmitter that are released in a SNARE-dependent manner are required for the toxic effects of $A\beta_{1-42}$ oligomers. This could be explained by the fact that Aβ has been shown to disrupt gliotransmission, by enhancing Ca^{2+} signaling in astrocytes. Therefore, this Ca^{2+}/gliotransmission alteration could underlie an important role of astrocytes in AD pathology. In fact, astrocytic Ca^{2+} signaling is abnormal in several models of AD: (1) in cultures of mixed astrocytes

and neurons, Aβ induces Ca^{2+} signals, mediated by Ca^{2+} influx across the plasma membrane selectively in astrocytes, causing sporadic fluctuations of Ca^{2+} concentrations, while having no apparent effect on Ca^{2+} dynamics in nearby neurons (Abramov et al., 2003); (2) Aβ interacts directly with the astrocyte network, and thus Ca^{2+} homeostasis and dynamic signaling are modulated by the direct effect of Aβ on the astrocyte network, and not derived from neuronal hyperactivity near Aβ deposits (Kuchibhotla et al., 2009); (3) astrocytic Ca^{2+}-signaling and homeostasis are disrupted in the APP/PS1 AD model (Kuchibhotla et al., 2009); (4) AD astrocytic processes are more synchronous but lose their ability to provide timely feedback at single tripartite synapses, which results in enhanced depletion of docked vesicles leading to the loss in correspondence between Ca^{2+} events and gliotransmitter release events (Pillai and Nadkarni, 2019). Thus, in accordance with the literature, our results are suggestive that neurotoxicity may be secondary to impaired astrocytic function in the support of neuronal viability. Nevertheless, one question is raised: which gliotransmitters are released by exocytosis that mediates the Aβ-toxicity in synaptic plasticity? And how do they contribute to LTP disruption?

The protocol used to study synaptic plasticity (Chapter 2.3.3) assesses LTP-mediated by NMDARs, which mediate learning and memory processes in the hippocampus (Sweatt, 2009). These receptors require the binding of a co-agonist (glycine or D-serine) and an agonist (glutamate) to GluN1 and GluN2A-D subunits, respectively (Hardingham and Bading, 2010; Shipton et al., 2014) and are divided into two different groups: neuroprotective sNMDAR (mainly enriched with GluN2A subunits) with a high affinity for D-serine, and neurotoxic eNMDARs (mainly containing GluN2B subunits) with a higher affinity for glycine (Armada-Moreira et al., 2020; Hardingham and Bading, 2010; Papouin et al., 2012). In addition, it is described that Aβ oligomers, even at low to subnanomolar concentrations, increase GluN2B-eNMDAR response (Li et al., 2011). Therefore, astrocytes through their supply of D-serine to synapses (Figure 21 and Henneberger et al.2010) appear to be key regulators of sNMDAR functions. Conversely, astrocytes also provide glutamate to eNMDARs (Angulo et al., 2004; Talantova et al., 2013). Thus, our results (Figures 20 and 33) propose that, in the presence of $Aβ_{1-42}$ oligomers, SNARE-dependent release of glutamate from astrocytes increases GluN2B-NMDARs (eNMDARs) activity, contributing to the synaptic plasticity deficits triggered $Aβ_{1-42}$ oligomers.

With this in mind, it is raised the possibility that neurotoxic effects in synaptic plasticity by $Aβ_{1-42}$ oligomers are a result of the perturbation between the balance of NMDARs activity. More

specifically, Aβ induces astrocytic Ca^{2+} dysregulation, which could induce an insufficient release of sNMDARs co-agonist, and simultaneously promote an increased release of glutamate, which in turn activates eNMDARs, that will antagonize the pro-survival signaling of sNMDAR, disturbing synaptic plasticity mechanisms. Nonetheless, there is, to date, no consistent evidence indicating between astrocytes (Henneberger et al., 2010) and neurons (Benneyworth et al., 2012) which is the major source of extracellular D-serine. Hence, we proposed to clarify astrocytes' contribution to D-serine-mediated NMDAR signaling. Considering that SR (D-serine producing enzyme) substrate, L-serine, is synthesized *de novo* in astrocytes, which express all the enzymes required to convert glucose into L-serine, we perfused hippocampal slices from dn-SNARE animals with compromised vesicular release of gliotransmitters, and respective controls, with D-serine and L-serine. Thus, it was anticipated that if D-serine release relied on astrocytic integrity, D-serine and L-serine produced different outcomes in dn-SNARE hippocampal slices. Our results (Figure 21) show that D-serine increases 48.90% LTP magnitude in hippocampal slices from animals with compromised gliotransmission, an effect that is not observed by L-serine perfusion, regardless L-serine concentration (Figure 22) (we used the same concentration as D-serine, and a known concentration that rescues LTP in animals lacking PHGDH in astrocytes (enzyme required for the synthesis of L-serine from glucose) (Le Douce et al., 2020)). This is suggestive that after L-serine perfusion, D-serine is produced, but cannot be released in hippocampal slices from animals with impaired SNARE-dependent gliotransmission. Moreover, these results corroborate the “Serine shuttle” model (Wolosker, 2011), whereby L-serine synthesized by astrocytes is shuttled to neurons to fuel the synthesis of D-serine that, once released by neurons, is taken up by astrocytes. Besides, even though the question of by what mechanisms D-serine is released from either cell-type has become a topic of debate, our results are suggestive that in the hippocampus, once produced, D-serine shuttles from neurons to astrocytes, where it accumulates in glial vesicles to be released in a SNARE-dependent manner. The SNARE-dependent exocytosis of D-serine from astrocytes has also been supported by the direct measurements of its extracellular level with microelectrode biosensors in the neocortex of dn-SNARE animals (Lalo et al., 2018). Although this experiment was done in a different brain region, our results are similar and strongly suggest astrocytes as the main source of D-serine. Nevertheless, studies that place neurons in the center of this pathway (Benneyworth et al., 2012) do not deny the ability of astrocytes to accumulate D-serine. Therefore, that theory continues to be compatible with our results, highlighting the cooperation between neurons and astrocytes to D-serine dynamics. Overall, our data fills substantial gaps in our understanding of the

D-serine releasing mechanism (Lalo et al., 2021a): (1) it elucidates the predominant role of astrocytes in D-serine release, and (2) proves that astrocyte-derived D-serine plays a crucial role in NMDAR-mediated synaptic plasticity.

Having unveiled the contribution of astrocytes for D-serine release, it becomes easier to study whether Aβ peptides contribute to the dysregulation in astroglial modulation of neuronal NMDRARs. The previous results demonstrate that $A\beta_{1-42}$ oligomers dysregulate astrocytes, triggering exacerbated astrocytic glutamate release, evoking excessive eNMDARs activation. However, if Aβ causes insufficient D-serine release, under activating sNMDAR, and thus suppressing the induction of LTP, remains an open question. For that purpose, we perfused hippocampal slices exposed to $A\beta_{1-42}$ oligomers from dn-SNARE and Wt animals with D-serine. We found that D-serine restores the deficits in LTP provoked by $A\beta_{1-42}$ oligomers (Figure 23), which is suggestive that poor activation of GluN2A-NMDARs (sNMDAR) may also underlie LTP impairments mediated by $A\beta_{1-42}$ oligomers. Along with this, hippocampal slices from dn-SNARE animals with compromised gliotransmission exposed to $A\beta_{1-42}$ oligomers but treated with D-serine show improved LTP magnitude in comparison to the blockade of gliotransmission alone (Figure 23), suggesting that, although D-serine by itself is sufficient to restore LTP, it can enhance the neuroprotective potential of blocking gliotransmission. It is documented that Aβ-mediated inhibition of LTP is rescued by GluN2B-NMDARs antagonists, but not by GluN2A-NMDARs antagonists (Li et al., 2011), which endorse the principle that decreasing eNMDARs overactivity is protective against Aβ-inhibited LTP, and that sNMDAR overactivity is not the root cause of LTP inhibition by Aβ. Besides, the degree of occupancy of the co-agonist binding site (where D-serine binds) directly dictates the ability of NMDARs to be activated by glutamate (Kleckner and Dingledine, 1988). Since glutamate is fully saturating to NMDARs during synaptic transmission (Clements, 1996), D-serine availability is the limiting factor to NMDAR activation. Therefore, results that point to high levels of D-serine in AD patients' samples (Chang et al., 2020; Madeira et al., 2015) could be caused by a compensatory mechanism to increase sNMDAR activity.

Overall, our work demonstrates that the etiology and treatment for AD can be mechanistically linked, via astrocytes. We show that: (1) impairing gliotransmission restores LTP inhibition mediated by Aβ; (2) astrocytes release more glutamate (sNMDARs and eNMDARs agonist) in the presence of Aβ; (3) and that D-serine (sNMDAR co-agonist) can successfully enhance sNMDARs activation and potentiate LTP induction in the presence of Aβ. These results provide mechanistic insights into the

effects of NMDAR modulators and highlight their potential to restore synaptic plasticity. Overall, our result places astrocyte at the central hub for synaptic plasticity dysfunction in AD, opening the search for innovative approaches and targets to the treatment of AD.

4.3. Role of gliotransmission in AD-like APP processing

Despite many years of research in AD, results from animal models have presented variable results, potentially due to the lack of translatable models of human AD. Transgenic models display much higher levels of APP and Aβ compared to the human situation, which may have toxic effects unrelated to the early phases of AD (Audrain et al., 2016). Therefore, we used an alternative model involving the production, *in vivo* in the mouse hippocampus, of moderate levels of amyloid derivatives, resembling as closely as possible the pattern of expression observed in the hippocampus of human AD patients (Audrain et al., 2016), to study the role of astrocytes in the consequences of initial amyloid pathway engagement.

To monitor vector-mediated APP expression, mice were euthanized after behavioral experiments. The AAV generators affirmed that human APP expression in AAV-APP/PS1 groups is not sufficient to be detected by immunohistochemistry, but a detectable signal should be observed in WB (Audrain et al., 2016). However, WB analysis of the whole hippocampus revealed no detectable signal of exogenous human APP expression (6E10 antibody) (Figure 24), questioning the viability of this antibody or the efficacy of the hippocampal injections. Curiously, our immunohistochemical analyses of hippocampal sections revealed widespread human APP immunoreactivity (Figure 25), a result that contradicts our WB data. This could be explained by the fact that hippocampal slices used in WB analyses were all the left-over slices from the electrophysiology experiments of these animals, which may have resulted in a loss of the slices they contained at the injection site. A possible solution would be to only use the slices of the coordinates of the injection, in order not to dilute the protein, which would make it undetectable. Besides, a fluorescent reporter could also be added to the construct of AAV-APP/PS1 to allow the visualization and relative quantification of the proteins. Nevertheless, although the WB has failed, the immunological, behavioral, and electrophysiological results suggest that the AAV injection is working and inducing the production of human APP.

In regards to the total amount of APP (human + murine forms), animals injected with AAV-APP/PS1 exhibit slightly (but not significant) increased APP expression in the hippocampus, in comparison to

animals injected with AAV-PS1 alone (Figure 25). These results are in accordance with the observations in immunohistochemical analysis (Figure 26) and indicate that potential early synaptic dysfunctions and cognitive deficits are not a result of APP overproduction. Moreover, the APP distribution profile is different between Wt and dn-SNARE animals. Interestingly, the blockade of vesicular gliotransmitters release in astrocytes decreases APP in cell-bodies of pyramidal neurons in CA1 after AAV-APP/PS1 injection (Figure 26). CA1 pyramidal neurons are known to show *in vivo* physiological responses to spatial changes, as well as to novel objects and fear, thus encoding both spatial and non-spatial memories (Masurkar, 2018). Synaptic and functional changes in area CA1 have been documented in the early stages of AD (Masurkar, 2018), however, a relevant role to this alteration was never attributed to the modulation of APP by astrocytes. Given the critical role of CA1 neurons in the formation, consolidation, and retrieval of hippocampal-dependent memories, our results bring the hypothesis that gliotransmitters also regulate the distribution of APP, especially the level of the most affected circuits in AD.

According to previous studies by the AAV-AD model generators, anxiety-related behavior was expected in animals injected with AAV-APP/PS1 in the OFT (Audrain et al., 2016). In contrast to the respective controls, Wt AAV-APP/PS1 shows a tendency to spend less time in the center of the arena (Figure 27), where the lighting is more intense, and so tends to be avoided when the animals show increased anxiety (Seibenhener and Wooten, 2015). By contrast, dn-SNARE AAV-APP/PS1 exhibit decreased thigmotaxis after AAV-APP/PS1 injection (Figure 27). Several transgenic models of AD, that show early elevated Aβ production and plaque formation in the hippocampus, have reported that mice spent more time in the center area and exhibit increased locomotor activity, which is suggestive of a disinhibitory tendency, an anxiety-related phenotype that involves the loss of awareness of what is appropriate behavior (Gil-Bea and Schliebs, 2007; Kelliny et al., 2021; Tavares et al., 2016; Wang et al., 2019). Since these animals do not mimic, as well as our model, the temporal events related to APP processing, the literature data suggests that at more advanced stages of AD, where there is a higher deposition of Aβ, there is an induction of behavioral disinhibition. Curiously, this is similar to what is observed in dn-SNARE AAV-APP/PS1 animals, which calls into question whether dysregulation in gliotransmission contributes to this behavioral disinhibition in later stages of the disease. Besides, the possibility that behavioral disinhibition is a result of locomotor impulsivity is excluded, since, in comparison to Wt AAV-APP/PS1, dn-SNARE AAV-APP/PS1 do not

present excessive locomotor activity, and therefore are not likely to overrun, which proposes that the result of the dn-SNARE AAV-APP/PS1 is exclusively due to the impairment of gliotransmission

After concluding that AAV-PS1 and AAV-APP/PS1 injection does not impact locomotor, exploratory, and anxious behavior, further tests were conducted to characterize Wt and dn-SNARE injected animals in what concerns their learning and memory performances. As discussed in Chapter 4.1, spatial recognition memory was assessed by OLT (Figure 29), but the results were not considered valid, since control animals failed to learn the test correctly. In the future, OLT will be optimized and the NOR test will be performed to evaluate non-spatial learning of object identity (Denninger et al., 2018) of Wt and dn-SNARE mice after AAV-PS1 and AAV-APP/PS1 injection.

Another test was the Y-maze spontaneous alternation test, which was conducted to evaluate spatial working memory performance of Wt and dn-SNARE mice after AAV-PS1 and AAV-APP/PS1 injection, that relies on the prefrontal cortex, parietal cortex and hippocampus areas for maintaining spatial information in working memory (Kraeuter and Guest, 2019; van Asselen et al., 2006). Here, it was expected that animals with working memory deficits failed to complete the expected arm sequence (animals visited the three different arms consecutively). The % of alternation in the Y-maze of animals injected with AAV-APP/PS1 did not indicate deficits in spatial working memory, as suggested by a similar score compared with control animals (Figure 29). The locomotor activity (number of arm visits) also did not differ between the five groups (Figure 29). These results agree with previous work that has shown no significant impairments in spatial working memory in Y-maze spontaneous alternation test in different AD animal models (Reiserer et al., 2007; Tournier et al., 2021). Besides, a study has shown that AD patients with moderate dementia exhibit impairment in spatial working memory while those with mild dementia do not (Guariglia, 2007). Although the sample size in our test is small, this may explain why we did not detect a tendency for spatial working memory impairment. Considering that the hippocampus is the brain structure that exhibits the earliest divergence between normal aging and AD (Coupé et al., 2019), it is expected that, at this disease stage, mice exhibit intact prefrontal cortical functions, and hence intact working memory. However, considering the last reference (Coupé et al., 2019), it is expected that alterations are detected at the level of hippocampus-dependent memory.

Due to the non-detectable cognitive impairments in the previously analyzed tasks, it was hypothesized that APP processing could specifically induce hippocampal-dependent spatial learning/memory impairment. Thereby, this type of memory was examined using the Barnes Maze

and MWM test, since adequate performance in this task has been shown to be highly dependent on the integrity of the hippocampus (O'Leary and Brown, 2009). In Barnes Maze, our results show no change in any of the parameters tested, revealing preserved spatial learning of Wt AAV-APP/PS1 animals during the 4-day acquisition phase, as well as absent memory impairment in the probe test. When performed by AD animal models, Barnes Maze has shown variable results. For instance, similarly to our results, in a study using APP/PS1 mice, the animals were able to solve the maze proficiently in the probe test (Reiserer et al., 2007). Contrarily, Barnes Maze has revealed spatial memory deficits in the TgCRND8 mouse model, that is an aggressive early-onset model of brain amyloidosis (Gortz et al., 2008), but also in APP/PS1 mice model (Ahn et al., 2014), which could be explained by different protocols being used. Nonetheless, the non-injected Wt animals were not able to perform the test successfully: (1) they did not show primary error reduction (Figure 30), (2) they have a preference for the serial strategy over strategies that require spatial learning (Figure 30), and (3) in the probe test they did not show a preference for the target hole (Figure 31), which overall reveals that the animals are aware of the existence of an escape route, but instead of using the special cues, they choose to travel in a circle until finding the target hole that hides the escape box. Although Barnes Maze has several advantages over the MWM, as it is less physically demanding and less stressful to mice (O'Leary and Brown, 2009), these could also be potential weaknesses, since the test could not be aversive enough to motivate the mice to find the escape box. Therefore, the Barnes Maze may be less sensitive than MWM in detecting mild changes in memory function. Regarding MWM results, the AAV-AD model authors reported no differences in the traveled distance in the learning phase between AAV-PS1 and AAV-APP/PS1 injected animals but, during the probe test, AAV-PS1 mice spent longer in the target quadrant than AAV-APP/PS1, indicating an alteration in the memory retention in AAV-APP/PS1 mice (Audrain et al., 2016). Although our results seem to agree with the authors, the sample size needs to be increased to more be conclusive. Several studies focusing on models of AD have addressed changes in performance in the MWM (Audrain et al., 2016; Huang et al., 2017; Stazi and Wirths, 2021; Zhang et al., 2014). Interestingly, these changes (that are also observed in our results) are more noticeable in the probe test than in the acquisition phase. This can be an indicator that sometimes, in the learning phase, the animal accidentally bumps against the platform and climbs on it. Furthermore, although the results are too preliminary to draw any conclusions about astrocytes contribution to long-term spatial memory deficits in early AD, the probe test seems to indicate that compromised gliotransmission increases the time spent in the correct quadrant and the number of crosses in the previous platform location

after AAV-APP/PS1 injection (Figure 32). Therefore, the absence of SNARE-dependent gliotransmission seems to reverse the deficits caused by APP-processing in MWM, suggesting that astrocytic gliotransmission may contribute to those spatial memory impairments. Nevertheless, which gliotransmitters are exerting toxic effects remains unanswered. In animal models of AD (namely the APP/PS1 and the Tg4-42 AD models), memantine, a low- to moderate-affinity uncompetitive NMDAR antagonist that preferentially blocks eNMDAR, has been shown to restore LTP impairments and improve behavioral performance in learning and memory tasks (Li et al., 2021; Stazi and Wirths, 2021). These data, together with our results that show an increase in glutamate release by astrocytes, supports the assumption of an excitotoxic mechanism induced by astrocytic glutamate and propose that memantine may exert protective effects by potentially blocking astrocytic glutamate activity. In the future, it would be of interest to confirm whether D-serine has the same protective effect *in vivo*, being able to restore the memory deficits of our AAV-AD animal model, highlighting the pivotal involvement of astrocytes in synaptic dysfunction and progressive memory impairment, that may therefore represent a promising therapeutic strategy for the treatment of AD.

5. Conclusion

The main aim of this master thesis was to assess the consequences of alterations in astrocyte-neuron communication in AD.

The work present in this thesis suggests that dysregulated NMDAR signaling, mediated by aberrant gliotransmission may be the underlying cause of synaptic plasticity impairments and consequent memory dysfunction in AD. Our results show for the first time that:

i. Impairment of gliotransmission is protective in the presence of $A\beta_{1-42}$ because it blocks SNARE-dependent release of glutamate from astrocytes.
ii. Astrocytes are the primary source of D-serine, by releasing it in a SNARE-dependent manner and contributing to the induction of LTP in area CA1-CA3 in the hippocampus.
iii. D-serine rescues LTP impairments in hippocampal slices from Wt animals pretreated with $A\beta_{1-42}$, by promoting sNMDAR-mediated activity, suggesting its promising neuroprotective effect for toxicity induced by Aβ.
iv. AAV-AD Wt animals show a tendency to spend less time in the target quadrant in MWM probe test, which is suggestive of poor spatial memory performance, while AAV-AD dn-SNARE animals exhibit intact spatial learning and memory.

These findings highlight the role of astrocytes and gliotransmission in AD, where astrocytic signaling contributes to synaptic dysfunction that ultimately results in cognitive impairment and eventually dementia. Nevertheless, there are still open questions and future tasks that arise from our results:

i. The correlation between GFP levels in the hippocampi of low and high dn-SNARE transgene “expression”, and their respective performance in behavioral tests and synaptic plasticity integrity should be assessed.
ii. The protocol for detection of human APP by WB should be optimized to validate the AAV-AD model in agreement with the creators of the model.
iii. The pattern of phospho-tau in AAV-APP/PS1 Wt and dn-SNARE mice should be evaluated, since it has been shown to be altered in this AD model and related to eNMDAR activation and Aβ presence (Audrain et al., 2016)

i. The $A\beta_{1-42}$ dispersion in the hippocampus of injected Wt and dn-SNARE animals should be detected to evaluate the implications of gliotransmission in neurotoxic Aβ deposition.

ii. To reduce the potential variability conferred by the imprecision of the injection site, only the animals in which the desired coordinates of injection are verified upon brain dissection, should be included in upcoming studies. For that purpose, a reporter gene should be encoded in the AAV.

iii. Test whether D -serine can improve hippocampal synaptic plasticity and performance in tasks related to spatial memory in animals injected with AAV-APP/PS1.

This work will pave new astrocytic mechanisms in AD that may contribute to the development of new therapeutic strategies based on astrocyte-neuron signaling mechanisms.

6. References

Abramov, A.Y., Canevari, L., Duchen, M.R., 2003. Changes in intracellular calcium and glutathione in astrocytes as the primary mechanism of amyloid neurotoxicity. J. Neurosci. 23, 5088–5095. https://doi.org/10.1523/jneurosci.23-12-05088.2003

Adamsky, A., Goshen, I., 2017. Astrocytes in memory function : Pioneering findings and future directions. Neuroscience 370, 14–26. https://doi.org/10.1016/j.neuroscience.2017.05.033

Agulhon, C., Petravicz, J., Mcmullen, A.B., Sweger, E.J., Minton, S.K., Taves, S.R., Casper, K.B., Fiacco, T.A., Mccarthy, K.D., 2008. What Is the Role of Astrocyte Calcium in Neurophysiology ? Neuron. https://doi.org/10.1016/j.neuron.2008.09.004

Agulhon, C., Sun, M., Murphy, T., Myers, T., Lauderdale, K., Fiacco, A., 2012. Calcium signaling and gliotransmission in normal vs . reactive astrocytes. Front. Pharmacol. 3, 1–16. https://doi.org/10.3389/fphar.2012.00139

Ahn, H.J., Glickman, J.F., Poon, K.L., Zamolodchikov, D., Jno-charles, O.C., Norris, E.H., Strickland, S., 2014. A novel Aβ -fibrinogen interaction inhibitor rescues altered thrombosis and cognitive decline in Alzheimer's disease mice. Histol. Histopathol. 211, 1049–1062. https://doi.org/10.1084/jem.20131751

Albensi, B.C., Oliver, D.R., Toupin, J., Odero, G., 2007. Electrical stimulation protocols for hippocampal synaptic plasticity and neuronal hyper-excitability : Are they effective or relevant ? Exp. Neurol. 204, 1–13. https://doi.org/10.1016/j.expneurol.2006.12.009

Allen, N.J., Barres, B.A., 2009. Neuroscience: Glia - More Than Just Brain Glue. Nature 457, 675–677. https://doi.org/10.1038/457675a

Andriezen, W.L., 1893. The Neuroglia Elements in the Human Brain. Br. Med. J. 2, 227–230. https://doi.org/10.1136/bmj.2.1700.227

Angulo, M.C., Kozlov, A.S., Charpak, S., Audinat, E., 2004. Glutamate released from glial cells synchronizes neuronal activity in the hippocampus. J. Neurosci. 24, 6920–6927. https://doi.org/10.1523/JNEUROSCI.0473-04.2004

Araque, A., Carmignoto, G., Haydon, P.G., Oliet, S.H.R., Robitaille, R., Volterra, A., 2014. Gliotransmitters travel in time and space. Neuron 81, 728–739.

https://doi.org/10.1016/j.neuron.2014.02.007

Araque, A., Parpura, V., Sanzgiri, R.P., Haydon, P.G., 1999. Tripartite synapses: Glia, the unacknowledged partner. Trends Neurosci. 22, 208–215. https://doi.org/10.1016/S0166-2236(98)01349-6

Araque, A., Parpura, V., Sanzgiri, R.P., Haydon, P.G., 1998a. Glutamate-dependent astrocyte modulation of synaptic transmission between cultured hippocampal neurons. Eur. J. Neurosci. 10, 2129–2142. https://doi.org/10.1046/j.1460-9568.1998.00221.x

Araque, A., Sanzgiri, R.P., Parpura, V., Haydon, P.G., 1998b. Calcium Elevation in Astrocytes Causes an NMDA Receptor- Dependent Increase in the Frequency of Miniature Synaptic Currents in Cultured Hippocampal Neurons. J. Neurosci. 18, 6822–6829. https://doi.org/10.1523/JNEUROSCI.18-17-06822.1998

Armada-Moreira, A., Gomes, J.I., Pina, C.C., Savchak, O.K., Gonçalves-Ribeiro, J., Rei, N., Pinto, S., Morais, T.P., Martins, R.S., Ribeiro, F.F., Sebastião, A.M., Crunelli, V., Vaz, S.H., 2020. Going the Extra (Synaptic) Mile: Excitotoxicity as the Road Toward Neurodegenerative Diseases. Front. Cell. Neurosci. 14, 1–27. https://doi.org/10.3389/fncel.2020.00090

Audrain, M., Fol, R., Dutar, P., Potier, B., Billard, J., Flament, J., Alves, S., Burlot, M., Dufayet-chaffaud, G., Bemelmans, A., Valette, J., Hantraye, P., Déglon, N., Cartier, N., Braudeau, J., 2016. Alzheimer ' s disease-like APP processing in wild-type mice identifies synaptic defects as initial steps of disease progression. Mol. Neurodegener. 11, 1–17. https://doi.org/10.1186/s13024-016-0070-y

Balu, D.T., Pantazopoulos, H., Huang, C.C.Y., Muszynski, K., Harvey, T.L., Uno, Y., Rorabaugh, J.M., Galloway, C.R., Botz-Zapp, C., Berretta, S., Weinshenker, D., Coyle, J.T., 2019. Neurotoxic astrocytes express the D-serine synthesizing enzyme, serine racemase, in Alzheimer's disease. Neurobiol. Dis. 130, 104511. https://doi.org/10.1016/j.nbd.2019.104511

Barnes, C.A., 2003. Long-term potentiation and the ageing brain. Philos. Trans. R. Soc. B Biol. Sci. 765–772. https://doi.org/10.1098/rstb.2002.1244

Barnes, C.A., 1979. Memory Deficits Associated With Senescence : A Neurophysiological and Behavioral Study in the Rat. J. Comp. Physiol. Psychol. 93, 74–104. https://doi.org/10.1037/h0077579

Bellot-Saez, A., Kékesi, O., Morley, J.W., Buskila, Y., 2017. Astrocytic modulation of neuronal excitability through K+ spatial buffering. Neurosci. Biobehav. Rev. 77, 87–97. https://doi.org/10.1016/j.neubiorev.2017.03.002

Bender, C.L., Calfa, G.D., Molina, V.A., 2016. Astrocyte plasticity induced by emotional stress: A new partner in psychiatric physiopathology? Prog. Neuro-Psychopharmacology Biol. Psychiatry 65, 68–77. https://doi.org/10.1016/j.pnpbp.2015.08.005

Benneyworth, M.A., Li, Y., Basu, A.C., Bolshakov, V.Y., Coyle, J.T., 2012. Cell selective conditional null mutations of serine racemase demonstrate a predominate localization in cortical glutamatergic neurons. Cell. Mol. Neurobiol. 32, 613–624. https://doi.org/10.1007/s10571-012-9808-4

Bitan, G., Kirkitadze, M.D., Lomakin, A., Vollers, S.S., Benedek, G.B., Teplow, D.B., 2003. Amyloid β-protein (Aβ) assembly: Aβ40 and Aβ42 oligomerize through distinct pathways. Proc. Natl. Acad. Sci. U. S. A. 100. https://doi.org/10.1073/pnas.222681699

Bliss, T.V.P., Collingridge, G.L., Morris, R.G.M., Reymann, K.G., 2018. Long-term potentiation in the hippocampus: Discovery, mechanisms and function. Neuroforum 24, A103–A120. https://doi.org/10.1515/nf-2017-A059

Bliss, T.V.P., Lømo, T., 1973. Long-lasting potentiation of synaptic transmission in the dentate area of the anaesthetized rabbit following stimulation of the perforant path. J. Physiol. 232, 331–356. https://doi.org/10.1113/jphysiol.1973.sp010273

Brito-Moreira, J., Paula-Lima, A.C., Bomfim, T.R., Oliveira, F.F., Sepúlveda, F.J., 2011. Aβ Oligomers Induce Glutamate Release from Hippocampal Neurons. Curr. Alzheimer Res. 552–562. https://doi.org/10.2174/156720511796391917

Brodziak, A., Kołat, E., Różyk-Myrta, A., 2014. In Search of Memory Tests Equivalent for Experiments on Animals and Humans. Med. Sci. Monit. 2733–2739. https://doi.org/10.12659/MSM.891056

Canada, A.S. of, 2014. Understanding Genetics and Alzheimer ' s Disease. https://doi.org/https://alzheimer.ca/simcoecounty/sites/simcoecounty/files/documents/understanding_genetics_e.pdf

Carlson, H.J., Campbell, R.E., 2009. Genetically encoded FRET-based biosensors for multiparameter fluorescence imaging. Curr. Opin. Biotechnol. 20, 19–27. https://doi.org/10.1016/j.copbio.2009.01.003

Carrillo-Mora, P., Luna, R., Colín-Barenque, L., 2014. Amyloid beta: Multiple mechanisms of toxicity and only some protective effects? Oxid. Med. Cell. Longev. 2014. https://doi.org/10.1155/2014/795375

Chang, C.-H., Kuo, H.-L., Ma, W.-F., Tsai, H.-C., 2020. Cerebrospinal Fluid and Serum d-Serine Levels in Patients with Alzheimer's Disease: A Systematic Review and Meta-Analysis. J. Clin. Med. 9, 3840. https://doi.org/10.3390/jcm9123840

Chasseigneaux, S., Allinquant, B., 2012. Functions of Aβ, sAPPα and sAPPβ: Similarities and differences. J. Neurochem. 120, 99–108. https://doi.org/10.1111/j.1471-4159.2011.07584.x

Chen, Q.S., Kagan, B.L., Hirakura, Y., Xie, C.W., 2000. Impairment of hippocampal long-term potentiation by Alzheimer amyloid β-peptides. J. Neurosci. Res. 60, 65–72. https://doi.org/10.1002/(SICI)1097-4547(20000401)60:1<65::AID-JNR7>3.0.CO;2-Q

Chow, S.K., Yu, D., MacDonald, C.L., Buibas, M., Silva, G.A., 2010. Amyloid β-peptide directly induces spontaneous calcium transients, delayed intercellular calcium waves and gliosis in rat cortical astrocytes. ASN Neuro 2, 15–23. https://doi.org/10.1042/AN20090035

Cipriani, G., Dolciotti, C., Picchi, L., Bonuccelli, U., 2011. Alzheimer and his disease: A brief history. Neurol. Sci. 32, 275–279. https://doi.org/10.1007/s10072-010-0454-7

Citri, A., Malenka, R.C., 2008. Synaptic Plasticity : Multiple Forms, functions, and mechanisms. Neuropharmacology 18–41. https://doi.org/10.1038/sj.npp.1301559

Clasadonte, J., Dong, J., Hines, D.J., Haydon, P.G., 2013. Astrocyte control of synaptic NMDA receptors contributes to the progressive development of temporal lobe epilepsy. Proc. Natl. Acad. Sci. U. S. A. 110, 17540–17545. https://doi.org/10.1073/pnas.1311967110

Clements, J.D., 1996. Transmitter timecourse in the synaptic cleft: its role in central synaptic function. Trends Neurosci. 19, 163–171. https://doi.org/10.1016/S0166-2236(96)10024-2

Cornell-Bell, A.H., Finkbeiner, S.M., Cooper, M.S., Smith, S.J., 1990. Glutamate Induces Calcium Waves in Cultured Astrocytes: Long-Range Glial Signaling. Science (80-.). 247, 2–5. https://doi.org/10.1126/science.1967852

Coupé, P., Manjón, J.V., Lanuza, E., Catheline, G., 2019. Lifespan Changes of the Human Brain In Alzheimer's Disease. Sci. Rep. 9, 1–12. https://doi.org/10.1038/s41598-019-39809-8

Coyle, J.T., Balu, D., Wolosker, H., 2020. d-Serine, the Shape-Shifting NMDA Receptor Co-agonist.

Neurochem. Res. 45, 1344–1353. https://doi.org/10.1007/s11064-020-03014-1

Dallérac, G., Chever, O., Rouach, N., 2013. How do astrocytes shape synaptic transmission ? Insights from electrophysiology. Front. Cell. Neurosci. 7, 1–19. https://doi.org/10.3389/fncel.2013.00159

Denninger, J.K., Smith, B.M., Kirby, E.D., 2018. Novel object recognition and object location behavioral testing in mice on a budget. J. Vis. Exp. 2018, 1–10. https://doi.org/10.3791/58593

Dézsi, L., Tuka, B., Martos, D., Vécsei, L., 2015. Alzheimer's disease, astrocytes and kynurenines. Curr. Alzheimer Res. 12, 462–480. https://doi.org/10.2174/1567205012051505261140000

Escartin, C., Galea, E., Lakatos, A., O'Callaghan, J.P., Petzold, G.C., Serrano-Pozo, A., Steinhäuser, C., Volterra, A., Carmignoto, G., Agarwal, A., Allen, N.J., Araque, A., Barbeito, L., Barzilai, A., Bergles, D.E., Bonvento, G., Butt, A.M., Chen, W.T., Cohen-Salmon, M., Cunningham, C., Deneen, B., De Strooper, B., Díaz-Castro, B., Farina, C., Freeman, M., Gallo, V., Goldman, J.E., Goldman, S.A., Götz, M., Gutiérrez, A., Haydon, P.G., Heiland, D.H., Hol, E.M., Holt, M.G., Iino, M., Kastanenka, K. V., Kettenmann, H., Khakh, B.S., Koizumi, S., Lee, C.J., Liddelow, S.A., MacVicar, B.A., Magistretti, P., Messing, A., Mishra, A., Molofsky, A. V., Murai, K.K., Norris, C.M., Okada, S., Oliet, S.H.R., Oliveira, J.F., Panatier, A., Parpura, V., Pekna, M., Pekny, M., Pellerin, L., Perea, G., Pérez-Nievas, B.G., Pfrieger, F.W., Poskanzer, K.E., Quintana, F.J., Ransohoff, R.M., Riquelme-Perez, M., Robel, S., Rose, C.R., Rothstein, J.D., Rouach, N., Rowitch, D.H., Semyanov, A., Sirko, S., Sontheimer, H., Swanson, R.A., Vitorica, J., Wanner, I.B., Wood, L.B., Wu, J., Zheng, B., Zimmer, E.R., Zorec, R., Sofroniew, M. V., Verkhratsky, A., 2021. Reactive astrocyte nomenclature, definitions, and future directions. Nat. Neurosci. 24, 312–325. https://doi.org/10.1038/s41593-020-00783-4

Fein, J.A., Sokolow, S., Miller, C.A., Vinters, H. V, Yang, F., Cole, G.M., Gylys, K.H., 2008. Co-Localization of Amyloid Beta and Tau Pathology in Alzheimer ' s Disease Synaptosomes. Am. J. Pathol. 172, 1683–1692. https://doi.org/10.2353/ajpath.2008.070829

Foltyn, V.N., Bendikov, I., Miranda, J. De, Panizzutti, R., Dumin, E., Shleper, M., Li, P., Toney, M.D., Kartvelishvily, E., Wolosker, H., 2005. Serine Racemase Modulates Intracellular D -Serine Levels through an α,β-Elimination Activity. J. Biol. Chem. 280, 1754–1763. https://doi.org/10.1074/jbc.M405726200

Fujita, T., Chen, M.J., Li, X.B., Smith, X.N.A., Peng, W., Sun, W., Toner, M.J., Kress, B.T., Wang, X.L.,

Benraiss, A., Takano, T., Wang, S., Nedergaard, M., 2014. Neuronal Transgene Expression in Dominant-Negative SNARE Mice. J. Neurosci. 34, 16594–16604. https://doi.org/10.1523/JNEUROSCI.2585-14.2014

Furman, J.L., Sama, D.M., Gant, J.C., Beckett, T.L., Murphy, M.P., Bachstetter, A.D., van Eldik, L.J., Norris, C.M., 2012. Targeting astrocytes Ameliorates neurologic changes in a mouse model of Alzheimer's disease. J. Neurosci. 32, 16129–16140. https://doi.org/10.1523/JNEUROSCI.2323-12.2012

Garwood, C.J., Ratcliffe, L.E., Simpson, J.E., Heath, P.R., Ince, P.G., Wharton, S.B., 2017. Review: Astrocytes in Alzheimer's disease and other age-associated dementias: a supporting player with a central role. Neuropathol. Appl. Neurobiol. 43, 281–298. https://doi.org/10.1111/nan.12338

Geisert, E.E., Frankfurter, A., 1989. The neuronal response to injury as visualized by immunostaining of class III β-tubulin in the rat. Neurosci. Lett. 102, 137–141. https://doi.org/10.1016/0304-3940(89)90068-2

Gil-Bea, F.J., Schliebs, R., 2007. Increase of Locomotor Activity Underlying the Behavioral Disinhibition in Tg2576 Mice. Behav. Neurosci. 121, 340–344. https://doi.org/10.1037/0735-7044.121.2.340

Gold, C.A., 2009. Memory loss in Alzheimer's disease: implications for development of therapeutics. Expert Rev. Neurother. 8, 1879–1891. https://doi.org/10.1586/14737175.8.12.1879.Memory

Gold, P.E., Newman, L.A., Scavuzzo, C.J., Korol, D.L., 2013. Modulation of multiple memory systems: From neurotransmitters to metabolic substrates. Hippocampus 23, 1053–1065. https://doi.org/10.1002/hipo.22182

Golgi, C., 1873. Suella struttura della sostanza grigia del cervello. Gazz. Med. Ital. Lombardia, 244–246.

Gonçalves-Ribeiro, J., Pina, C.C., Sebastião, A.M., Vaz, S.H., 2019. Glutamate Transporters in Hippocampal LTD / LTP : Not Just Prevention of Excitotoxicity. Front. Cell. Neurosci. 13, 1–7. https://doi.org/10.3389/fncel.2019.00357

González-arias, C., Perea, G., 2019. Gliotransmission at Tripartite Synapses, in: Computational Glioscience. Springer International Publishing, pp. 213–226. https://doi.org/10.1007/978-3-

030-00817-8

González-Reyes, R.E., Nava-Mesa, M.O., Vargas-Sánchez, K., Ariza-Salamanca, D., Mora-Muñoz, L., 2017. Involvement of astrocytes in Alzheimer's disease from a neuroinflammatory and oxidative stress perspective. Front. Mol. Neurosci. 10, 1–20. https://doi.org/10.3389/fnmol.2017.00427

Gordon, G.R., Mulligan, S.J., MacVicar, B.A., 2007. Astrocyte Control of the Cerebrovasculature. Glia 1214–21. https://doi.org/10.1002/glia.20543

Gortz, N., Lewejohann, L., Tomm, M., Ambr, O., Keyvani, K., Paulus, W., Sachser, N., 2008. Effects of environmental enrichment on exploration , anxiety , and memory in female TgCRND8 Alzheimer mice. Behav. Brain Res. 191, 43–48. https://doi.org/10.1016/j.bbr.2008.03.006

Graeber, M.B., Kösel, S., Egensperger, R., Banati, R.B., Müller, U., Bise, K., Hoff, P., Möller, H.J., Fujisawa, K., Mehraein, P., 1997. Rediscovery of the case described by Alois Alzheimer in 1911: Historical, histological and molecular genetic analysis. Neurogenetics 1, 73–80. https://doi.org/10.1007/s100480050011

Gralle, M., Ferreira, S.T., 2007. Structure and functions of the human amyloid precursor protein: The whole is more than the sum of its parts. Prog. Neurobiol. 82, 11–32. https://doi.org/10.1016/j.pneurobio.2007.02.001

Graziano, A., Petrosini, L., Bartoletti, A., 2003. Automatic recognition of explorative strategies in the Morris water maze. J. Neurosci. Methods 130, 33–44. https://doi.org/10.1016/S0165-0270(03)00187-0

Guariglia, C.C., 2007. Spatial working memory in Alzheimer's disease: A study using the Corsi block-tapping test. Dement. Neuropsychol. 1, 392–395. https://doi.org/10.1590/s1980-57642008dn10400011

Guercio, G.D., Panizzutti, R., 2018. Potential and challenges for the clinical use of D-Serine as a cognitive enhancer. Front. Psychiatry 9, 1–10. https://doi.org/10.3389/fpsyt.2018.00014

Guerra-Gomes, S., Sousa, N., Pinto, L., Oliveira, J.F., 2018. Functional Roles of Astrocyte Calcium Elevations : From Synapses to Behavior. Front. Cell. Neurosci. 11, 1–7. https://doi.org/10.3389/fncel.2017.00427

Haery, L., Deverman, B.E., Matho, K., Cetin, A., Woodard, K., Guerin, K.I., Rego, M.A., Ersing, I.,

Bachle, S.M., Fan, M., 2019. Adeno-Associated Virus Technologies and Methods for Targeted Neuronal Manipulation. Front. Neuroanat. https://doi.org/10.3389/fnana.2019.00093

Haim, L. Ben, Rowitch, D., 2016. Functional diversity of astrocytes in neural circuit regulation. Nat. Publ. Gr. 18, 31–41. https://doi.org/10.1038/nrn.2016.159

Halassa, M.M., Florian, C., Fellin, T., Munoz, J.R., Lee, S.Y., Abel, T., Haydon, P.G., Frank, M.G., 2009. Astrocytic Modulation of Sleep Homeostasis and Cognitive Consequences of Sleep Loss. Neuron 61, 213–219. https://doi.org/10.1016/j.neuron.2008.11.024

Hardingham, G.E., Bading, H., 2010. Synaptic versus extrasynaptic NMDA receptor signalling: implications for neurodegenerative disorders. Nat. Rev. Neurosci. 11. https://doi.org/10.1038/nrn2911

Hashimoto, A., Kumashiro, S., Nishikawa, T., Oka, T., Takahashi, K., Mito, T., Takashima, S., Doi, N., Mizutani, Y., Yamazaki, T., Kaneko, T., Ootomo, E., 1993a. Embryonic Development and Postnatal Changes in Free d-Aspartate and d-Serine in the Human Prefrontal Cortex. J. Neurochem. 61, 348–351. https://doi.org/10.1111/j.1471-4159.1993.tb03575.x

Hashimoto, A., Nishikawa, T., Hayashi, T., Fujii, N., Harada, K., Oka, T., Takahashi, K., 1992. The presence of free D-serine in rat brain. FEBS Lett. 296, 33–36. https://doi.org/10.1016/0014-5793(92)80397-Y

Hashimoto, A., Nishikawa, T., Konno, R., Niwa, A., Yasumura, Y., Oka, T., Takahashi, K., 1993b. Free d-serine, d-aspartate and d-alanine in central nervous system and serum in mutant mice lacking d-amino acid oxidase. Neurosci. Lett. 152, 33–36. https://doi.org/10.1016/0304-3940(93)90476-2

Hassel, B., Tessler, S., Faull, R.L.M., Emson, P.C., 2008. Glutamate uptake is reduced in prefrontal cortex in Huntington's disease. Neurochem. Res. 33, 232–237. https://doi.org/10.1007/s11064-007-9463-1

He, Y., Zheng, M.M., Ma, Y., Han, X.J., Ma, X.Q., Qu, C.Q., Du, Y.F., 2012. Soluble oligomers and fibrillar species of amyloid β-peptide differentially affect cognitive functions and hippocampal inflammatory response. Biochem. Biophys. Res. Commun. 429, 125–130. https://doi.org/10.1016/j.bbrc.2012.10.129

Hebb, D.O., 1949. The organization of behavior: a neurophychological theory. Wiley, New York.

Hefendehl, J.K., LeDue, J., Ko, R.W.Y., Mahler, J., Murphy, T.H., MacVicar, B.A., 2016. Mapping synaptic glutamate transporter dysfunction in vivo to regions surrounding Aβ plaques by iGluSnFR two-photon imaging. Nat. Commun. 7. https://doi.org/10.1038/ncomms13441

Henneberger, C., Papouin, T., Oliet, S.H.R., Rusakov, D.A., 2010. Long-term potentiation depends on release of d-serine from astrocytes. Nature 463, 232–236. https://doi.org/10.1038/nature08673

Hines, D.J., Schmitt, L.I., Hines, R.M., Moss, S.J., Haydon, P.G., 2013. Antidepressant effects of sleep deprivation require astrocyte-dependent adenosine mediated signaling. Transl. Psychiatry 3, e212-9. https://doi.org/10.1038/tp.2012.136

Hu, X., Crick, S.L., Bu, G., Frieden, C., Pappu, R. V., Lee, J.M., 2009. Amyloid seeds formed by cellular uptake, concentration, and aggregation of the amyloid-beta peptide. Proc. Natl. Acad. Sci. U. S. A. 106, 20324–20329. https://doi.org/10.1073/pnas.0911281106

Hu, X., Yuan, Y., Wang, D., Su, Z., 2016. Heterogeneous astrocytes: active players in CNS. Brain Res. Bull. https://doi.org/10.1016/j.brainresbull.2016.03.017

Huang, Y., Shen, W., Su, J., Cheng, B., Li, D., Liu, G., Zhou, W.X., Zhang, Y.X., 2017. Modulating the Balance of Synaptic and Extrasynaptic NMDA Receptors Shows Positive Effects against Amyloid-β-Induced Neurotoxicity. J. Alzheimer's Dis. 57, 885–897. https://doi.org/10.3233/JAD-161186

Illouz, T., Madar, R., Clague, C., Griffioen, K., Louzoun, Y., 2016. Unbiased classification of spatial strategies in the Barnes maze. Bioinformatics. https://doi.org/10.1093/bioinformatics/btw376

Ivanov, A.D., Mothet, J.P., 2019. The plastic D-serine signaling pathway: Sliding from neurons to glia and vice-versa. Neurosci. Lett. 689, 21–25. https://doi.org/10.1016/j.neulet.2018.05.039

Jong, T.V. De, Moshkin, Y.M., Guryev, V., 2021. Gene expression variability : the other dimension in transcriptome analysis. Physiol. Genomics 145–158. https://doi.org/10.1152/physiolgenomics.00128.2018

Kang, J., Jiang, L., Goldman, S.A., Nedergaard, M., 1998. Astrocyte-mediated potentiation of inhibitory synaptic transmission. Nat. Neurosci. https://doi.org/10.1038/3684

Kelliny, S., Lin, L., Deng, I., Xiong, J., Zhou, F., Al-hawwas, M., Bobrovskaya, L., Zhou, X., 2021. A New Approach to Model Sporadic Alzheimer's Disease by Intracerebroventricular Streptozotocin

Injection in APP/PS1 Mice. Mol. Neurobiol. https://doi.org/10.1007/s12035-021-02338-5

Kleckner, N.W., Dingledine, R., 1988. Requirement for Glycme in Activation of NMDA- Receptors Expressed in Xenopus Oocytes. Science (80-.). 2–4. https://doi.org/10.1126/science.2841759

Kölliker, A., 1889. Handbuch der Gewebelehre des Menschen. ournal Anat. Physiol.

Kondori, N.R., Paul, P., Robbins, J.P., Liu, K., Hildyard, J.C.W., Wells, D.J., de Belleroche, J.S., 2018. Focus on the role of D-serine and D-amino acid oxidase in Amyotrophic Lateral Sclerosis/motor neuron disease (ALS). Front. Mol. Biosci. 5. https://doi.org/10.3389/fmolb.2018.00008

Kraeuter, A., Guest, P.C., 2019. The Y-Maze for Assessment of Spatial Working and Reference Memory in Mice. Pre-Clinical Model. Tech. Protoc. 1916, 105–111. https://doi.org/10.1007/978-1-4939-8994-2_10

Kuchibhotla, K. V., Lattarulo, C.R., Hyman, B.T., Bacskai, B.J., 2009. Synchronous hyperactivity and intercellular calcium waves in astrocytes in Alzheimer mice. Science (80-.). 323, 1211–1215. https://doi.org/10.1126/science.1169096

Kumar, A., Singh, A., 2015. Pharmacological Reports Review article A review on Alzheimer ' s disease pathophysiology and its management : an update. Pharmacol. Reports 67, 195–203. https://doi.org/10.1016/j.pharep.2014.09.004

Lalo, U., Bogdanov, A., Pankratov, Y., 2018. Diversity of Astroglial Effects on Aging- And Experience-Related Cortical Metaplasticity. Front. Mol. Neurosci. 11, 1–14. https://doi.org/10.3389/fnmol.2018.00239

Lalo, U., Koh, W., Lee, C.J., Pankratov, Y., 2021a. The tripartite glutamatergic synapse. Neuropharmacology 199, 108758. https://doi.org/10.1016/j.neuropharm.2021.108758

Lalo, U., Rasooli-Nejad, S., Bogdanov, A., More, L., Koh, W., Muller, J., Wall, M., Lee, C.J., Pankratov, Y., 2021b. Synergy between vesicular and non-vesicular gliotransmission regulates synaptic plasticity and working memory. Cell Rep. https://doi.org/Lalo, Ulyana and Rasooli-Nejad, Seyed and Bogdanov, Alexander and More, Lorenzo and Koh, Wuhyun and Muller, Jurgen and Wall, Mark J. and Lee, C. Justin and Pankratov, Yuriy, Synergy Between Vesicular and Non-Vesicular Gliotransmission Regulates Synaptic Plasticity and Working Memory. Available at SSRN: https://ssrn.com/abstract=3872944 or http://dx.doi.org/10.2139/ssrn.3872944

Lalo, U., Rasooli-Nejad, S., Pankratov, Y., 2014. Exocytosis of gliotransmitters from cortical

astrocytes: Implications for synaptic plasticity and aging. Biochem. Soc. Trans. 42, 1275–1281. https://doi.org/10.1042/BST20140163

Lanciotti, A., Brignone, M.S., Bertini, E., Petrucci, T.C., Aloisi, F., Ambrosini, E., 2013. Astrocytes: Emerging stars in leukodystrophy pathogenesis. Transl. Neurosci. 4, 144–164. https://doi.org/10.2478/s13380-013-0118-1

Landeghem, F.K.H. Van, Weiss, T., Oehmichen, M., Von Deimling, A., 2006. Decreased expression of glutamate transporters in astrocytes after human traumatic brain injury. J. Neurotrauma 23, 1518–1528. https://doi.org/10.1089/neu.2006.23.1518

Le Bail, M., Martineau, M., Sacchi, S., Yatsenko, N., Radzishevsky, I., Conrod, S., Ouares, K.A., Wolosker, H., Pollegioni, L., Billard, J.M., Mothet, J.P., Snyder, S.H., 2015. Identity of the NMDA receptor coagonist is synapse specific and developmentally regulated in the hippocampus. Proc. Natl. Acad. Sci. U. S. A. 112, E204–E213. https://doi.org/10.1073/pnas.1416668112

Le Douce, J., Maugard, M., Veran, J., Matos, M., Jégo, P., Vigneron, P.A., Faivre, E., Toussay, X., Vandenberghe, M., Balbastre, Y., Piquet, J., Guiot, E., Tran, N.T., Taverna, M., Marinesco, S., Koyanagi, A., Furuya, S., Gaudin-Guérif, M., Goutal, S., Ghettas, A., Pruvost, A., Bemelmans, A.P., Gaillard, M.C., Cambon, K., Stimmer, L., Sazdovitch, V., Duyckaerts, C., Knott, G., Hérard, A.S., Delzescaux, T., Hantraye, P., Brouillet, E., Cauli, B., Oliet, S.H.R., Panatier, A., Bonvento, G., 2020. Impairment of Glycolysis-Derived L-Serine Production in Astrocytes Contributes to Cognitive Deficits in Alzheimer's Disease. Cell Metab. 31, 503-517.e8. https://doi.org/10.1016/j.cmet.2020.02.004

Lenhossek, M. von, 1891. No Zur Kenntnis der Neuroglia des menschlichen Rückenmarkes. Verh. Anat. Ges. 5, 193–221.

Lever, C., Burton, S., Keefe, J.O., 2006. Rearing on Hind Legs , Environmental Novelty , and the Hippocampal Formation. Rev. Neurosci. 17, 111–133. https://doi.org/10.1515/REVNEURO.2006.17.1-2.111

Lewis, J., Lewis, J., Dickson, D.W., Lin, W., Chisholm, L., Corral, A., Jones, G., Yen, S., Sahara, N., Skipper, L., Yager, D., Eckman, C., Hardy, J., Hutton, M., Mcgowan, E., 2013. Enhanced Neurofibrillary Degeneration in Transgenic Mice Expressing Mutant Tau and APP. Science (80-.). 1487. https://doi.org/10.1126/science.1058189

Li, P., Xu, J., Gu, H., Peng, H., Yin, Y., Zhuang, J., 2021. Memantine ameliorates cognitive deficit in AD

mice via enhancement of entorhinal – CA1 projection. BMC Neurosci. 1–8. https://doi.org/10.1186/s12868-021-00647-y

Li, S., Jin, M., Koeglsperger, T., Shepardson, N.E., Shankar, G.M., Selkoe, D.J., 2011. Soluble Aβ Oligomers Inhibit Long-Term Potentiation through a Mechanism Involving Excessive Activation of Extrasynaptic NR2B-Containing NMDA Receptors. J. Neurosci. 31, 6627–6638. https://doi.org/10.1523/JNEUROSCI.0203-11.2011

Lim, D.A., Alvarez-Buylla, A., 1999. Interaction between astrocytes and adult subventricular zone precursors stimulates neurogenesis. Proc. Natl. Acad. Sci. U. S. A. 96, 7526–7531. https://doi.org/10.1073/pnas.96.13.7526

Liu, H., Li, S., Yang, C., Jia, H., Gu, Z., Tu, X., Tian, S., 2020. D-serine Ameliorates Motor and Cognitive Impairments in β -amyloid 1-42 Injected Mice by Inhibiting JNK Signaling Pathway. J. Chem. Neuroanat. 109, 101852. https://doi.org/10.1016/j.jchemneu.2020.101852

Liu, L., He, F., Yu, Y., Wang, Y., 2020. Application of FRET Biosensors in Mechanobiology and Mechanopharmacological Screening. Front. Bioeng. Biotechnol. 8, 1–17. https://doi.org/10.3389/fbioe.2020.595497

Madeira, C., Lourenco, M. V., Vargas-Lopes, C., Suemoto, C.K., Brandão, C.O., Reis, T., Leite, R.E.P., Laks, J., Jacob-Filho, W., Pasqualucci, C.A., Grinberg, L.T., Ferreira, S.T., Panizzutti, R., 2015. D-serine levels in Alzheimer's disease: Implications for novel biomarker development. Transl. Psychiatry 5. https://doi.org/10.1038/tp.2015.52

Mahmoud, S., Gharagozloo, M., Simard, C., Gris, D., 2019. Astrocytes Maintain Glutamate Homeostasis in the CNS by Controlling the Balance between Glutamate Uptake and Release. Cells 8, 184. https://doi.org/10.3390/cells8020184

Malarkey, E.B., Parpura, V., 2008. Mechanisms of glutamate release from astrocytes. Neurochem. Int. 52, 142–154. https://doi.org/10.1016/j.neuint.2007.06.005

Malikowska-racia, N., Podkowa, A., Sa, K., 2018. Phencyclidine and Scopolamine for Modeling Amnesia in Rodents : Direct Comparison with the Use of Barnes Maze Test and Contextual Fear Conditioning Test in Mice. Neurotox. Res. https://doi.org/10.1007/s12640-018-9901-7

Martineau, M., Parpura, V., Mothet, J.P., 2014. Cell-type specific mechanisms of D-serine uptake and release in the brain. Front. Synaptic Neurosci. 6, 1–9.

https://doi.org/10.3389/fnsyn.2014.00012

Martineau, M., Shi, T., Puyal, J., Knolhoff, A.M., Dulong, J., Gasnier, B., Klingauf, J., Sweedler, J. V., Jahn, R., Mothet, J.P., 2013. Storage and uptake of D-serine into astrocytic synaptic-like vesicles specify gliotransmission. J. Neurosci. 33, 3413–3423. https://doi.org/10.1523/JNEUROSCI.3497-12.2013

Masliah, E., Alford, M., DeTeresa, R., Mallory, M., Hansen, L., 1996. Deficient glutamate transport is associated with neurodegeneration in Alzheimer's disease. Ann. Neurol. 40, 759–766. https://doi.org/10.1002/ana.410400512

Masurkar, A. V, 2018. Towards a Circuit-Level Understanding of Hippocampal CA1 Dysfunction in Alzheimer's Disease Across Anatomical Axes. J. Alzheimer's Dis. Park. 08, 1–6. https://doi.org/10.4172/2161-0460.1000412

Molofsky, A. V, Krenick, R., Ullian, E., Molofsky, A. V, Krenick, R., Ullian, E., Tsai, H., Deneen, B., Richardson, W.D., Barres, B.A., Rowitch, D.H., 2012. Astrocytes and disease : a neurodevelopmental perspective Astrocytes and disease : a neurodevelopmental perspective. Genes Dev. 891–907. https://doi.org/10.1101/gad.188326.112

Mothet, J.P., Parent, A.T., Wolosker, H., Brady, R.O., Linden, D.J., Ferris, C.D., Rogawski, M.A., Snyder, S.H., 2000. D-serine is an endogenous ligand for the glycine site of the N-methyl-D-aspartate receptor. Proc. Natl. Acad. Sci. U. S. A. 97, 4926–4931. https://doi.org/10.1073/pnas.97.9.4926

Murai, T., Okuda, S., Tanaka, T., Ohta, H., 2007. Characteristics of object location memory in mice : Behavioral and pharmacological studies. Physiol. Behav. 90, 116–124. https://doi.org/10.1016/j.physbeh.2006.09.013

Nabavi, S., Fox, R., Proulx, C.D., Lin, J.Y., Tsien, R.Y., Malinow, R., 2014. Engineering a memory with LTD and LTP. Nature. https://doi.org/10.1038/nature13294

Nanclares, C., Baraibar, A.M., Araque, A., Kofuji, P., 2021. Dysregulation of Astrocyte – Neuronal Communication in Alzheimer's Disease. Int. J. Mol. Sci. https://doi.org/10.3390/ijms22157887

Neame, S., Safory, H., Radzishevsky, I., Touitou, A., Marchesani, F., Marchetti, M., Kellner, S., Berlin, S., Foltyn, V.N., Engelender, S., Billard, J.M., Wolosker, H., 2019. The NMDA receptor activation by D-serine and glycine is controlled by an astrocytic Phgdh-dependent serine shuttle. Proc.

Natl. Acad. Sci. U. S. A. 116, 20736–20742. https://doi.org/10.1073/pnas.1909458116

Neves, G., Cooke, S.F., Bliss, T.V.P., 2008. Synaptic plasticity, memory and the hippocampus: A neural network approach to causality. Nat. Rev. Neurosci. 9, 65–75. https://doi.org/10.1038/nrn2303

Nuzzo, T., Miroballo, M., Casamassa, A., Mancini, A., Gaetani, L., Nisticò, R., Eusebi, P., Katane, M., Homma, H., Calabresi, P., Errico, F., Parnetti, L., Usiello, A., 2020. Cerebrospinal fluid and serum D-serine concentrations are unaltered across the whole clinical spectrum of Alzheimer's disease. Biochim. Biophys. Acta - Proteins Proteomics 1868, 140537. https://doi.org/10.1016/j.bbapap.2020.140537

O'Leary, T.P., Brown, R.E., 2009. Visuo-spatial learning and memory deficits on the Barnes maze in the 16-month-old APPswe / PS1dE9 mouse model of Alzheimer ' s disease. Behav. Brain Res. 201, 120–127. https://doi.org/10.1016/j.bbr.2009.01.039

Oberheim, N.A., Goldman, S.A., Nedergaard, M., 2011. Heterogeneity of Astrocytic Form and Function. Methods Mol. Biol. 814, 23–45. https://doi.org/10.1007/978-1-61779-452-0

Okumoto, S., Looger, L.L., Micheva, K.D., Reimer, R.J., Smith, S.J., Frommer, W.B., 2005. Detection of glutamate release from neurons by genetically encoded surface-displayed FRET nanosensors. Proc. Natl. Acad. Sci. U. S. A. 102, 8740–8745. https://doi.org/10.1073/pnas.0503274102

Ota, Y., Zanetti, A.T., Hallock, R.M., 2013. The role of astrocytes in the regulation of synaptic plasticity and memory formation. Neural Plast. 2013. https://doi.org/10.1155/2013/185463

Otto, T., Eichenbaum, H., Wiener, S.I., Wible, C.G., 1991. Learning-related patterns of CA1 spike trains parallel stimulation parameters optimal for inducing hippocampal long- term potentiation. Hippocampus 1, 181–192. https://doi.org/10.1002/hipo.450010206

Pankratov, Y., Lalo, U., 2015. Role for astroglial α1-adrenoreceptors in gliotransmission and control of synaptic plasticity in the neocortex. Front. Cell. Neurosci. 9, 1–11. https://doi.org/10.3389/fncel.2015.00230

Papouin, T., Ladépêche, L., Ruel, J., Sacchi, S., Labasque, M., Hanini, M., Groc, L., Pollegioni, L., Mothet, J.P., Oliet, S.H.R., 2012. Synaptic and extrasynaptic NMDA receptors are gated by different endogenous coagonists. Cell 150, 633–646. https://doi.org/10.1016/j.cell.2012.06.029

Park, Hyungju, Oh, S.J., Han, K.S., Woo, D.H., Park, Hyekyung, Mannaioni, G., Traynelis, S.F., Lee, C.J., 2009. Bestrophin-1 encodes for the Ca2+-activated anion channel in hippocampal astrocytes. J. Neurosci. 29, 13063–13073. https://doi.org/10.1523/JNEUROSCI.3193-09.2009

Parpura, V., Zorec, R., 2010. Gliotransmission : Exocytotic release from astrocytes. Brain Res. Rev. 63, 83–92. https://doi.org/10.1016/j.brainresrev.2009.11.008

Pascual, O., Casper, K.B., Kubera, C., Zhang, J., Revilla-Sanchez, R., Sul, J.Y., Takano, H., Moss, S.J., McCarthy, K., Haydon, P.G., 2005. Astrocytic purinergic signaling coordinates synaptic networks. Science (80-.). 310, 113–116. https://doi.org/10.1126/science.1116916

Perea, G., Araque, A., 2009. GLIA modulates synaptic transmission. Brain Res. Rev. 63, 93–102. https://doi.org/10.1016/j.brainresrev.2009.10.005

Perea, G., Araque, A., 2007. Astrocytes Potentiate Transmitter Release at Single Hippocampal Synapses. Science (80-.). 16–18. https://doi.org/10.1126/science.1144640

Perea, G., Navarrete, M., Araque, A., 2009. Tripartite synapses: astrocytes process and control synaptic information. Trends Neurosci. 32, 421–431. https://doi.org/10.1016/j.tins.2009.05.001

Perez, B.A., Shutterly, A., Chan, Y.K., Byrne, B.J., Corti, M., 2020. Management of Neuroinflammatory Responses to AAV-Mediated Gene Therapies for Neurodegenerative Diseases. Brain Sci. 10. https://doi.org/10.3390/brainsci10020119

Petralia, R.S., Wang, Y.X., Hua, F., Yi, Z., Zhou, A., Ge, L., Stephenson, F.A., Wenthold, R.J., 2010. Organization of NMDA receptors at extrasynaptic locations. Neuroscience 167, 68–87. https://doi.org/10.1016/j.neuroscience.2010.01.022

Petravicz, J., Fiacco, T.A., Mccarthy, K.D., 2008. Loss of IP3 Receptor-Dependent Ca 2+ Increases in Hippocampal Astrocytes Does Not Affect Baseline CA1 Pyramidal Neuron Synaptic Activity. J. Neurosci. 28, 4967–4973. https://doi.org/10.1523/JNEUROSCI.5572-07.2008

Pillai, A.G., Nadkarni, S., 2019. Amyloid pathology disrupts gliotransmitter release in astrocytes. https://doi.org/10.1101/679860

Pinto-Duarte, A., Sejnowski, T.J., Roberts, A.J., Ouyang, K., 2019. Impairments in remote memory caused by the lack of Type 2 IP 3 receptors. Glia 1–14. https://doi.org/10.1002/glia.23679

Pitts, M.W., 2018. Barnes Maze Procedure for Spatial Learning and Memory in Mice. Bio-protocol 8,

139–148. https://doi.org/10.21769/bioprotoc.2744.Barnes

Piubelli, L., Pollegioni, L., Rabattoni, V., Mauri, M., Cariddi, L.P., Versino, M., Sacchi, S., 2021. Serum D -serine levels are altered in early phases of Alzheimer ' s disease : towards a precocious biomarker. Transl. Psychiatry. https://doi.org/10.1038/s41398-021-01202-3

Ramón y Cajal, S., 1913. Sobre un nuevo proceder de impregnación de la neuroglia y sus resultados en los centros nerviosos del hombre y animales. Trab. del Lab. Investig. Biológicas 11, 103–112.

Rei, N., Rombo, D.M., Ferreira, M.F., Baqi, Y., Müller, C.E., Ribeiro, J.A., Sebastião, A.M., Vaz, S.H., 2020. Hippocampal synaptic dysfunction in the SOD1 G93A mouse model of Amyotrophic Lateral Sclerosis : Reversal by adenosine A 2A R blockade. Neuropharmacology 171, 108106. https://doi.org/10.1016/j.neuropharm.2020.108106

Reiserer, R.S., Harrison, F.E., Syverud, D.C., 2007. Impaired spatial learning in the APP Swe+PSEN1E9 bigenic mouse model of Alzheimer's disease. Genes, Brain Behav. (54–65. https://doi.org/10.1111/j.1601-183X.2006.00221.x

Reiss, A.B., Arain, H.A., Stecker, M.M., Siegart, N.M., Kasselman, L.J., 2018. Amyloid toxicity in Alzheimer's disease. Rev. Neurosci. 29, 613–627. https://doi.org/10.1515/revneuro-2017-0063

Rothstein, J.D., Dykes-hoberg, M., Pardo, C.A., Bristol, L.A., Jin, L., Kuncl, R.W., Kanai, Y., Hediger, M.A., Wang, Y., Schielke, J.P., Welty, D.F., 1996. Knockout of Glutamate Transporters Reveals a Major Role for Astroglial Transport in Excitotoxicity and Clearance of Glutamate. Neuron 16, 675–686. https://doi.org/10.1016/s0896-6273(00)80086-0

Santello, M., Calì, C., Bezzi, P., 2012. Gliotransmission and the tripartite synapse. Adv. Exp. Med. Biol. 970, 307–331. https://doi.org/10.1007/978-3-7091-0932-8_14

Santello, M., Toni, N., Volterra, A., 2019. Astrocyte function from information processing to cognition and cognitive impairment. Nat. Neurosci. https://doi.org/10.1038/s41593-018-0325-8

Sardinha, V.M., Tavares, G., Martins, M., Reis, J.S., Correia, J.S., Teixeira-castro, A., Pinto, L., Sousa, N., Oliveira, F., 2017. Astrocytic signaling supports hippocampal – prefrontal theta synchronization and cognitive function. Glia 1–17. https://doi.org/10.1002/glia.23205

Schildge, S., Bohrer, C., Beck, K., Schachtrup, C., 2013. Isolation and culture of mouse cortical astrocytes. J. Vis. Exp. 1–7. https://doi.org/10.3791/50079

Scoville, W.B., Milner, B., 1957. Loss of recent memory after bilateral hippocampal lesions. J. Neurol. Neurosurg. Psychiatry 20, 11–21. https://doi.org/10.1136/jnnp.20.1.11

Seibenhener, M.L., Wooten, M.C., 2015. Use of the Open Field Maze to Measure Locomotor and Anxiety-like Behavior in Mice. J. Vis. Exp. 1–6. https://doi.org/10.3791/52434

Shipton, O.A., Paulsen, O., Paulsen, O., 2014. GluN2A and GluN2B subunit-containing NMDA receptors in hippocampal plasticity. Philos. Trans. R. Soc. B Biol. Sci. https://doi.org/10.1098/rstb.2013.0163

Skowrońska, K., Obara-Michlewska, M., Zielińska, M., Albrecht, J., 2019. NMDA Receptors in Astrocytes : In Search for Roles in Neurotransmission and Astrocytic Homeostasis. Int. J. Mol. Sci. https://doi.org/10.3390/ijms20020309

Socodato, R., Melo, P., Ferraz-Nogueira, J.P., Portugal, C.C., Relvas, J.B., 2020. A Protocol for FRET-Based Live-Cell Imaging in Microglia. STAR Protoc. 1. https://doi.org/10.1016/j.xpro.2020.100147

Stazi, M., Wirths, O., 2021. Chronic Memantine Treatment Ameliorates Behavioral Deficits , Neuron Loss , and Impaired Neurogenesis in a Model of Alzheimer ' s Disease. Mol. Neurobiol. 204–216. https://doi.org/10.1007/s12035-020-02120-z

Sturman, O., Germain, P., Bohacek, J., 2018. Exploratory rearing : a context- and stress-sensitive behavior recorded in the open-field test. Stress 0, 1–10. https://doi.org/10.1080/10253890.2018.1438405

Sultan, S., Li, L., Moss, J., Petrelli, F., Cassé, F., Gebara, E., Lopatar, J., Pfrieger, F.W., Bezzi, P., Bischofberger, J., Toni, N., 2015. Synaptic Integration of Adult-Born Hippocampal Neurons Is Locally Controlled by Astrocytes. Neuron 88, 957–972. https://doi.org/10.1016/j.neuron.2015.10.037

Sweatt, J.D., 2009. Mechanisms of Memory, Second Edi. ed. Academic Press. https://doi.org/https://doi.org/10.1016/B978-0-12-374951-2.00004-4

Tabata, H., 2015. Diverse subtypes of astrocytes and their development during corticogenesis. Front. Neurosci. 9, 1–7. https://doi.org/10.3389/fnins.2015.00114

Takahashi, R.H., Capetillo-zarate, E., Lin, M.T., Milner, T.A., Gouras, G.K., 2010. Co-occurrence of Alzheimer ' s disease β-amyloid and tau pathologies at synapses. Neurobiol. Aging 31, 1145–

1152. https://doi.org/10.1016/j.neurobiolaging.2008.07.021

Takano, T., Han, X., Deane, R., Zlokovic, B., Nedergaard, M., 2007. Two-photon imaging of astrocytic Ca2+ signaling and the microvasculature in experimental mice models of Alzheimer's disease. Ann. N. Y. Acad. Sci. 1097, 40–50. https://doi.org/10.1196/annals.1379.004

Talantova, M., Sanz-Blasco, S., Zhang, X., Xia, P., Akhtar, M.W., Okomoto, S., Dziewczapolskib, G., Nakamuraa, T., Cao, G., Pratt, A.E., Kang, Y.-J., Tu, S., Molokanovaa, E., McKerchera, S.R., Hires, S.A., Sason, H., Stoufferf, D.G., Lipton, S.A., 2013. Aβ induces astrocytic glutamate release, extrasynaptic NMDA receptor activation, and synaptic loss. Proc. Natl. Acad. Sci. U. S. A. 110, 13691. https://doi.org/10.1073/pnas.1313266110

Tanzi, R.E., 2021. FDA Approval of Aduhelm Paves a New Path for Alzheimer ' s Disease. ACS Chem. Neurosci. 2714–2715. https://doi.org/10.1021/acschemneuro.1c00394

Tavares, E., Antequera, D., López-gonzález, I., Ferrer, I., Miñano, F.J., Carro, E., 2016. Potential Role of Aminoprocalcitonin in the Pathogenesis of Alzheimer Disease. Am. J. Pathol. 1–14. https://doi.org/10.1016/j.ajpath.2016.06.006

Temido-Ferreira, M., Coelho, J.E., Pousinha, P.A., Lopes, L. V., 2019. Novel Players in the Aging Synapse: Impact on Cognition. J. Caffeine Adenosine Res. 9, 104–127. https://doi.org/10.1089/caff.2019.0013

Tournier, B.B., Barca, C., Fall, A.B., Gloria, Y., Meyer, L., Ceyzériat, K., Millet, P., 2021. Spatial reference learning deficits in absence of dysfunctional working memory in the TgF344-AD rat model of Alzheimer's disease. Genes, Brain Behav. 20, 1–10. https://doi.org/10.1111/gbb.12712

Trudler, D., Sanz-blasco, S., Eisele, Y.S., Ghatak, S., Bodhinathan, K., Akhtar, M.W., Lynch, W.P., Piña-crespo, J.C., Talantova, M., Kelly, J.W., Lipton, S.A., 2021. α-Synuclein Oligomers Induce Glutamate Release from Astrocytes and Excessive Extrasynaptic NMDAR Activity in Neurons , Thus Contributing to Synapse Loss. J. Neurosci. 41, 2264–2273. https://doi.org/10.1523/JNEUROSCI.1871-20.2020

Tu, S., Okamoto, S., Lipton, S.A., Xu, H., 2014. Oligomeric A β -induced synaptic dysfunction in Alzheimer ' s disease. Mol. Neurodegener. 9, 1–12. https://doi.org/10.1186/1750-1326-9-48

Vago, D.R., Wallenstein, G. V., Morris, L.S., 2014. Hippocampus. Encycl. Neurol. Sci. 2, 566–570.

https://doi.org/10.1016/B978-0-12-385157-4.01151-9

Van-Horn, M.R., Sild, M., Ruthazer, E.S., 2013. D-serine as a gliotransmitter and its roles in brain development and disease. Front. Cell. Neurosci. 7, 1–13. https://doi.org/10.3389/fncel.2013.00039

van Asselen, M., Kessels, R.P.C., Neggers, S.F.W., Kappelle, L.J., Frijns, C.J.M., Postma, A., 2006. Brain areas involved in spatial working memory. Neuropsychologia 44, 1185–1194. https://doi.org/10.1016/j.neuropsychologia.2005.10.005

Vaz, S.H., Pinto, S., Sebastião, A.M., Brites, D., Araki, T., 2021. Astrocytes in Amyotrophic Lateral Sclerosis, in: Exon Publications, Brisbane, A. (Ed.), Amyotrophic Lateral Sclerosis [Internet]. https://doi.org/10.36255/exonpublications.amyotrophiclateralsclerosis.astrocytes.2021

Verkhratsky, A., Nedergaard, M., Hertz, L., 2014. Why are Astrocytes Important? Neurochem. Res. 40, 389–401. https://doi.org/10.1007/s11064-014-1403-2

Virchow, R., 1856. Gesammelte Abbildung zur wissenschaftlichen Medizin. Verlag von Meidinger Sohn Comp.

Vitvitsky, V.M., Garg, S.K., Keep, R.F., Albin, R.L., Banerjee, R., 2012. Biochimica et Biophysica Acta Na + and K + ion imbalances in Alzheimer ' s disease. BBA - Mol. Basis Dis. 1822, 1671–1681. https://doi.org/10.1016/j.bbadis.2012.07.004

Vorhees, C. V., Williams, M.T., 2006. Morris water maze: Procedures for assessing spatial and related forms of learning and memory. Nat. Protoc. 1, 848–858. https://doi.org/10.1038/nprot.2006.116

Wang, Z.-J., Zhao, F., Wang, C.-F., Zhang, X.-M., Xiao, Y., Zhou, F., Wu, M.-N., Zhang, J., Qi, J.-S., Ynag, W., 2019. Xestospongin C, a Reversible IP3 Receptor Antagonist, Alleviates the Cognitive and Pathological Impairments in APP/PS1 Mice of Alzheimer's Disease. J. Alzheimer's Dis. https://doi.org/10.3233/JAD-190796

Willbold, E., Layer, P.G., 1998. Muller glia cells and their possible roles during retina differentiation in vivo and in vitro. Histol. Histopathol. 531–552. https://doi.org/10.14670/HH-13.531

Williams, S.M., Diaz, C.M., Macnab, L.T., Sullivan, R.K.P., 2006. Immunocytochemical Analysis of D-Serine Distribution in the Mammalian Brain Reveals Novel Anatomical Compartmentalizations in Glia and Neurons. Glia 53, 401–411. https://doi.org/10.1002/glia

Wolosker, H., 2018. The Neurobiology of D-Serine Signaling, 1st ed, Advances in Pharmacology. Elsevier Inc. https://doi.org/10.1016/bs.apha.2017.08.010

Wolosker, H., 2011. Serine racemase and the serine shuttle between neurons and astrocytes. Biochim. Biophys. Acta - Proteins Proteomics 1814, 1558–1566. https://doi.org/10.1016/j.bbapap.2011.01.001

Yang, J.H., Wada, A., Yoshida, K., Miyoshi, Y., Sayano, T., Esaki, K., Kinoshita, M.O., Tomonaga, S., Azuma, N., Watanabe, M., Hamase, K., Zaitsu, K., MacHida, T., Messing, A., Itohara, S., Hirabayashi, Y., Furuya, S., 2010. Brain-specific Phgdh deletion reveals a pivotal role for l-serine biosynthesis in controlling the level of D-serine, an N-methyl-D-aspartate receptor co-agonist, in adult brain. J. Biol. Chem. 285, 41380–41390. https://doi.org/10.1074/jbc.M110.187443

Zhang, Q., Pangršič, T., Kreft, M., Kržan, M., Li, N., Sul, J.Y., Halassa, M., Van Bockstaele, E., Zorec, R., Haydon, P.G., 2004. Fusion-related Release of Glutamate from Astrocytes. J. Biol. Chem. 279, 12724–12733. https://doi.org/10.1074/jbc.M312845200

Zhang, Y., Lu, L., Jia, J., Jia, L., Geula, C., Pei, J., Xu, Z., Qin, W., Liu, R., Li, D., Pan, N., 2014. A Lifespan Observation of a Novel Mouse Model : In Vivo Evidence Supports A b Oligomer Hypothesis. PLoS One 9. https://doi.org/10.1371/journal.pone.0085885

Zheng, H., Koo, E.H., 2006. The amyloid precursor protein: beyond amyloid. Mol. Neurodegener. 1, 1–12. https://doi.org/10.1186/1750-1326-1-5

Ziervogel, B.K., Roux, B., 2013. The binding of antibiotics in OmpF porin. Structure 21, 76–87. https://doi.org/10.1016/j.str.2012.10.014